Linear Parameter Varying Path-Tracking Control Design for Autonomous Ground Vehicles

Amir Afsharinejad

A Thesis

in

The Department

of

Mechanical, Industrial & Aerospace Engineering

Presented in Partial Fulfillment of the Requirements

for the Degree of

Master of Applied Science (Mechanical Engineering) at

Concordia University

Montréal, Québec, Canada

October 2025

CONCORDIA UNIVERSITY

School of Graduate Studies

This is to certify that the thesis prepared

By: **Amir Afsharinejad**
Entitled: **Linear Parameter Varying Path-Tracking Control Design for Autonomous Ground Vehicles**
and submitted in partial fulfillment of the requirements for the degree of
Master of Applied Science (Mechanical Engineering)
complies with the regulations of this University and meets the accepted standards with respect to originality and quality.
Signed by the Final Examining Committee:

_____ Chair
Dr. Youmin Zhang

_____ External Examiner
Dr. Wen-Fang Xie

_____ Examiner
Dr. Youmin Zhang

_____ Supervisor
Dr. Hamid Taghavifar

_____ Co-supervisor
Dr. Anh-Tu Nguyen

Approved by

_____
Dr. Muthkumaran Packrisamy, Chair
Department of Mechanical, Industrial & Aerospace Engineering

_____ October 2025

_____
Dr. Mourad Debbabi, Dean
Dean Gina Cody School of Engineering and Computer Science

ABSTRACT

Linear Parameter Varying Path-Tracking Control Design for Autonomous Ground Vehicles

Amir Afsharinejad

Navigating Autonomous Ground Vehicles (AGVs) demands handling complex traffic conditions with safety, comfort, and precision across diverse operating conditions. An essential constituent of AGV navigation is the development of effective path-following strategies to track a desired trajectory while dealing with dynamic variables such as changing vehicle speeds, external disturbances, and actuator limitations. Such systems must combine robust control methods to handle uncertainties and nonlinearities inherent in vehicle dynamics and provide reliable performance in complex driving conditions. This research focuses on developing a lateral control framework for AGVs through a novel Linear Parameter Varying (LPV) modeling approach. By treating the vehicle's longitudinal velocity as a varying parameter, an LPV representation of the road-vehicle system is formulated. To reduce the conservatism inherent in traditional LPV models, a polytopic LPV framework that employs a varying parameter and utilizes a first-order Taylor approximation is introduced. This approach reduces the number of vertices required in the polytopic vehicle model, thus improving computational efficiency and performance of the path tracking control design. This polytopic LPV model, employed for an H_2 LPV control design, has the dual objectives of disturbance attenuation and guaranteeing passenger safety and comfort. The control design process utilizes Lyapunov theory to guarantee the stability and performance of the closed-loop system. Both Quadratic Lyapunov Functions (QLF) and Poly-Quadratic Lyapunov Functions (PQLF) are explored, with PQLF suggesting a substantial reduction in the conservatism typically associated with LPV systems. The controller design is recast as a convex optimization problem under Linear Matrix Inequality (LMI) constraints. This method avoids the drawbacks of heuristic optimization methods while ensuring a systematic and robust solution. Additionally, a Linear Quadratic Regulator (LQR) control scheme is developed as a benchmark that is further validated through numerical simulations. The performance of the proposed controllers and LPV models is extensively assessed through comparative simulations with their nonlinear counterparts, which emphasizes their effectiveness in dealing with the dynamic challenges of AGV lateral control.

Acknowledgments

I would like to express my deepest gratitude to my first supervisor, Dr. Hamid Taghavifar, for his incredible support, patience, and guidance throughout this research. From him, I have learned invaluable lessons not only for my academic work but also for life. His encouragement and insight have been truly inspiring.

I am also deeply thankful to my second supervisor, Dr. Anh-Tu Nguyen, for always being helpful and supportive, even from afar and across different time zones. His guidance has greatly contributed to the completion of this work.

I am profoundly grateful to my family, especially my mother, for their love, encouragement, understanding, and constant support throughout this journey.

Finally, I wish to thank my friends for their support and motivation along this path.

I dedicate this thesis to my beloved companion, Aida.

Your courage and unwavering spirit inspire me more than words can express.
Beyond that, your patience and tolerance throughout this journey have been truly remarkable.
This achievement is, in many ways, a reflection of your strength.

I stand with you and believe in you.

Table of Contents

List of Figures

Chapter One

Chapter Two

Chapter Three

Chapter Four

List of Tables

Chapter One

Chapter Two

Chapter Four

Chapter 1

Introduction and Literature Review

1.1. Background and Motivation

Autonomous Ground Vehicles (AGVs) offer a transformative opportunity for the realization of future intelligent transportation systems. Integrating AGVs with smart cities significantly improves traffic efficiency, road safety, and passenger comfort. This demand arises from the urgent need to address issues in current road transportation, where human error accounts for about 94% of fatal accidents. By utilizing robust and safe control methods, AGVs have the potential to considerably mitigate these risks, reduce traffic-related fatalities, and enhance the overall efficiency of transportation systems. Beyond safety, AGVs can improve driving comfort through precise and adaptive vehicle control [1]. These advancements not only address critical safety concerns but also overcome the inherent limitations of human drivers, providing a level of reliability and consistency unattainable with conventional vehicles. This limitation can be addressed by AGVs, where advanced intelligence takes control of the car, remaining unaffected by human vulnerabilities such as fatigue, sleepiness, and distractions. In terms of comfort, AGVs utilize high-tech sensors, powerful processors, and state-of-the-art telecommunication systems. This improvement is particularly useful for individuals with visual or hearing impairments or physical disabilities, offering them greater independence and accessibility while enhancing the overall convenience of transportation for all users [2]. Fig. 1.1 provides a general overview of an AGV, including its onboard sensors, computer, and other components.

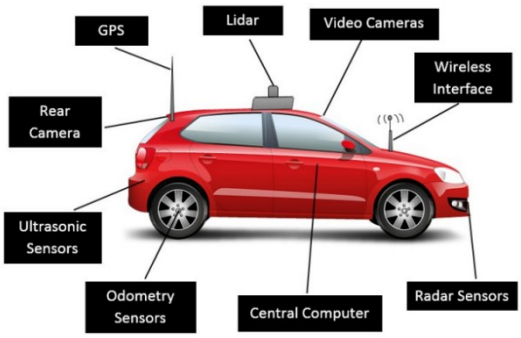

Fig. 1.1. The sketch of an autonomous vehicle and its on-board equipment [3]

The field of automated driving is extensive and encompasses a diversity of focus and applications, each with its own set of requirements and concerns, with lane-keeping and lateral path-tracking control as a primary one. This task involves the intelligent vehicle utilizing input data obtained from onboard sensors, as well as various vehicle parameters, to navigate and maintain a desired path, a fundamental goal in the development of autonomous vehicles.

Active safety systems, such as steering assistance technologies, have been implemented over the past two decades to facilitate automatic lane-keeping control, also known as lateral control and higher levels of autonomy for self-driving cars. These systems seek to prevent lane departure, thereby significantly reducing road accidents and consequent road casualties. [4]. Such a task covers various scenarios, such as *i)* lane tracking, *ii)* lane changing, and *iii)* obstacle avoidance, which can be tackled by designing control laws through steering commands [5].

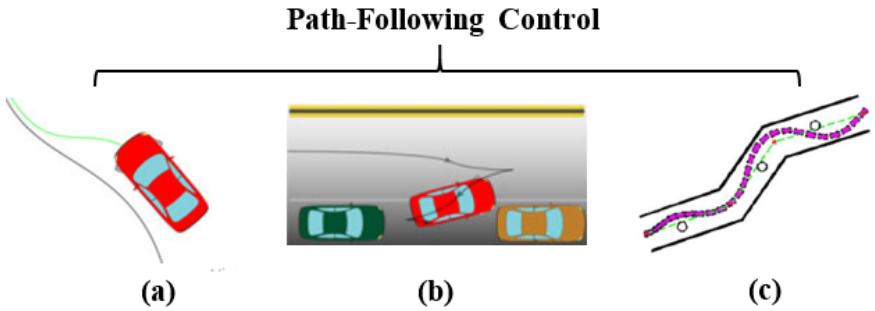

Fig. 1.2. Different goals in path-following control of an AGV: **(a)** Lane tracking [1], **(b)** Lane changing [1], **(c)** Obstacle avoidance [6]

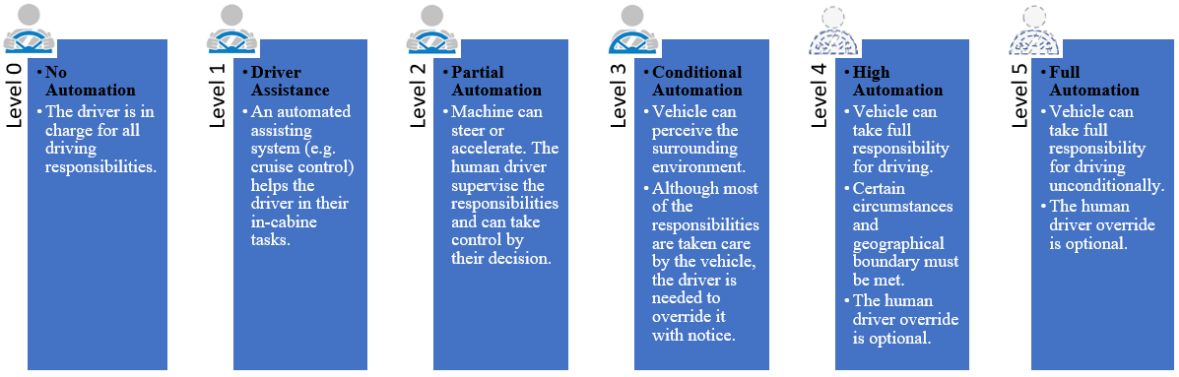

Fig. 1.3. AGVs' autonomy levels

Fig. 1.3 exhibits the different autonomy levels of AGVs based on the SAE definition [7]. The SAE levels of autonomy, ranging from Level 0 (no automation) to Level 5 (full automation), outline the increasing capabilities of automated systems and the decreasing reliance on human intervention. As vehicles progress toward higher levels of autonomy, the complexity of system responsibilities grows. While the SAE levels provide a framework for vehicle automation, the lateral path tracking task, including lane-keeping performance, remains a critical challenge across all levels, especially for driverless and highly autonomous vehicles. This highlights the enduring importance of robust control strategies for this fundamental task.

1.2. Literature Review

AGVs have been in the spotlight of the research activities done by both academia and the automotive industry during the past decades [8], [9] with one desired goal, contributing to the safety of and comfort in the daily commuting of individuals in society [10]. There are some key areas in the field of controlling AGVs, including trajectory planning and optimization, where optimal paths or trajectories for the AGV are generated through designed algorithms [11], [12], [13] and [14]; adaptive cruise control systems take the responsibility of keeping a safe following distance from other vehicles by manipulating the vehicle's velocity by developing control strategies [15], [16], [17] and [18]; platooning control, where several autonomous vehicles are coordinated together to achieve a desired objective [19], [20], [21] and [22]; parking assistance control systems which make automatic parking possible for AGVs regardless of the physical geometry of the parking space [23], [24], [25] and [26]; the context of sensor fusion and localization in which generated data by LiDAR or cameras is utilized to define the vehicle's position and orientation [27], [28], [29] and [30]; and finally, designing control systems targeted to provide efficient collaboration between human drivers and autonomous systems [31], [32], [33] and [34]. Lane-keeping control has consistently remained a primary focus due to its significance in intelligent vehicles, while path-following control, which includes lane-keeping, plays a crucial role in mitigating the inherent hazards of driving by ensuring safe and accurate vehicle guidance [1], [35], [36], [37], and [38].

Table 1.1. Key areas in the field of controlling AGVs

Area	Example Studies
Trajectory Planning and Optimization	[11], [12], [13], [14]
Adaptive Cruise Control Systems	[15], [16], [17], [18]
Platooning Control	[19], [20], [21], [22]
Parking Assistance Control Systems	[23], [24], [25], [26]
Sensor Fusion and Localization	[27], [28], [29], [30]
Control of the Human-Machine Interaction	[31], [32], [33], [34]
Path-Following Control	[1], [35], [36], [37], [38]

The steering control in vision-based AGVs was investigated by designing a nested proportional-integral differential (PID) structure in [39], where experimental tests were conducted regarding designing a path-following controller for roads with uncertain curvature. In this study, the steering wheel angle was defined as the input control signal and was generated based on the yaw rate and the lateral offset. Yaw rate and lateral offset were measured using a gyroscope and a vision system working based on the distance between the road centerline and a virtual point at a fixed distance from the vehicle. A PID control with a double integral action built the external control loop for attenuating the disturbance on the curvature. Finally, the variations in the vehicle speed, along with the uncertainty in its parameters, were considered to examine the robustness of the control scheme against such parametric uncertainties. In another study [40], the lateral control of AGVs was investigated through three different adaptive nonlinear controllers: *i)* a sliding mode controller, *ii)* an immersion and invariance principle-based controller (or simply I&I controller), and *iii)* a passivity-based adaptive PI controller that benefits from the output feedback with a passive output (PBC controller). It was concluded that the SMC, despite the simplicity in design, has issues related to the chattering problems, and that the I&I controller exhibited greater robustness when handling significant variations in curvature. Additionally, the I&I control method provides smooth steering commands. Finally, by ensuring passivity in the closed-loop system, the PBC controller not only enabled energy-based analysis but also guaranteed that the system did not produce more energy than it consumed, resulting in robust and efficient performance. Despite different approaches, none of these methods demonstrated a clear advantage in terms of lateral error. Although one method (*e.g.*, the I&I controller) may offer a better transient response, another excels in steady-state performance, leading to an overall error that remains comparable over the entire operating period.

Given that the main benefits of these strategies lie in their robustness against uncertainties, noise, and variations in road curvature, a more directly comparable approach, such as H_∞-based methods, could have been assessed as well. A study focused on lane-keeping while considering passenger comfort and addressing disturbances and uncertainties in the vehicle's parameters [41]. Consequently, three criteria become advantageous in this exploration: i) lane tracking, ii) robustness, and iii) passenger comfort, which are managed by three different controllers: i.e., PID and Linear-Quadratic-Gaussian and H_∞. It was concluded that H_∞ demonstrated a greater performance in lane-keeping tasks and robustness. However, it was still sensitive to changes in look-ahead distance and the center of gravity location. The performance of AGVs dealing with obstacle avoidance was also studied in [42] using a nonlinear nonconvex control method implemented in two stages. In the first stage, a nonlinear model predictive controller used a simplified vehicle model to generate both a collision-free trajectory and the optimal input, leveraging the generalized minimal residual method along with a continuation method for optimization. In the second stage, a linear feedback controller with a preview component compensated for the discrepancy between the simplified model and a single-track (bicycle) model. Because this optimization problem was nonconvex, achieving global optimality remained an issue.

Another study in [43] addressed both longitudinal and lateral control of AGVs. A nonlinear model predictive controller was used to manage the steering system for lateral control, while a simplified vehicle model served as the basis for designing a Lyapunov-based nonlinear controller for longitudinal speed tracking. In [44], an active front steering system was controlled using a model predictive control strategy to track the desired trajectory at high speeds on icy, snow-covered roads. The controller used the predicted trajectory at each time interval to generate the steering angle. Two approaches were tested: one employed a nonlinear vehicle model, while the other utilized successive online linearization of the vehicle model, resulting in different computational demands. The authors demonstrated that the second approach achieved comparable performance to the nonlinear model predictive control but with a significantly lower computational cost. In [45], a robust controller was designed for path-following control in AGVs using a linear model predictive control strategy. The design incorporated a robust control action alongside a feed-forward control signal to compensate for discrepancies between the trajectory tracking error model used in the control design and the actual system. The study in [46] integrated trajectory tracking, vehicle

stability, and collision avoidance into a unified control structure. In cases where stabilization and collision avoidance control signals conflicted, the proposed approach prioritized collision avoidance. The design combined feedback controllers with model predictive methodologies. In [47], a stochastic model predictive controller was employed to predict the behavior of other vehicles and enable safe lane-changing scenarios. However, [47], similar to other studies using model predictive control approaches, faced significant computational challenges due to the need for solving online optimization problems, a limitation particularly pronounced in nonlinear model predictive techniques, as mentioned in [45].

In the study [48], a shared controller was developed to assist drivers with trajectory following using a gain-scheduling robust approach. This approach accounted for varying driving conditions, vehicle dynamics, and driver characteristics (e.g., delay time, preview time, and steering gain). Additionally, uncertainties such as tire cornering stiffness variations and modeling errors were incorporated as bounded disturbances. The performance optimization considered tracking error, control effort, and the physical and mental workload of the driver. Constraints on the closed-loop system's pole placement were introduced to improve transient response, leveraging the relationship between eigenvalues and system stability.

Similar to [48], studies in [2], [49], and [50] explored trajectory following and lane-keeping with robust control strategies. These works employed static and dynamic output feedback controllers, focusing on regional pole placement via the D-stability concept to enhance transient response. The static output feedback controllers in [2] and [49] simplified real-time implementation, while [50] utilized a dynamic output feedback controller but noted limitations in its application to scenarios with large heading angles, such as J-turns.

Incorporating fuzzy and robust control methods, studies in [51], [52], and [53] designed lane-keeping assist (LKA) systems and trajectory-following controllers. These works addressed human-machine conflicts by including driver activity variables and employing T-S fuzzy techniques to manage variations in driver behavior and vehicle velocity. The control designs reduced conservatism using parameter-dependent Lyapunov functions, with optimization problems solved via LMIs for efficiency. However, dynamic output feedback schemes, as used in [51], added complexity to real-time implementation.

Several studies ([4], [5], [54], and [55]) investigated static output feedback controllers for lane-keeping and trajectory-following tasks. These controllers leveraged LPV or polytopic LPV models to address speed variations, included road geometry as a feedforward action, and incorporated physical constraints (e.g., acceleration bounds) to improve robustness and reduce conservatism. For example, [4] incorporated vehicle-road dynamics into the control law for improved cornering performance, while [5] combined LMI and genetic algorithms to design an H_∞ robust control strategy.

Control systems addressing disturbances and constraints were discussed in [56], [57], and [58]. These studies used shared steering frameworks and switching strategies to handle lane departures, obstacle avoidance, and stability control. Methods included Lyapunov-based techniques, composite Lyapunov functions, and polyhedral invariant sets to ensure stability and robust performance under uncertainties. In [57], an MPC-based shared steering system mitigated driver-system conflicts but faced computational challenges due to non-convex optimization. Studies [58], [59], and [60] focused on driver-automation interaction and used T-S fuzzy models and time-varying driver activity parameters to address human-machine collaboration in semi-autonomous vehicles. While [58] and [59] emphasized safety and comfort by incorporating physical constraints into the control design, [60] focused on using measured outputs to simplify implementation and full-state information. Lastly, [61], [62], and [63] addressed shared control structures and driver assistance systems under uncertainties, employing LPV and reduced-order LPV controllers to handle variations in road adhesion, vehicle mass, and wind disturbances. These studies highlighted the trade-offs between controller complexity, robustness, and real-time feasibility.

In [64], a robust H_2 control approach based on LPV modeling was used to design a direct tilt control strategy to improve the lateral stability of narrow tilting vehicles. The design incorporated constraints on system states and actuators to enhance safety and passenger comfort. The authors utilized parameter-dependent Lyapunov functions to reduce conservatism and solved the optimization problem using LMIs, ensuring efficient computation. Trajectory tracking and performance improvement of AGVs were addressed in [65] with an integral sliding mode control approach, focusing on yaw stabilization. The control strategy used a robust Kalman filter and neural networks to estimate states and manage uncertainties, targeting transient performance and considering actuator saturation. Similarly, [66] proposed a linear MPC controller for lane-keeping

and obstacle avoidance, using decoupled lateral and longitudinal dynamics to simplify real-time implementation. However, this approach was limited to low-curvature roads. Path-following applications were further explored in [67], [68], and [69]. In [67], a two-layer control system combined fuzzy logic and PID control for precise steering adjustment. In [68], a weighted gain-scheduling H_∞control strategy was designed, considering parameters such as steering hysteresis and longitudinal velocity variations, but lacked fast trajectory-tracking error convergence. The study in [69] addressed uncertainties in steering angle, tire forces, and load transfer with a combination of feedback-feedforward robust control and adaptive SMC.

Several studies, including [70], [71], [72], and [73], tackled vehicle dynamics and parametric uncertainties in path-following tasks. In [70], a robust fuzzy control system handled external disturbances and velocity variations, ensuring asymptotic stability. The study in [71] used an adaptive controller to manage tire cornering stiffness variations and lateral errors with constrained functions. In [72], an adaptive neural controller simultaneously addressed lateral and longitudinal dynamics in a model-independent manner but without considering control signal optimality. Localization errors and tire slip effects were considered in [73] using a polytopic model and an observer-based H_∞ and L_1control strategy for improved trajectory tracking. Slope road path-following was investigated in [74], where an MPC-LPV approach addressed unequal tire force distribution and gravity effects. The study integrated a torque allocation scheme and gyro sensor data but assumed constant longitudinal velocity, limiting its real-world applicability. The study in [75] extended MPC to include constraints such as sideslip, rollover, and vehicle envelopes, improving lateral stability and smooth transitions but lacked a non-MPC benchmark for comparison. Switched and nonlinear control strategies were discussed in [76], [77], and [78]. The study in [76] proposed a switched polytopic LPV model for varying vehicle velocities, ensuring stability using multiple Lyapunov functions. However, it did not compare different switching methods. In [77], a nonlinear H_∞control strategy combined neural networks and policy iteration to manage input limitations and disturbances but did not address parametric uncertainties. The work in [78] extended H_∞control to account for delays, data dropouts, and tire stiffness uncertainties, though its time-invariant assumptions introduced conservatism. Lastly, [79] designed a robust H_∞controller for trajectory tracking using active front steering and direct yaw moment control. The design employed LMIs, Lyapunov stability, and D-stability concepts to

address model uncertainties, system constraints, and external disturbances, achieving improved transient response.

Table 1.2. Literature Review Summary

Path-following Control Approaches	**References**
Classical Linear Control	
PID	[39], [41], [67]
LQG	[41]
H_∞	[5], [48], [41], [68], [69], [73], [76], [78], [79]
Mixed H_∞/L_1	[73]
Nonlinear H_∞	[77]
H_2	[2], [4], [52], [62], [64]
Nonlinear Control (Adaptive Control)	[40], [65], [69], [71], [72]
MPC Control:	
Nonlinear MPC	[44], [42], [43]
LTV MPC	[44]
Linear MPC	[45], [46], [57], [66], [75]
LPV MPC	[74]
Stochastic MPC	[47]
LPV and T-S Control	
LPV	[5], [4], [50], [61], [63], [64], [69]
Switched-LPV	[76]
Gain-scheduling	[48], [56], [68]
Fuzzy	[51], [67], [70]
T-S Fuzzy	[2], [53], [58], [59], [60]

1.3. Research Scope and Objectives

Safety and comfort are critical priorities in developing intelligent vehicles and AGVs. The effectiveness of a vehicle control system directly impacts these priorities while maintaining closed-loop stability as a fundamental requirement. By enhancing feedback control performance, the controlled system becomes more efficient, mitigating the inherent risks of driving and reducing the driver's workload. In lane-keeping control, one of the primary objectives in intelligent vehicle systems, real-time road curvature information can significantly improve the control system's effectiveness by enabling the prediction of potential vehicle trajectories. This enhancement is

achieved by integrating a feedforward gain with a feedback gain, forming the overall control law proposed in this thesis for the path-following task of AGVs.

Vehicle dynamics, which model AGV behavior, vary significantly under different operating conditions, including changes in speed, vehicle parameters (such as tire cornering stiffness), road conditions, and control objectives like lane tracking, lane changing, and obstacle avoidance. Consequently, different performance criteria must be employed to address the diverse traffic scenarios vehicles encounter. Designing a model-based controller that meets performance objectives across a wide range of operating conditions remains a major challenge. Robust control strategies are essential to address these varying conditions and achieve diverse performance goals. Such control algorithms must ensure passenger comfort, minimize conservatism, and be practical for real-world applications. Before deployment on test tracks or real roads, these algorithms must be rigorously validated through high-fidelity numerical simulations. The stability of the closed-loop system is a requirement, ensuring reliability and safety under all operating scenarios.

This M.A.Sc. project specifically focuses on developing advanced robust controller schemes for AGVs to meet various performance objectives across the full operating range in the context of lane-keeping control. The specific goals of the research activity are as follows.

- To tackle the challenges arising from variations in the vehicle's longitudinal velocity and its resulting dynamics, the polytopic LPV framework will be employed in both the modeling and controller design phases. The approach utilizes quadratic and parameter-dependent Lyapunov functions to address two key aspects: simplifying the complexity of control system implementation and mitigating the inherent conservatism associated with this control methodology.
- The stability analysis and performance guarantees are rigorously established using Lyapunov stability theory.
- Convex optimization techniques, under LMI constraints, are employed to solve the design conditions and determine the required controller gains. This approach avoids heuristic optimization methods, which often lack guarantees for finding a globally optimal solution and involve significant computational costs.

- The system's responsiveness and the amplitude bound of the controller's gains are carefully considered during the controller design process. Responsiveness ensures the method's applicability to practical scenarios, such as emergency lane changes in obstacle avoidance for AGVs, while bounded controller gains guarantee the practicality and feasibility of implementation.
- The effectiveness of the proposed solutions will be evaluated through validated numerical simulations using standard test scenarios in the context of autonomous vehicles. An LQR control will be designed and utilized as a benchmark, providing a basis for fair comparisons to validate the strategies presented in this thesis further.
- The developed polytopic LPV models for an AGV are validated through numerical simulations, with the original nonlinear dynamics of the AGV serving as the reference model.

Chapter 2

Modeling Vehicle Dynamics

Developing control systems typically involves two key steps: (i) modeling the system under study and (ii) formulating the control strategy. Accurate modeling is essential for effective controller design, as it provides the basis for understanding system dynamics and predicting behavior. Without a reliable model, the control strategy may fail to achieve stability or desired performance. A well-represented model enables the development of a robust and efficient control system and helps guarantee stability and optimal performance in diverse operating conditions.

Modeling includes developing mathematical representations describing physical systems' behavior and dynamics, which form a basis for control design, analysis, and simulation. These models vary depending on the nature of the system: for continuous-time systems, differential equations are used, while difference equations express discrete-time systems. These models are derived from fundamental physical laws, such as Newton's laws of motion for mechanical systems. Accurate modeling explains the essential dynamics and comprises system-specific constraints and external influences, which help the development of control strategies specific to the system's characteristics. This chapter focuses on vehicle modeling with an emphasis on achieving lateral control objectives. In Section 2.1, nonlinear vehicle dynamics are represented, path coordinates are investigated in Section 2.2, and steering system dynamics are addressed in Section 2.3. Then, an introduction to Linear Parameter Varying (LPV) systems is given in Section 2.4, followed by a polytopic LPV representation for a general control-based road-vehicle model in Section 2.5. The aforementioned general model is gathered from the dynamics in Sections 2.1-2.3. Lastly, Section 2.6 addresses the validation of the two models presented in this chapter for AGV control compared to its nonlinear model.

2.1. Vehicle Nonlinear Dynamics

Nonlinear models are essential for accurately representing physical systems because they capture complex dynamics and nonlinear behaviors that linear models cannot, primarily when the system operates over a wide range of conditions or exhibits significant nonlinearities. This thesis focuses on the automatic path-tracking application for vehicle systems. Consequently, the nonlinear single-

track (bicycle) model is employed to characterize the vehicle's handling dynamics in the horizontal plane [40]. This model simplifies the vehicle dynamics by making several assumptions: it assumes symmetry between the left and right sides of the vehicle, considers high suspension stiffness to neglect roll and pitch motions, and presumes equal weight distribution between the wheels. These assumptions allow the model to effectively describe the essential lateral dynamics required for control design while providing computational efficiency. Fig. 2.1 illustrates the schematic of the vehicle lateral dynamics and its relationship with the lane centerline during path tracking. Additionally, the values for vehicle model parameters are given in Table 2.1.

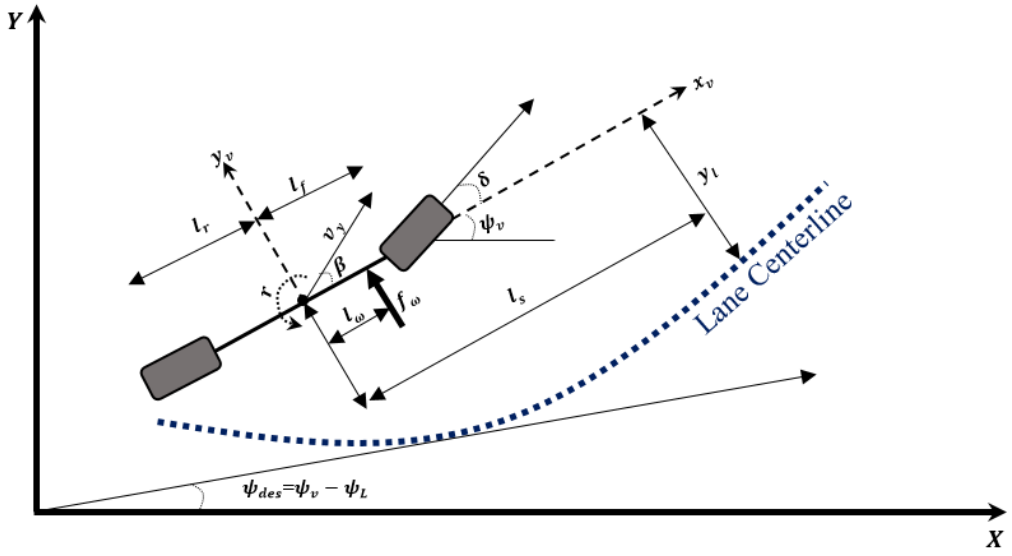

Fig. 2.1. Schematic representation of vehicle lateral dynamics and path tracking relative to the lane centerline

Table 2.1. Vehicle parameters [4]

Parameter	Description	Value
M	Vehicle mass	$1{,}476\ kg$
l_ω	Distance between the vehicle C.G. and the center of the wind force effect	$0.4\ m$
l_f	Distance between the vehicle's C.G. and front axle	$1.13\ m$
l_r	Distance between the vehicle's C.G. and rear axle	$1.49\ m$
l_s	Look-ahead distance	$5\ m$
η_t	Tire length contact	$0.13\ m$
I_{eff}	Effective longitudinal inertia	$442.8\ kgm^2$
I_z	Yaw moment of inertia of the vehicle	$1{,}810\ kgm^2$
I_s	Yaw moment of inertia of the steering setup	$0.02\ kgm^2$
R_s	Ratio for the steering gear	16
B_s	Damping of the steering setup	3.7
K_p	Manual steering column coefficient	0.13
c_f	Cornering stiffness of the front tires	$57\ kN/rad$
c_r	Cornering stiffness of the rear tires	$59\ kN/rad$
c_x	Coefficient of the longitudinal aerodynamic drag	0.35
c_y	Coefficient of the lateral aerodynamic drag	0.45

The nonlinear vehicle dynamics, obtained from the Newton-Euler equations, are represented as [4]:

$$\begin{aligned} \dot{v}_x &= \frac{T_{eng} - c_x v_x^2}{I_{eff}} + v_y r, \\ \dot{v}_y &= \frac{F_{yf} + F_{yr} - c_y v_y^2 + f_\omega}{M} - v_x r, \end{aligned} \tag{2.1}$$

$$\dot{r} = \frac{1}{I_z}\left(l_f F_{yf} - l_r F_{yr} + l_\omega f_\omega\right),$$

where v_x and v_y represent the vehicle speed and lateral velocity, the yaw rate is represented by r, and the net engine or brake torque is denoted by T_{eng}. This torque acts as the control input for the longitudinal dynamics of the vehicle. Lateral disturbance (wind force) is included by f_ω and lateral forces at the front and rear tires are F_{yf} and F_{yr}, respectively. In addition, the magic formula is used to model tire cornering forces as [4]:

$$\begin{aligned} F_{yi}(\alpha_i) &= D_i \sin(\nabla_i), \\ \nabla_i &= C_i \arctan[(1 - E_i)B_i\alpha_i + E_i \arctan(B_i\alpha_i)], \end{aligned} \tag{2.2}$$

where the superscript i with f and r represents the front and rear axle tires, respectively. Additionally, B_i, C_i, D_i, and E_i are Pacejka parameters influenced by tire characteristics, road contamination, and vehicle operating conditions [80]. Furthermore, the tire slip angles at the front and rear axles are [4]:

$$\begin{aligned} \alpha_f &= \delta - arctan\frac{v_y + l_f r}{v_x}, \\ \alpha_r &= arctan\frac{v_y - l_r r}{vx}. \end{aligned} \tag{2.3}$$

where δ is the front wheel steering angle, and l_f and l_r are the distances from the center of gravity of the vehicle to the front and rear axles, respectively.

To obtain a simplified representation model, the following assumptions are made: i) By considering the vehicle speed as a time-varying parameter with a bounded variation rate, the longitudinal dynamics, as well as the aerodynamic forces are ignored; ii) The lateral tire forces are proportional to their corresponding axles' side-slip angles; and iii) it is assumed that the side-slip angles are small. The mentioned assumptions hold in designing vehicle lateral control structures for normal driving situations [81], [54] , and [39]. Therefore, the lateral tire forces can be represented by [4]:

$$F_{yf} = 2c_f\left(\delta - \frac{v_y + l_f r}{v_x}\right), \tag{2.4}$$

$$F_{yr} = 2c_r\left(\frac{v_y - l_r r}{v_x}\right),$$

where c_f and c_r represent the front and rear tire cornering stiffness respectively. Finally, the simplified dynamics representing the lateral behavior of the vehicle is given by [4]:

$$\begin{bmatrix}\dot{\beta}\\ \dot{r}\end{bmatrix} = \begin{bmatrix}a_{11} & a_{12}\\ a_{21} & a_{22}\end{bmatrix}\begin{bmatrix}\beta\\ r\end{bmatrix} + \begin{bmatrix}b_1\\ b_2\end{bmatrix}\delta + \begin{bmatrix}e_1\\ e_2\end{bmatrix}f_\omega, \tag{2.5}$$

where β represents the side-slip angle at the center of the gravity of the vehicle. This parameter is defined as $\beta = \frac{v_y}{v_x}$. The elements of the matrices in (2.5) are as follows:

$$a_{11} = -\frac{2(c_r + c_f)}{Mv_x}, a_{12} = \frac{2(l_r c_r - l_f c_f)}{Mv_x^2} - 1,$$
$$a_{21} = \frac{2(l_r c_r - l_f c_f)}{I_z}, a_{22} = \frac{-2(l_r^2 c_r + l_f^2 c_f)}{I_z v_x},$$
$$b_1 = \frac{2c_f}{Mv_x}, b_2 = \frac{2l_f c_f}{I_z}, e_1 = \frac{1}{Mv_x}, e_2 = \frac{l_\omega}{I_z},$$

where M, I_z, and l_ω represent the total mass of the vehicle, the yaw moment of inertia of the vehicle, and the distance from the vehicle's center of gravity to the effective center of the wind force, respectively.

2.2. Path Coordinates

Monitoring the vehicle's position within the road frame is a critical component of lane-keeping control in autonomous vehicles. Accordingly, the dynamic representations of lateral deviation error y_L, and heading error ψ_L must be included in the equation (2.5). These dynamics equations are as follows [4]:

$$\dot{y}_L = \beta v_x + l_p r + \psi_L v_x,$$
$$\dot{\psi}_L = r - \rho_r v_x, \tag{2.6}$$

where ρ_r is the road curvature with R_r as its curvature radius and l_p is the look-ahead distance. The schematic representation of y_L and ψ_L can be observed in Fig 2.1. It is worth noting that the given dynamics of y_L and ψ_L have been employed in the literature for control purposes of AGVs, e.g., [58], [62], [81], and [39].

2.3. Steering System Dynamics

The electronic power steering (EPS) system acts as the primary mechanism for executing lane-keeping operations by receiving commands from the controller, translating them into precise steering actions, and helping the vehicle remain on the desired path. In addition to providing steering assistance, the EPS enhances vehicle stability and reduces driver effort. Its dynamic behavior, including the torque and angle relationships, is modeled as follows [81]:

$$\ddot{\delta}_d = \frac{T_{s\beta}}{I_s}\beta + \frac{T_{sr}}{I_s}r - \frac{T_{s\beta}}{R_s I_s}\delta_d - \frac{B_s}{I_s}\dot{\delta}_d + \frac{1}{I_s}T_s \tag{2.7}$$

where the steering wheel angle is denoted by δ_d and is computed as $\delta_d = R_s\delta$, where R_s is the steering gear ratio, and the steering torque is represented by T_s. Furthermore, $T_{s\beta}$ and T_{sr} are given by [4]:

$$T_{s\beta} = \frac{2K_p c_f \eta_t}{R_s},\ T_{sr} = \frac{2K_p c_f \eta_t l_f}{R_s v_x},$$

where the manual steering column coefficient and the tire length contact are represented by η_t and K_p respectively.

2.4. Preliminaries on LPV Systems

In this section, an overview of linear parameter varying (LPV) systems is provided, followed by an analysis of their stability and performance. Finally, the two Lyapunov functions employed in this research are presented.

- Introduction

Nonlinear and time-varying systems are pervasive in nature, with most real-world systems exhibiting such characteristics. While many systems can be approximated by linear models under the assumption that their behavior remains close to nominal operating conditions, this approximation often falls short for applications requiring high precision or when the system operates under varying conditions. For instance, the dynamics of a surgical robot involve complex nonlinear behaviors that demand high precision, making linear approximations insufficient for accurate control. In such cases, controllers based on linearized models may perform well on the

linearized system but fail to effectively manage the actual nonlinear system, necessitating the use of nonlinear control strategies [82].

Advanced linearization techniques, such as Parameterized Jacobian Linearization, offer a partial solution to address system nonlinearity. Instead of linearizing around a single equilibrium point, this method linearizes the system at multiple equilibrium points parameterized by a scheduling variable. The control task is then accomplished using the gain-scheduling approach, which designs linear controllers for each operating point and interpolates between them based on the system's operating conditions. In essence, the controller parameters adapt to varying conditions to ensure robust performance [83]. To overcome the limitations of traditional gain-scheduling, Linear Parameter Varying (LPV) systems provide a systematic and theoretically grounded approach [84]. In LPV systems, the system matrices explicitly depend on time-varying parameters. A specific subset, known as quasi-LPV (q-LPV) systems, allows the scheduling parameters to depend on the states of the nonlinear system. By leveraging this framework, many nonlinear systems can be effectively addressed using LPV techniques. However, LPV approaches require both the parameters and their variations to be bounded and well-defined [85].

Compared to gain-scheduling, LPV approaches offer several advantages. Notably, LPV control does not require slow transitions between operating points, which is often a limitation in gain-scheduling. Additionally, gain scheduling typically requires a large number of linearized models to achieve satisfactory performance, adding complexity to the design process [84]. Fig. 2.2 illustrates the gain-scheduling methodology, highlighting the challenges posed by the need for multiple linearized models.

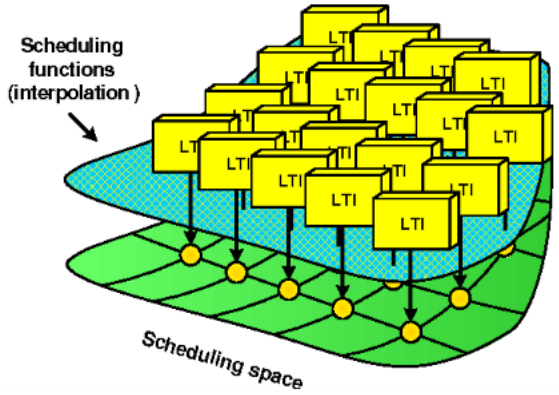

Fig. 2.2. A view of the gain scheduling approach [86]

When comparing LPV and robust control approaches, it is important to note a key distinction. In robust control theory, a static controller is designed to handle all possible variations in the system's parameters, ensuring closed-loop stability. In contrast, the LPV approach dynamically measures both the parameters and their rates of variation online. This additional information allows the controller to adapt online, resulting in improved performance and reduced conservatism compared to robust control methods [87].

Furthermore, the difference between controlling LPV systems and time-varying systems lies in the information available about the system model. In controlling time-varying systems, it is assumed that the system model is fully known over the entire time interval $[0, \infty)$. Conversely, in LPV systems, the system model is only identified at the current sample time t and within the interval $[0, t)$, making the LPV approach more suitable for systems with evolving dynamics [88]. Fig. 2.3 illustrates the generality of LPV systems compared to other modeling approaches, highlighting their flexibility and adaptability.

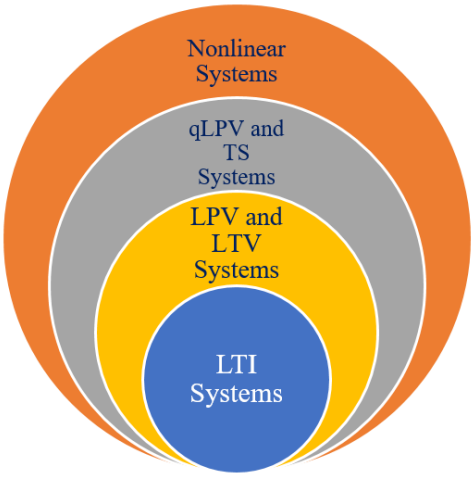

Fig. 2.3. The place of the LPV systems among various systems

- Different Types of LPV systems [89]

An LPV system can be considered as follows:

$$G(\theta): \begin{cases} \dot{x}(t) = A(\theta)x(t) + B_1(\theta)\omega(t) + B_2(\theta)u(t) \\ z(t) = C_1(\theta)x(t) + D_{11}(\theta)\omega(t) + D_{12}(\theta)u(t), \\ y(t) = C_2(\theta)x(t) + D_{21}(\theta)\omega(t) + D_{22}(\theta)u(t) \end{cases} \tag{2.8}$$

where $x(t) \in \mathbb{R}^{n_x}$ is the state vector, $y(t) \in \mathbb{R}^{p}$ represents the measured output vector, $u(t) \in \mathbb{R}^{m}$ denotes the input vector, and the vector $z(t) \in \mathbb{R}^{n_z}$ embodies the controlled output vectors. Additionally, $\omega(t) \in \mathbb{R}^{\mathrm{w}}$ represents the vector of exogenous inputs and $\theta \in \mathbb{R}^{n_p}$ stands for the vector related to measurable varying parameters.

Different Types of LPV systems have been in the literature [89]. The difference between the classes of LPV systems is mainly associated with defining the time-varying parameter vector θ. Some of the main classes of LPV systems are summarized in the following parts.

i) LPV systems with bounded parameters in which the varying parameter vector contains external parameters, $\theta = \theta(t)$ and belong to $\mathcal{P}$, where $\mathcal{P}$ is defined as:

$$\mathcal{P} \coloneqq \left\{\theta(.) \coloneqq \begin{bmatrix}\theta_1 & \dots & \theta_{n_p}\end{bmatrix}^T \in \mathbb{R}^{n_p}, \theta_i \in \begin{bmatrix}\underline{\theta_i} & \overline{\theta}_i\end{bmatrix} \forall i = 1, \dots, n_p\right\}. \tag{2.9}$$

In other words, the varying parameter vector is considered a vector of exogenous inputs.

ii) Quasi-LPV systems in which where the varying parameter vector θ is the function of the state vector, $\theta = \theta(x(t))$. In other words, the varying parameter vector varies as a function of states, inputs, and/or outputs.

iii) Polytopic LPV systems in which the varying parameters satisfy the convex sum. It should be noted that $D_{22}(\theta) = 0$, leading to a strictly proper system. The varying parameter vector (θ) belongs to the convex polytopic region $(\mathcal{P})$, defined as the convex combination of the varying parameters' extremums. The formulation of the aforementioned varying parameter is as follows [89]:

$$\theta = \sum_{i=1}^{2^{n_p}} \eta_i v_i, \sum_{i=1}^{2^{n_p}} \eta_i = 1, \eta_i \geq 0 \; \forall i = 1, \dots, 2^{n_p}, \tag{2.10}$$

where v_i represents each vertex of the above-mentioned convex polytope, and

$$\eta_i = \prod_{i=1}^{2^{n_p}} \gamma_i,$$
$$\gamma_i = \left|\frac{\overline{\theta_1} - \theta_1}{\overline{\theta_1} - \underline{\theta_1}}\right| or \left|\frac{\theta_1 - \underline{\theta_1}}{\overline{\theta_1} - \underline{\theta_1}}\right| \times \dots \times \left|\frac{\overline{\theta_{n_p}} - \theta_{n_p}}{\overline{\theta_{n_p}} - \underline{\theta_{n_p}}}\right| or \left|\frac{\theta_{n_p} - \underline{\theta_{n_p}}}{\overline{\theta_{n_p}} - \underline{\theta_{n_p}}}\right|, \tag{2.11}$$

depending on whether the vertex corresponds to $\overline{\theta_k}$ or $\underline{\theta_k}$ in that dimension θ_k, where $k = 1, \dots, n_p$. It should be noted that the n_p represents the number of varying parameters, and 2^{n_p} represents the number of vertices of their resultant convex polytope.

As a result, the polytopic LPV representation of a system with varying parameter θ is formulated as the convex combination of the state-space realizations of the linear time-invariant systems as given in the following:

$$\begin{bmatrix} A_{pol}(\theta) & B_{1_{pol}}(\theta) & B_{2_{pol}} \\ C_1(\theta)_{pol} & D_{11_{pol}}(\theta) & D_{12_{pol}} \\ C_{2_{pol}} & D_{21_{pol}} & 0 \end{bmatrix} = \sum_{i=1}^{2^{n_p}} \eta_i(\theta) \begin{bmatrix} A(v_i) & B_1(v_i) & B_2 \\ C_1(v_i) & D_{11}(v_i) & D_{12} \\ C_2 & D_{21} & 0 \end{bmatrix} \tag{2.12}$$

where pol briefly represents polytopic LPV.

2.5. Polytopic LPV Modeling for Vehicle Dynamics

In the following, the simplified road-vehicle system in (2.5), the dynamic equations for lateral deviation and heading errors in (2.6), and power steering system dynamics in (2.7) are combined to formulate a polytopic LPV representation for the lateral dynamics of the AGVs as follows [4]:

$$\Sigma_v(v_x): \ \dot{x} = A_{(v_x)}x + B_{u(v_x)}u + B_{\omega(v_x)}\omega, \tag{2.13}$$

where $x = [\beta \quad r \quad \psi_L \quad y_L \quad \delta \quad \dot{\delta}]^T$ is the state vector of the vehicle,; $\omega = [f_\omega \quad \rho_r]^T$ is the input disturbance vector, and the steering torque T_s acts as the input control signal u. The state-space matrices in (2.13) are given by

$$A_{(v_x)} = \begin{bmatrix} a_{11} & a_{12} & 0 & 0 & b_1 & 0 \\ a_{21} & a_{22} & 0 & 0 & b_2 & 0 \\ 0 & 1 & 0 & 0 & 0 & 0 \\ v_x & l_s & v_x & 0 & 0 & 0 \\ 0 & 0 & 0 & 0 & 0 & 1 \\ a_{61} & a_{62} & 0 & 0 & a_{65} & a_{66} \end{bmatrix}, B_{\omega(v_x)} = \begin{bmatrix} e_1 & 0 \\ e_2 & 0 \\ 0 & -v_x \\ 0 & 0 \\ 0 & 0 \\ 0 & 0 \end{bmatrix},$$

$$B_u = \begin{bmatrix} 0 & 0 & 0 & 0 & 0 & \frac{1}{R_s I_s} \end{bmatrix}^T,$$

where

$$a_{61} = \frac{T_{s\beta}}{R_s I_s}, a_{62} = \frac{T_{sr}}{R_s I_s}, a_{65} = -\frac{T_{s\beta}}{R_s I_s}, a_{66} = -\frac{B_s}{I_s}.$$

Note that the values for a_{11}, a_{12}, a_{21}, and a_{22} are brought in section 2.1, and the output of the vehicle system in (2.13) is formulated as follows:

$$y = C_y x, \tag{2.14}$$

where

$$C_y = \begin{bmatrix} 1 & 0 & 0 & 0 & 0 & 0 \\ 0 & 1 & 0 & 0 & 0 & 0 \\ 0 & 0 & 1 & 0 & 0 & 0 \\ 0 & 0 & 0 & 1 & 0 & 0 \\ 0 & 0 & 0 & 0 & 1 & 0 \\ 0 & 0 & 0 & 0 & 0 & 1 \end{bmatrix}.$$

Using C_y as an identity matrix imposes a high cost due to the requirement for additional sensors to measure all the vehicle states. However, this configuration enables the use of state-feedback controllers instead of output-feedback systems, which not only leads to simple control design but also can further improve the path following control performance with a reduced design conservatism.

In the following sections, a performance output z is introduced for the control methodology, which will be detailed in Chapter 4. For lane-keeping control, the performance vector z incorporates variables related to lane departure and passenger comfort to emphasize comprehensive performance evaluation [4]. This goal can be accomplished by considering i) heading error (ψ_L), ii) lane departure with respect to the centerline of the road (y_{act}), iii) lateral acceleration (a_y), and iv) steering torque (T_s). Heading angle error provides information regarding both the lane-keeping performance and the future anticipated error in the vehicle position, while lane departure ensures performance regarding the vehicle position within the road frames. Additionally, lateral acceleration considers the comfort of passengers and is approximated by $a_y \approx v_x\dot{\beta}$ and steering torque accounts for the consumed energy by the power steering system [4]. Moreover, the steering torque directly impacts passenger comfort, as excessive or abrupt torque values can result in undesirable steering actions, causing discomfort for both the driver and passengers [90]. Consequently, the performance output (z) is given by [4]:

$$\begin{aligned} z &= \mathcal{W}[\psi_L \quad y_{act} \quad a_y \quad T_s]^T, \\ \mathcal{W} &= diag\left(\omega_{\psi_L}, \omega_{y_{act}}, \omega_{a_y}, \omega_{T_s}\right), \end{aligned} \tag{2.15}$$

where ω_{ψ_L}, $\omega_{y_{act}}$, ω_{a_y}, and ω_{T_s} are weighting gains; and the state variables are given by:

$$\begin{bmatrix} \psi_L \\ y_{act} \\ a_y \\ T_s \end{bmatrix} = \begin{bmatrix} 0 & 0 & 1 & 0 & 0 & 0 \\ 0 & 0 & -l_s & 1 & 0 & 0 \\ v_x a_{11} & v_x a_{12} & 0 & 0 & v_x b_1 & 0 \\ 0 & 0 & 0 & 0 & 0 & 0 \end{bmatrix} x + \begin{bmatrix} 0 \\ 0 \\ 0 \\ 1 \end{bmatrix} T_s, \tag{2.16}$$

where a_{12} and a_{21} are given in Section 2.1. One can rewrite the performance vector z as follows:

$$z = C_{z(v_x)} x + D_z u, \tag{2.17}$$

with

$$C_{z(v_x)=\mathcal{W}} \begin{bmatrix} 0 & 0 & 1 & 0 & 0 & 0 \\ 0 & 0 & -l_s & 1 & 0 & 0 \\ v_x a_{11} & v_x a_{12} & 0 & 0 & v_x b_1 & 0 \\ 0 & 0 & 0 & 0 & 0 & 0 \end{bmatrix}, D_z = \mathcal{W} \begin{bmatrix} 0 \\ 0 \\ 0 \\ 1 \end{bmatrix}.$$

Additionally, the vehicle dynamics represented in (2.13), and the performance vector represented in (2.17) are dependent on the vehicle speed denoted by v_x through the common terms with v_x including $\frac{1}{v_x}$, and $\frac{1}{v_x^2}$. Also, the vehicle speed is bounded by the given range:

$$v_{\min} \leq v_x \leq v_{max}, v_{min} = 5m/s, v_{max} = 25m/s. \tag{2.18}$$

It is important to note that the dependence of Equation (2.13) on v_x is nonlinear, owing to the terms $\frac{1}{v_x}$ and $\frac{1}{v_x^2}$. For the control purposes discussed in Chapter 4, a polytopic LPV representation of Equation (2.13) is required. To achieve this, v_x, $\frac{1}{v_x}$, and $\frac{1}{v_x^2}$ can be considered as scheduling variables θ_1, θ_2, and θ_3, respectively. selecting these scheduling variables ignores the mathematical relationship between θ_1, θ_2, and θ_3 introducing conservatism into the control design [4]. Furthermore, as outlined in [91], using three scheduling variables translates into eight vertices in the resulting polytopic LPV model, posing computational challenges for semi-definite programming solvers when searching for the controller's gain within a feasible solution set, if one exists. To address this issue, as suggested by [61] and [58], $\frac{1}{v_x}$ is chosen as the scheduling variable of the LPV model via the time-varying parameter θ, followed by approximating v_x and $\frac{1}{v_x^2}$ by employing the first-order Taylor's approximation [4]:

$$\frac{1}{v_x} = \frac{1}{v_0} + \frac{1}{v_1}\theta, \tag{2.19}$$

$$v_x \cong v_0\left(1-\frac{v_0}{v_1}\theta\right),$$
$$\frac{1}{v_x^2} \cong \frac{1}{v_0^2}\left(1+2\frac{v_0}{v_1}\theta\right).$$

The time-varying parameter θ represents the variation of v_x between the bounds v_{min} and v_{max} as:

$$\theta_{min} \le \theta \le \theta_{max}, \theta_{min} = -1, \theta_{max} = +1. \tag{2.20}$$

Also, v_0 and v_1 in (2.19) are defined as:

$$v_0 = \frac{2v_{min}v_{max}}{v_{min}+v_{max}}, v_1 = \frac{2v_{min}v_{max}}{v_{min}-v_{max}}. \tag{2.21}$$

By substituting (2.19) in (2.13), the following dynamics are derived for the vehicle model [4]:

$$\Sigma_v(\theta): \begin{cases} \dot{x} = A_{(\theta)}x + B_{u(\theta)}u + B_{\omega(\theta)}\omega \\ z = C_{z(\theta)}x + D_{z(\theta)}u \end{cases}. \tag{2.22}$$

It is clear that Eq. (2.22) has a linear dependence on the parameter θ, instead of the nonlinear dependence on v_x. Applying the sector nonlinearity decomposition [91] to represent the vehicle model in (2.22) in a polytopic LPV representation gives:

$$\Sigma_v(\theta): \begin{cases} \dot{x} = \sum_{i=1}^{2} \eta_i(\theta)(A_i x + B_i^u u + B_i^\omega \omega) \\ z = \sum_{i=1}^{2} \eta_i(\theta)(C_i^z x + D_i^z u) \end{cases}, \tag{2.23}$$

where η_i, $i = 1,2$, are the scalar Membership Functions (MFs), computed as follows:

$$\eta_1(\theta) = \frac{1-\theta}{2}, \eta_2(\theta) = 1 - \eta_1(\theta), \tag{2.24}$$

and

$$A_1 = A_{(\theta_{min})}, \quad B_1^u = B_u, \quad B_1^\omega = B_{\omega(\theta_{min})},$$
$$A_2 = A_{(\theta_{max})}, \quad B_2^u = B_u, \quad B_2^\omega = B_{\omega(\theta_{max})},$$
$$C_1^z = C_{z(\theta_{min})}, \quad C_1^z = C_{z(\theta_{max})}, \quad D_1^z = D_2^z = D_z.$$

The polytopic LPV representation of model (2.13), which is derived by applying sector nonlinearity decomposition [91], has $2^3 = 8$ vertices. In comparison, having one scheduling

parameter θ leads to a polytopic LPV representation with $2^1 = 2$ vertices or linear submodels. This approach reduces conservatism in the design and facilitates real-time implementation by lowering computational burden and improving the feasibility of finding a solution for the controller's gain. Further insights into these advantages are provided in Chapter 4, where the proposed polytopic LPV model is utilized in the control design procedure. Fig. 2.4 presents a flow chart summarizing the steps discussed above, leading to the development of a control-oriented polytopic LPV model for the lateral control of an AGV.

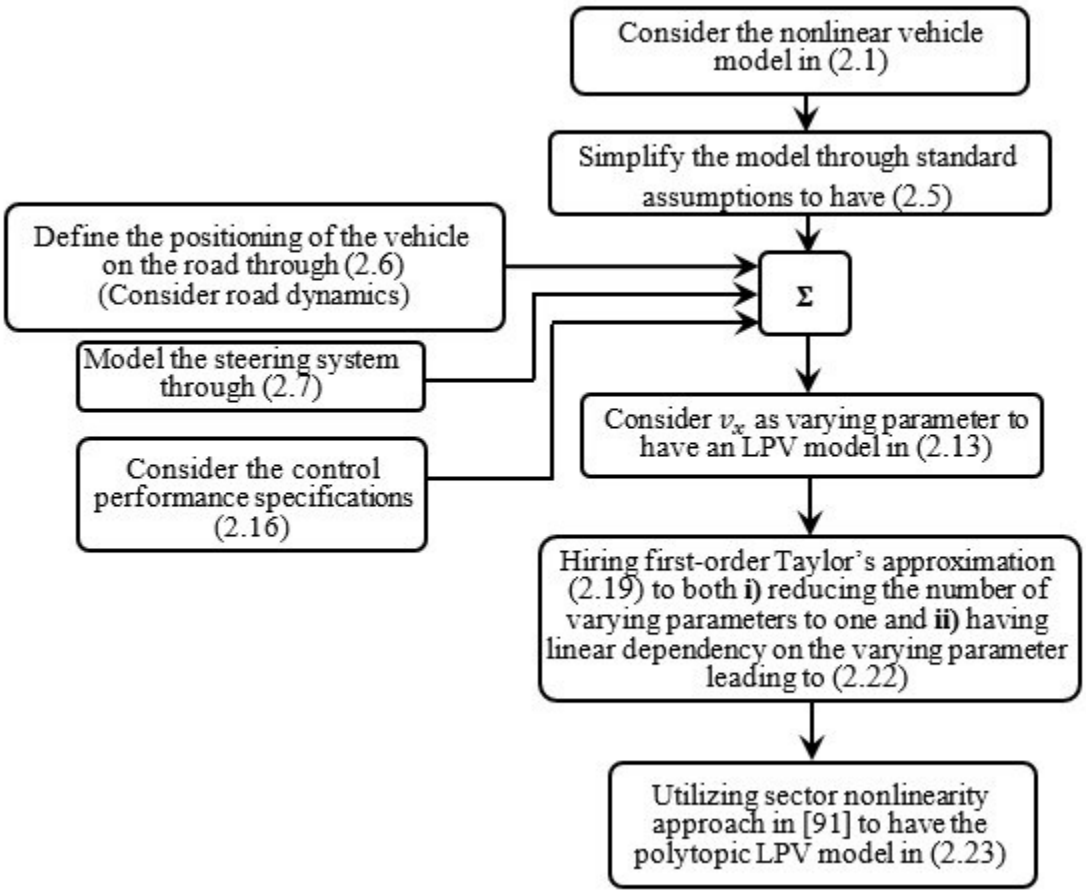

Fig. 2.4. The flowchart of deriving a control-based polytopic LPV model for AGVs

Lastly, for the control design outlined in Chapter 4, bounds on vehicle acceleration can be considered in a manner analogous to the bounds on vehicle speed described in Equation (2.18), as follows:

$$a_{\min} \leq a_x = \dot{v}_x \leq a_{max}, a_{min} = -4m/s^2, a_{max} = 3m/s^2. \tag{2.25}$$

These bounds on acceleration are determined to limit the vehicle's theoretical kinematic centripetal acceleration [4]. The physical bounds on acceleration can be translated to the bounds on the in-hand scheduling variable θ, where from (2.19) and (2.25) one has [4]:

$$\frac{a_{min}}{a_0} \leq \dot{\theta} \leq \frac{a_{max}}{a_0}, \tag{2.26}$$

with $a_0 = -\frac{v_0^2}{v_1}$. This consideration aims to reduce the conservatism of the design procedure. In essence, providing the control strategy with more detailed information from the model under study leads to a greater reduction in conservatism. The theoretical details of this approach will be further elaborated in Chapter 4, where parameter-dependent Lyapunov functions are employed in the control design process. Finally, Fig. 2.5 illustrates the control-oriented standard model for AGVs, depicting the inputs and outputs of the proposed framework.

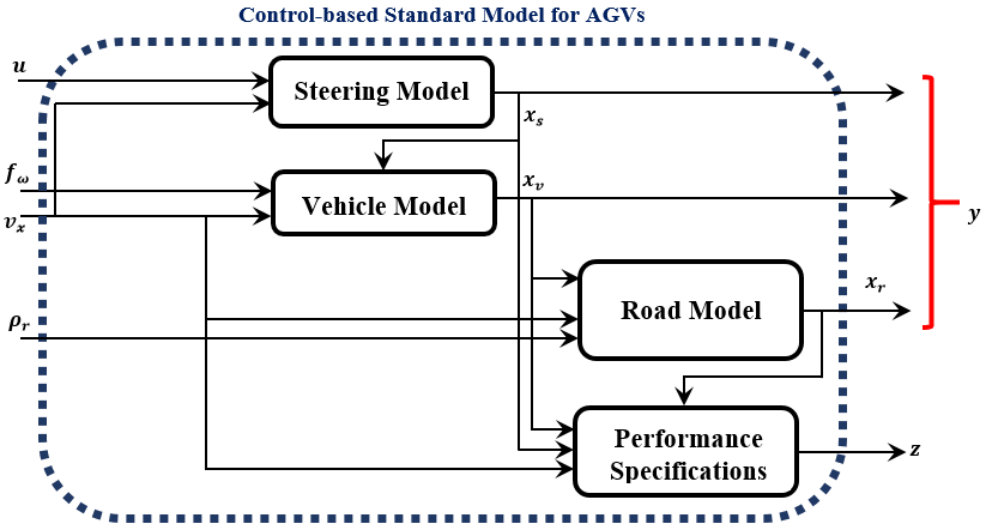

Fig. 2.5. The schematic of the control-based standard model for AGVs

2.6. Model Validation Results

Here, the general control-based road-vehicle model has been formulated using the nonlinear vehicle dynamics described in (2.1)–(2.3), combined with (2.6) and (2.7) in their LPV representation in (2.13) and subsequently in polytopic LPV form (2.23). In the upcoming chapters, the polytopic LPV representation will be used to synthesize the control structure, while the LPV representation will facilitate closed-loop system simulations. However, an important question

remains: to what extent do the LPV and polytopic LPV representations accurately capture the behavior of the nonlinear road-vehicle dynamics? This question is particularly critical for closed-loop system simulations, where the validity of the model directly impacts the system's ability to meet stability and performance criteria in both simulations and experimental tests.

In this section, the three representations (nonlinear, LPV, and polytopic LPV models) are evaluated using the same step steering torque as the control input, as shown in Fig. 2.7, along with identical vehicle speed and road curvature profiles, see Figs. 2.6(a) and 2.6(b). A comparison is then conducted by analyzing the system states for each representation. The results demonstrate that both the LPV and polytopic LPV models closely approximate the behavior of the nonlinear vehicle dynamics. This confirms their suitability for modeling, controller design, and validation phases. The simulations were implemented in MATLAB R2022b, using the vehicle parameters listed in Table 2.1 to generate the state trajectories of the closed-loop system, as shown in Figs. 2.8 to 2.13.

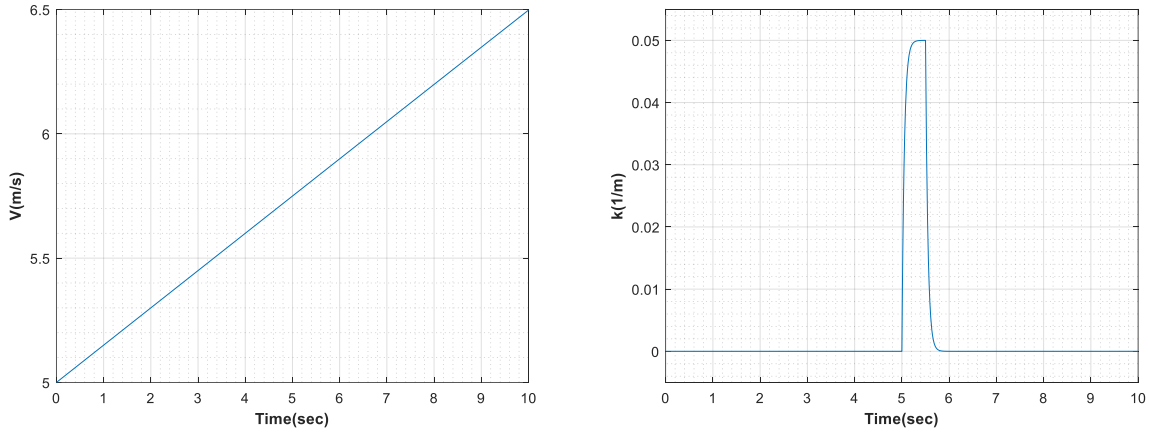

(a) **(b)**

Fig. 2.6. Validation test scenario. **(a)** vehicle longitudinal velocity and **(b)** road curvature

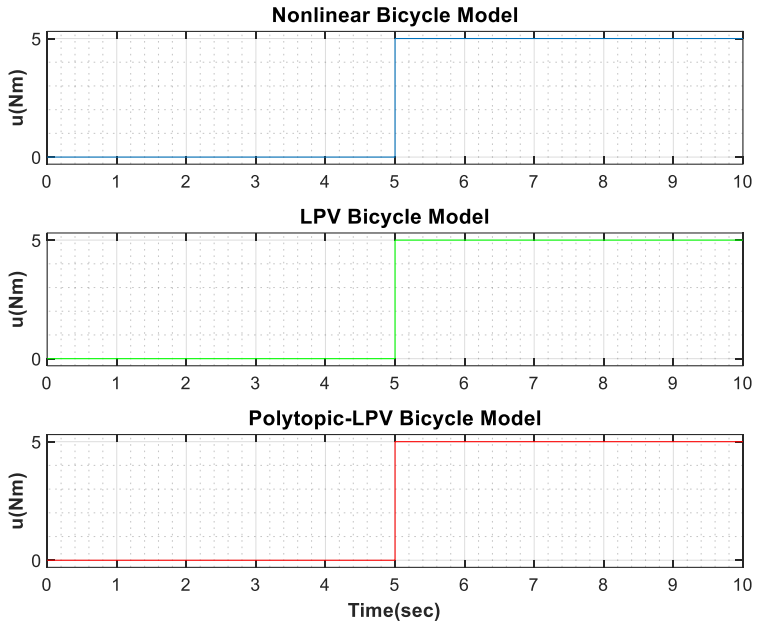

Fig. 2.7. Steering torque for **nonlinear**, **LPV**, and **polytopic LPV** models

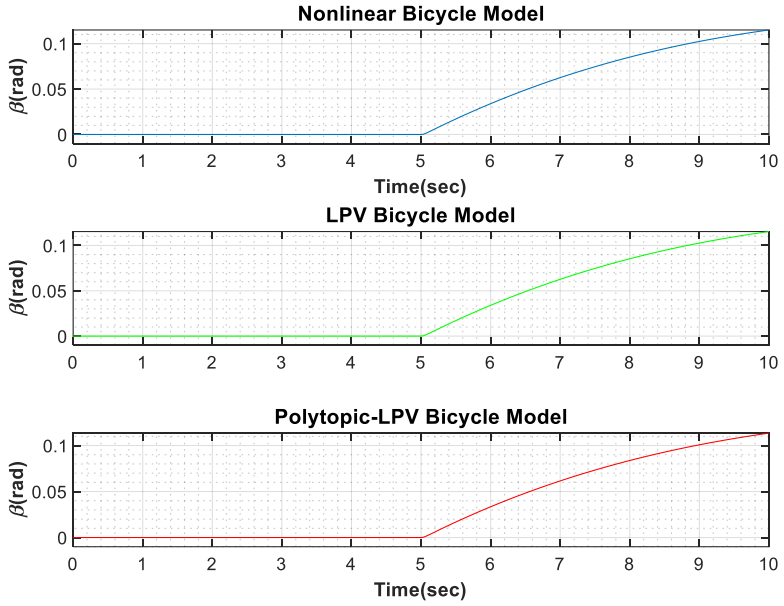

Fig. 2.8. Side-slip angle for **nonlinear**, **LPV**, and **polytopic LPV** models

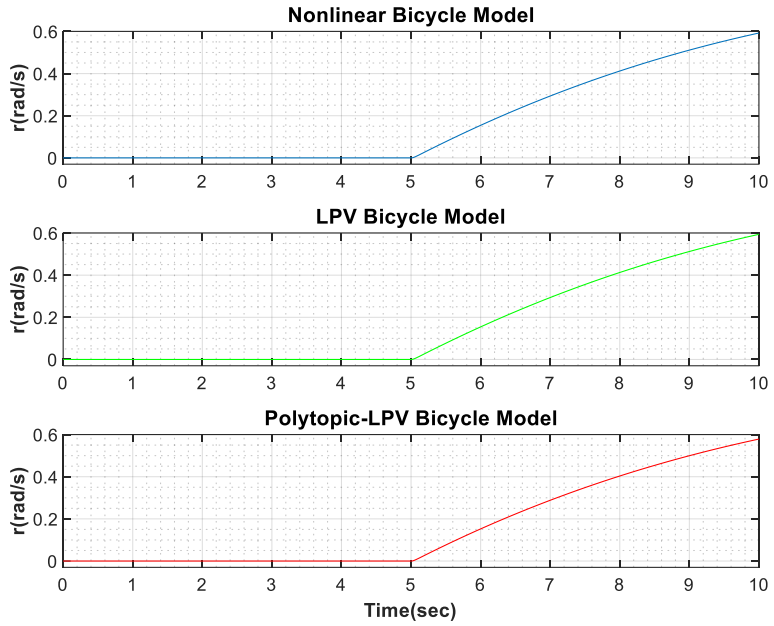

Fig. 2.9. Yaw rate for **nonlinear**, **LPV**, and **polytopic LPV** models

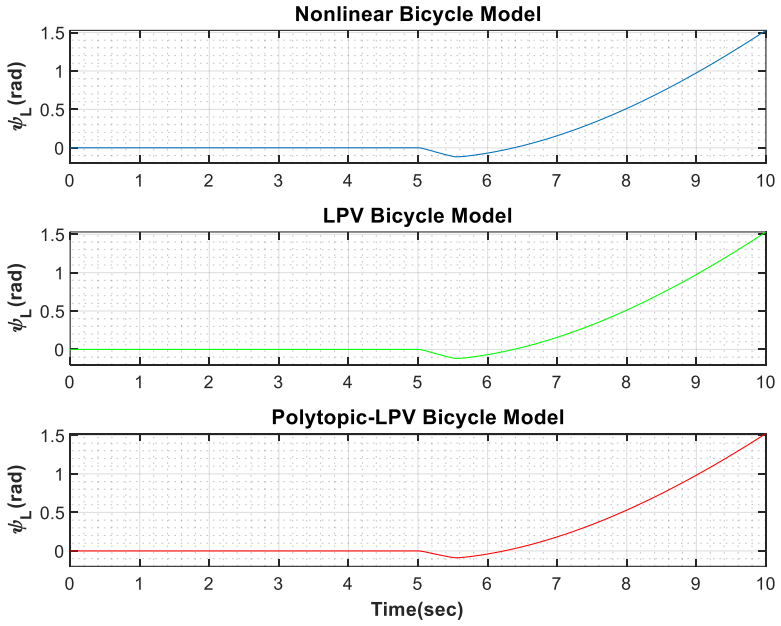

Fig. 2.10. Heading error for **nonlinear**, **LPV**, and **polytopic LPV** models

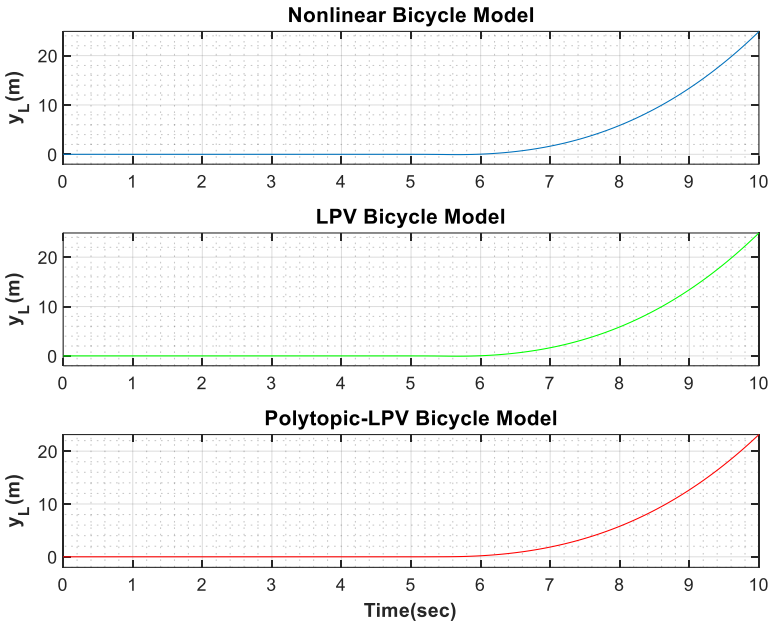

Fig. 2.11. Lateral deviation error at the look-ahead distance for **nonlinear**, **LPV**, and **polytopic LPV** models

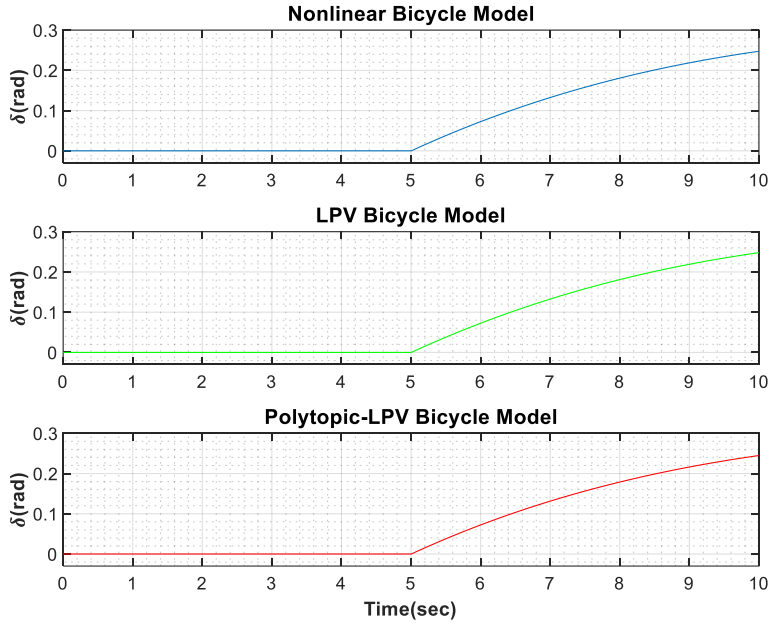

Fig. 2.12. Steering angle for **nonlinear**, **LPV**, and **polytopic LPV** models

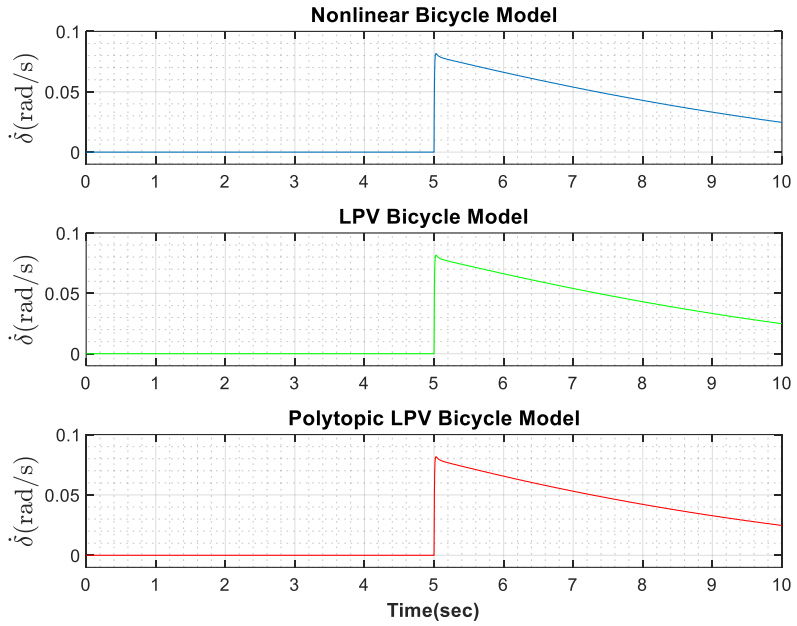

Fig. 2.13. Steering rate for nonlinear, LPV, and polytopic LPV models

In addition to Figs. 2.8-2.13, Table 2.2 gives a clear insight and quantitative results of the provided figures. In Table 2.2, the Root Mean Square (rms) of errors between the state trajectories obtained from the nonlinear bicycle model to a sample control input, as the reference model, and those of LPV and polytopic LPV models to the same control input, as the proposed models, are investigated. Although both models show good results in recreating the behavior of the original nonlinear model, the LPV model, as expected, acts better since it does not deploy the first-order Taylor approximation to reduce the number of its varying parameters.

Table 2.2. The RMS of errors between the obtained state trajectories from the reference nonlinear model and, LPV and polytopic LPV models to a sample control input

State	RMS of error	
	LPV	Polytopic LPV
Yaw rate	0.0002	0.0011
Side-slip angle	0.001	0.0077
Heading error	0.0027	0.0165
Lateral deviation error at the look-ahead distance	0.0479	0.5518
Steering angle	2.1427	2.1445
Steering rate	0.6996	0.7001

Chapter 3

LQR Path Tracking Control

In control theory, optimal control design focuses on determining a control signal that satisfies predefined constraints while optimizing a performance criterion. This process involves three primary steps: *(i)* modeling the system by deriving its dynamic equations to capture its behavior, *(ii)* mathematically formulating the physical constraints or limitations inherent to the system, and *(iii)* defining a performance criterion, often referred to as the cost function, which quantifies the desired objectives, such as minimizing energy consumption or trajectory tracking error. The goal of optimal control design is to minimize the cost function while ensuring that all constraints are respected, thereby achieving an optimal and feasible solution.

The linear quadratic regulator (LQR) is a widely used control strategy for determining an optimal control law for linear dynamical systems. This approach employs a state-space representation to model the system and a quadratic cost function to capture the trade-off between system performance (state deviations from desired values) and control effort (energy expenditure). The effectiveness of the LQR control method, combined with its simplicity in design and implementation, has made it a popular choice in vehicle dynamics control systems [92].

In this chapter, we present an LQR-based approach to control a road-vehicle model optimally. This control strategy is formulated around a quadratic performance (objective) function. The proposed controller is developed by solving a minimization problem that targets the upper bound of the objective function, making it a suboptimal design. However, the use of this approach allows the design conditions to be expressed as Linear Matrix Inequalities (LMIs), significantly simplifying the design procedure [91], as well as rendering a convex optimization problem with its own advantages mentioned in earlier chapters.

The reader may refer to Appendices for a better understanding of the notions regarding convex optimization problems and LMIs utilized in this chapter, as well as upcoming chapters.

3.1. Linearized Model for Path Tracking Control Design

In this section, a linearized model for path tracking control design is developed, motivated by two key reasons. First, a linearized model with reasonable simplifications is sufficient to handle control designs under normal driving conditions. Second, the Linear Quadratic Regulator (LQR) strategy, which is the focus of this chapter, is inherently based on the linear state-space representation of the system. Considering these factors, a linearized state-space representation of the road-vehicle control-based model is presented. This model is derived from the nonlinear bicycle model, which captures the vehicle's handling dynamics in the horizontal plane. Unlike LPV models discussed in Chapter 2, the linearized model assumes a constant longitudinal speed for simplicity. Given the similarities between the steps for deriving a linearized model and those for LPV models, only the final representation is provided here. Readers may refer to Chapter 2 for detailed derivations and vehicle parameters. By incorporating the simplified vehicle dynamics from (2.5), the lane tracking equations from (2.6), and the power steering model from (2.7), a linear representation of the road-vehicle system can be derived as follows:

$$\dot{x} = Ax + B_u u + B_\omega \omega, \tag{3.1}$$

where, $x = [\beta \quad r \quad \psi_L \quad y_L \quad \delta \quad \dot{\delta}]^T$ is the state vector of the vehicle, $\omega = [f_\omega \quad \rho_r]^T$ is the input disturbance vector, and steering torque T_s acts as the input control signal u. The system matrices in (3.1) are as follows:

$$A = \begin{bmatrix} a_{11} & a_{12} & 0 & 0 & b_1 & 0 \\ a_{21} & a_{22} & 0 & 0 & b_2 & 0 \\ 0 & 1 & 0 & 0 & 0 & 0 \\ v_x & l_s & v_x & 0 & 0 & 0 \\ 0 & 0 & 0 & 0 & 0 & 1 \\ a_{61} & a_{62} & 0 & 0 & a_{65} & a_{66} \end{bmatrix}, B_\omega = \begin{bmatrix} e_1 & 0 \\ e_2 & 0 \\ 0 & -v_x \\ 0 & 0 \\ 0 & 0 \\ 0 & 0 \end{bmatrix},$$

$$B_u = \begin{bmatrix} 0 & 0 & 0 & 0 & 0 & \frac{1}{R_s I_s} \end{bmatrix}^T,$$

where

$$a_{11} = -\frac{2(c_r + c_f)}{M v_x}, a_{12} = \frac{2(l_r c_r - l_f c_f)}{M v_x^2} - 1,$$

$$a_{21} = \frac{2(l_r c_r - l_f c_f)}{I_z}, a_{22} = \frac{-2(l_r^2 c_r + l_f^2 c_f)}{I_z v_x},$$

$$b_1 = \frac{2c_f}{Mv_x}, b_2 = \frac{2l_f c_f}{I_z}, e_1 = \frac{1}{Mv_x}, e_2 = \frac{l_\omega}{I_z},$$
$$a_{61} = \frac{T_{s\beta}}{R_s I_s}, a_{62} = \frac{T_{sr}}{R_s I_s}, a_{65} = -\frac{T_{s\beta}}{R_s I_s}, a_{66} = -\frac{B_s}{I_s}.$$

Recall that the output of the vehicle system, as represented in Equation (2.13) is formulated as $y = C_y x$ with C_y as the identity matrix. The disturbance input is not utilized during the control design phase in the LQR method. However, it is accounted for in the performance evaluation of the developed LQR controller.

3.2. LQR Control Design

Consider the following linear system:

$$\begin{cases} \dot{x}(t) = Ax(t) + Bu(t), \\ y(t) = Cx(t), \end{cases} \tag{3.2}$$

with the following performance function:

$$J(t) = \int_0^\infty \{x(t)^T Q x(t) + u(t)^T R u(t)\} dt, \tag{3.3}$$

and control law as given in the following:

$$u = Kx(t). \tag{3.4}$$

The objective is to design an optimal state-feedback control law that minimizes the performance function specified in Equation (3.3) by targeting its upper bound, ensuring the asymptotic stability of the closed-loop system. The following theorem forms the foundation of this design methodology.

Theorem 3.1 [91]**:** The system described by (3.2) can be stabilized using the control law in (3.4) while minimizing the cost function (3.3) if there exists a positive definite matrix S and a matrix M of appropriate dimensions, and a positive scalar γ such that the following LMI-based optimization problem is verified:

$$min\,\gamma \;\; s.t.:$$
$$\begin{bmatrix} \gamma & x^T(0) \\ x(0) & S \end{bmatrix} \geq 0, \tag{3.5}$$

$$\begin{bmatrix} SA^T + AS + M^T B^T + BM & S & M^T \\ S & -Q^{-1} & 0 \\ M & 0 & -R^{-1} \end{bmatrix} \leq 0,$$

$$S > 0.$$

Moreover, the objective function, defined in (3.3), satisfies

$$J < x^T(0)Px(0), \tag{3.6}$$

where $x^T(0)Px(0)$ serves as the upper bound of the cost function J, wih $P = S^{-1}$

Proof: Let us define a new variable as follows:

$$\hat{J} = x^T(t)Qx(t) + u^T(t)Ru(t). \tag{3.7}$$

In addition, consider the following Lyapunov function:

$$V(t) = x^T(t)Px(t), \tag{3.8}$$

where P is a positive definite matrix. Based on the Lyapunov stability theorem [93], and the quadratic form of the new variable $\hat{J}$

$$\dot{V}(t) + \hat{J}(t) \leq 0, \tag{3.9}$$

which results in:

$$\hat{J}(t) \leq -\dot{V}(t). \tag{3.10}$$

Integrating both sides of (3.10) from 0 to ∞, we obtain

$$\int_0^\infty \hat{J}(t) \leq -\int_0^\infty \dot{V}(t) \Rightarrow \int_0^\infty \hat{J}(t) \leq -\big(V(\infty) - V(0)\big). \tag{3.11}$$

Since $V(\infty) > 0$, it follows that

$$\int_0^\infty \hat{J}(t) \leq V(0). \tag{3.12}$$

As a result, an upper bound is obtained for the cost function in (3.3). The cost function can be minimized by reducing its upper bound, *i.e.*, minimizing $V(0)$, where $V(0) = x^T(0)Px(0)$. To achieve this, the following expression is derived:

$$\begin{aligned} &\min \gamma \ \ s.t.: \\ &x^T(0)Px(0) \leq \gamma, \end{aligned} \tag{3.13}$$

which results in $\gamma - x^T(0)Px(0) \geq 0$. By applying the Schur complement, the first LMI in (3.5) is obtained. Readers may refer to Appendix 2 for a detailed explanation of the Schur complement. In the subsequent step, by substituting (3.4) into (3.2), and considering the Lyapunov function defined in (3.8), along with the quadratic cost function in (3.3), the following conditions are derived based on the Lyapunov stability theorem:

$$\dot{V} = x^T[(A + BK)^T P + P(A + BK)]x + x^T[Q + K^T RK]x \leq 0, \tag{3.14}$$

Applying the congruence transformation lemma, along with certain mathematical simplifications, results in the following expression:

$$A^T P + K^T B^T P + PA + PBK + Q + K^T RK \leq 0. \tag{3.15}$$

Pre- and post-multiplying (3.15) with P^{-1},it follows that

$$P^{-1}A^T + P^{-1}K^T B^T + AP^{-1} + BKP^{-1} + P^{-1}QP^{-1} + P^{-1}K^T RKP^{-1} \leq 0, \tag{3.16}$$

where by changes of variables $P^{-1} \triangleq S$, and $KP^{-1} \triangleq M$ the following expression is obtained:

$$SA^T + AS + M^T B^T + BM + SQS + M^T RM \leq 0. \tag{3.17}$$

Employing Schur complement, the second LMI in (3.5) is derived, and the third LMI is obtained from Lyapunov stability. ■

The steps for designing an LQR controller for an AGV, utilizing LMI techniques and a convex optimization strategy, are summarized in the flowchart shown in Fig. 3.1.

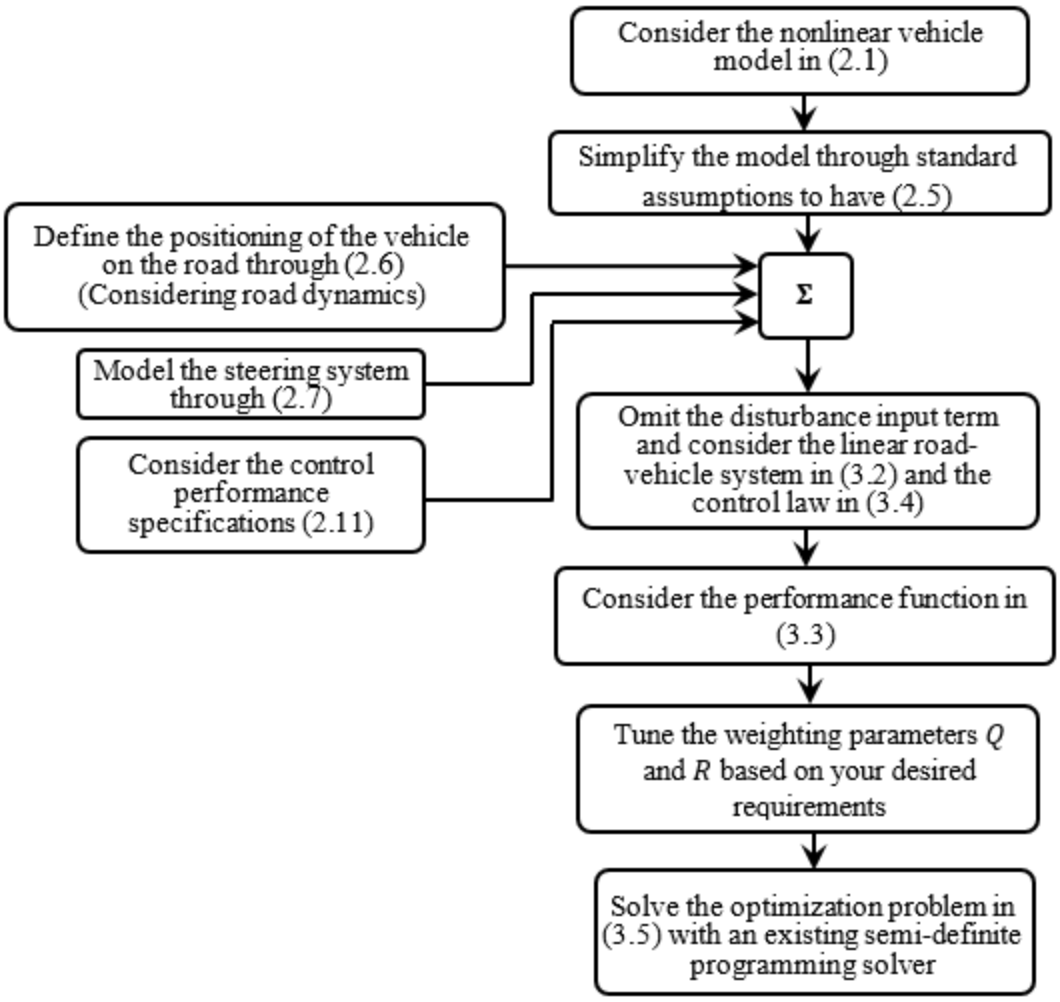

Fig. 3.1. The flowchart of designing an LQR controller for AGVs by using LMI techniques

3.3. Simulation Results and Discussions

In this subsection, the Q and R parameters, which serve as weighting factors in the LQR controller structure, are tuned. Parameter Q defines the importance of the states' trajectories of the controlled system, whilst R determines the significance of the control input cost of the control structure. For the system in (3.2), these parameters were selected as $Q = diag(1,1,6,12,1,1)$ and $R = 0.01$.

Proper tuning of these parameters is crucial, as the LQR controller designed in this chapter will serve as a benchmark for the advanced controllers developed in Chapter 4, which are the core focus of this thesis. A poorly tuned benchmark would lead to an unfair comparison and compromise the validation of the targeted controllers. During the tuning phase, a constant nominal longitudinal vehicle velocity of $v_x = 18\, m/s$, is considered alongside a road curvature profile

(Fig. 3.2), representing a single lane-change test scenario. To verify the effectiveness of the tuned optimal controller for the linearized road-vehicle system, the lateral position and heading errors (Fig. 3.3), steering torque (Fig. 3.4), and the global XY trajectory of the vehicle compared to the desired one (Fig. 3.5) are presented. In addition, the state trajectories of the closed-loop system, as well as the lateral forces of the front and rear tires, are examined and plotted in Fig. 3.6 to further validate the controller's performance.

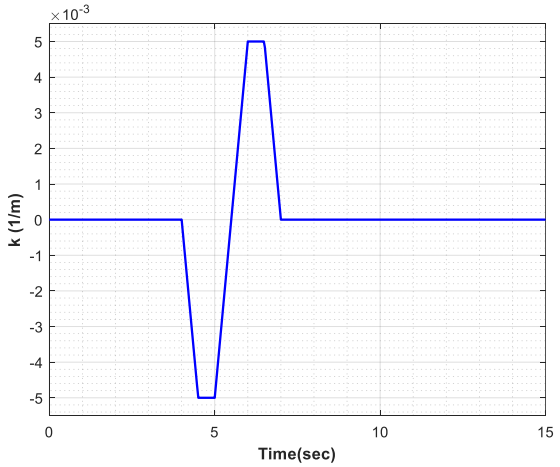

Fig. 3.2. Road curvature

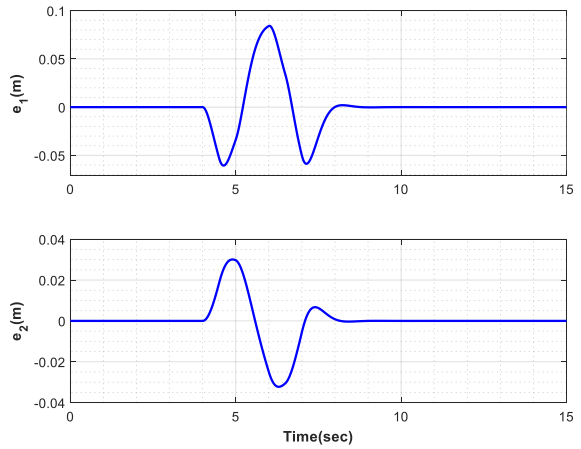

Fig. 3.3. **(Top)** Lateral position error, **(Bottom)** Heading error

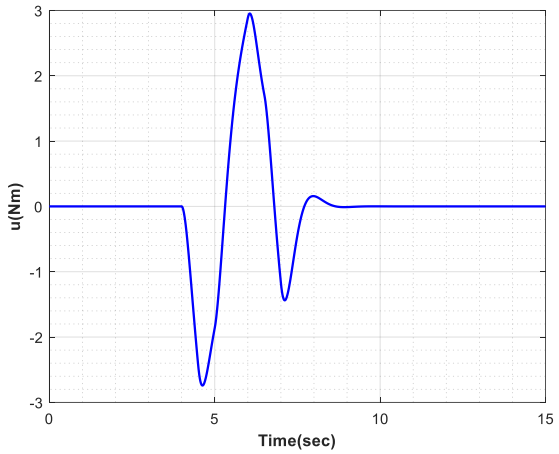

Fig. 3.4. Steering torque

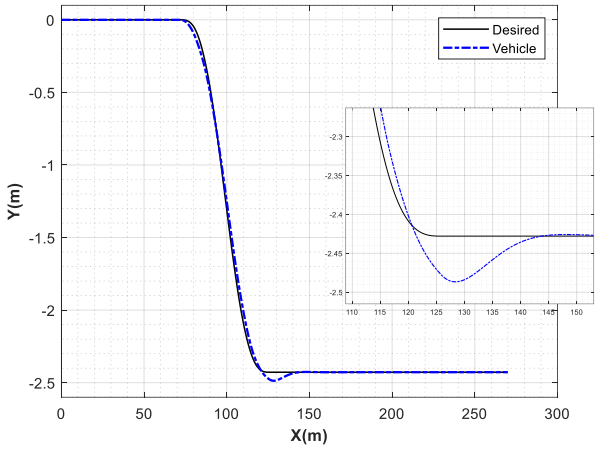

Fig. 3.5. Global vehicle XY trajectory

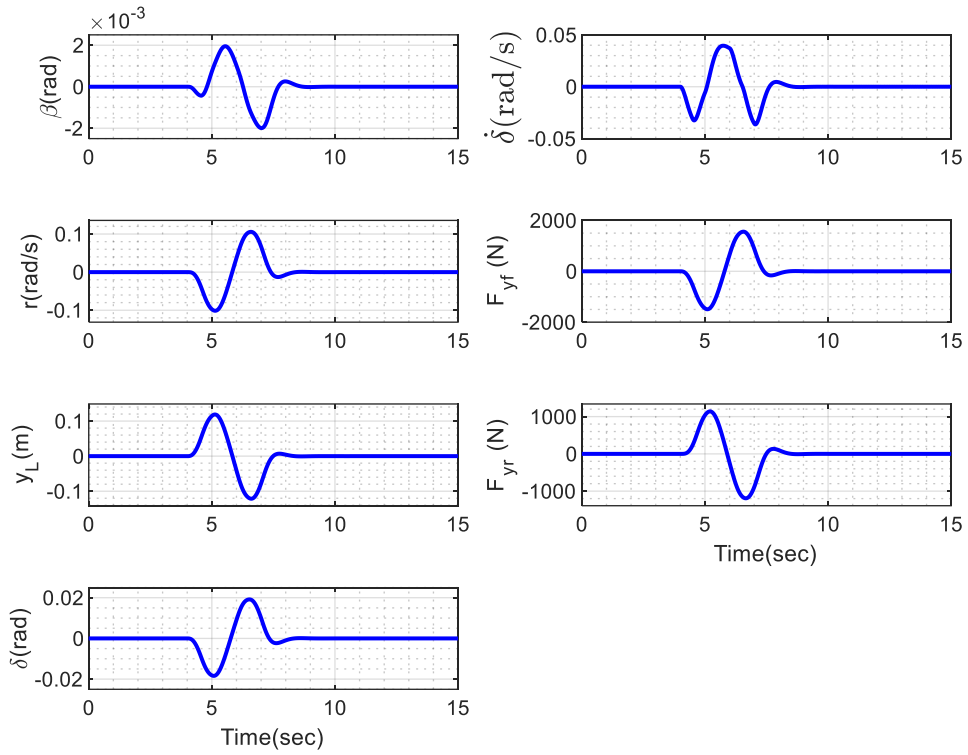

Fig. 3.6. From top to bottom: **(1)** Side-slip angle, **(2)** Yaw rate, **(3)** Lateral deviation error at the look-ahead distance, **(4)** Steering angle, **(5)** Steering rate, **(6)** Front lateral force, **(7)** Rear lateral force

Readers may refer to the first subsection of the simulation results in Chapter 4 to gain a better insight into the simulation results shown in this chapter regarding the lateral position error, the global vehicle *XY* trajectory, and the global desired *XY* trajectory.

Chapter 4

LPV Path-Tracking Control

4.1. Stability Analysis of LPV Systems

Representing the dynamics of physical systems using state-space models is a widely used and effective approach for developing control algorithms and analyzing stability. However, it is essential to acknowledge that variations in one or more system parameters introduce uncertainty into the model itself. Typically, these parameters and their variation ranges are defined and known in advance. Given that even small variations in system parameters can result in significant changes to the system's dynamic behavior, analyzing and addressing these variations is critical to ensuring robust and reliable control design [94].

Before analyzing the stability of LPV systems, it is essential to review the concept of Lyapunov stability. The direct Lyapunov stability theorem is a standard approach for ensuring the stability of closed-loop systems. However, in this dissertation, to derive controller design conditions in terms of Linear Matrix Inequalities (LMIs), specific Lyapunov candidates with particular properties are required. These properties enable the computation of unknown LMI variables using convex numerical techniques. The following section investigates two Lyapunov candidates commonly employed in LMI-based problems:

i) Quadratic Lyapunov function (QLF)

One of the simplest Lyapunov candidates is the Quadratic Lyapunov Function (QLF). The main advantage of utilizing QLF is that it provides a simple procedure for deriving the controller design conditions regarding LMIs. The structure of this function is as follows:

$$V_1 = x^T P x, \tag{4.1}$$

where P is the common positive definite Lyapunov matrix [91]. However, QLF is not the best solution to guarantee the stability of nonlinear systems. This fact is also true for Takagi-Sugeno (TS) fuzzy systems, as well as LPV systems. In other words, stable TS fuzzy/LPV systems exist whose stability cannot be assured by the QLFs. Furthermore, by increasing the number of fuzzy rules (the number of vertices), the TS fuzzy system (the LPV system) exhibits a more nonlinear nature. Consequently, deriving LMI controller design conditions based on the QLF may lead to

infeasible solutions for TS fuzzy systems with a high number of fuzzy rules, as well as LPV systems with a high number of vertices. This fact shows the inherent conservativeness of QLFs for nonlinear TS/LPV systems [95].

ii) Non-quadratic Lyapunov function (NQLF)

The Non-Quadratic Lyapunov Function (NQLF) is a fuzzy blending of multiple quadratic Lyapunov functions. The structure of the NQLF is as follows:

$$V_2 = \sum_{i=1}^{r} \eta_i \, x^T P_i x, \tag{4.2}$$

where η_i for $i = 1, \dots, r$ are the membership functions, and P_i for $i = 1, \dots, r$ are the Lyapunov matrices [95]. As can be seen in (4.2), NQLF is a fuzzy mixture of several QLFs. Therefore, this function is also known as fuzzy Lyapunov function. One should note that in the NQLF-based stability analysis, time-derivatives of membership functions appear, and their upper bounds have to be known prior to designing a fuzzy/LPV controller, which can pose some challenges to the synthesis procedure since the mentioned time-derivatives are proportional to not only states but also inputs, making it difficult to evaluate the aforementioned upper bounds [96] and [97].

By using the Lyapunov stability theorem and recalling the state-space realization of the polytopic LPV representation of a system, one can address the stability analysis of systems with time-varying parameters.

Theorem 4.1 [98]**:** The system $\dot{x}(t) = A\big(\theta(t)\big)x(t)$ is stable if:

$$\exists P = P^T > 0 \;\; s.t. A\big(\theta(t)\big)^T P + PA\big(\theta(t)\big) < 0 \;\; \forall \;\; \theta(t) \in \Delta, \tag{4.3}$$

where $\theta(t)$ is the time-varying parameter vector, and $\Delta \in \mathbb{R}^p$ is the varying parameter set. The stability of the system $\dot{x}(t) = A\big(\theta(t)\big)x(t)$ is subject to the validity of the equation (4.3) for all admissible time-varying parameters in the varying parameter set Δ. To conduct the stability analysis of such systems, the following theorem can be utilized:

Theorem 4.2 [98]**:** If $A(\theta(t))$ is an affine function in $\theta(t)$, and Δ_0 is the set of vertex points of the varying parameter set Δ, such that $\Delta = conv(\Delta_0)$, then, the system $\dot{x}(t) = A\big(\theta(t)\big)x(t)$ is stable if:

$$\exists P = P^T > 0 \;\; s.t. A\big(\theta(t)\big)^T P + PA\big(\theta(t)\big) < 0 \;\; \forall \; \theta(t) \in \Delta_0. \tag{4.4}$$

Therefore, it is sufficient to ensure the stability of the system at the vertex points of the varying parameter set Δ, rather than investigating the stability across the entire set.

4.2. LPV Path Tracking Control Design

Different control approaches can be considered to stabilize an LPV system, such as linear and gain-scheduling controllers. In Chapter 3, the application of a Linear Quadratic Regulator (LQR) was discussed. However, since the LPV system contains measurable time-varying parameters, a gain-scheduling controller is a better choice. Inspired by the polytopic LPV representation, we can consider a gain-scheduling controller with almost the same time-varying parameters as the LPV system. This consideration improves the closed-loop performance and reduces the conservativeness.

Moreover, as mentioned in Section 4.1, the selection of the Lyapunov function is of great importance due to its direct influence on the design's conservativeness. Several Lyapunov functions have been presented dealing with polytopic LPV systems, including quadratic Lyapunov function [99], and poly-quadratic Lyapunov function [95]. The quadratic Lyapunov function is a straightforward selection for the stability analysis of the LPV systems, as it offers a simple procedure to derive the conditions in terms of LMIs. However, it fails to involve the time-varying parameters in its definition, which increases the conservativeness of the derived conditions. Such an issue is alleviated by considering other types of Lyapunov functions. The other choice for the Lyapunov function is the poly-quadratic Lyapunov function. This function is a gain-scheduled version of the conventional quadratic Lyapunov function. Although time derivatives of the time-varying parameter appear in a design procedure using poly-quadratic Lyapunov functions, in several cases, the lower and/or upper bound(s) for these terms is/are provided, enabling us to solve the controller design conditions with LMI solvers. This fact makes the poly-quadratic Lyapunov function a decent choice for trajectory-following control systems.

The following subsections develop two control design methodologies. The first employs a quadratic Lyapunov function, while the second is based on a poly-quadratic Lyapunov function.

4.2.1. LPV Control Design with a Quadratic Lyapunov Function

In this subsection, Linear Matrix Inequalities (LMIs) targeted to design an H_2 LPV state feedback controller are developed. The rationale behind the choice of the state feedback controller lies in its simple control structure, while the H_2 scheme helps the control system to satisfy some performance criteria such as passengers' comfort and/or input disturbance attenuation like gust wind. The theoretical framework is built on polytopic LPV systems, incorporating a parameter-dependent controller designed to handle a wide range of variations in the vehicle's longitudinal velocity. Additionally, a quadratic Lyapunov function is utilized to ensure both the stability and performance of the control synthesis.

The polytopic LPV representation, previously introduced as Equation (2.23) in Chapter 2, is restated here as follows:

$$\Sigma_v(\theta): \begin{cases} \dot{x} = \sum_{i=1}^{2} \eta_i(\theta)(A_i x + B_i^u u + B_i^\omega \omega), \\ z = \sum_{i=1}^{2} \eta_i(\theta)(C_i^z x + D_i^z u), y = C_y x, \end{cases} \tag{4.5}$$

where $x \in \mathbb{R}^{n_x}$ represents the state, $u \in \mathbb{R}^{n_u}$ represents the control input, $\omega \in \mathbb{R}^{n_\omega}$ represents the disturbance, $z \in \mathbb{R}^{n_z}$ represents the performance output, and $y \in \mathbb{R}^{n_y}$ represents the system output. The parameter $\theta \in \mathbb{R}^p$ is the scheduling variable of the polytopic LPV representation. The real matrices A_i, B_i^u, B_i^ω, C_i^z, D_i^z and C_y, $i = \{1,2, \dots, N\}$ are constant. The membership functions $\eta_i(\theta)$, $i = \{1,2, \dots, N\}$ satisfy the given properties:

$$\eta_i(\theta) \geq 0, \qquad \sum_{i=1}^{N} \eta_i(\theta) = 1. \tag{4.6}$$

The number of vertices, $N = 2^p$, is determined using sector nonlinearity decomposition [91] which is employed to derive the polytopic LPV representation in the form of Equation (4.5). For the polytopic LPV system (4.5), consider the following parameter-dependent controller:

$$u = K(\theta)x + L_\omega(\theta)\omega, \tag{4.7}$$

where both $K(\theta)$ and $L_\omega(\theta)$ are linear functions of the time-varying parameters, as follows:

$$u = \sum_{i=1}^{N} \eta_i(\theta) K_i x + \sum_{i=1}^{N} \eta_i(\theta) L_i^{\omega} \omega, \tag{4.8}$$

where $L_i^{\omega} = \begin{bmatrix} 0 & k_i^{\rho_r} \end{bmatrix}$. It should be noted that the term $L_{\omega}(\theta)$ acts as a feedforward gain for the control synthesis considering the road curvature information to reduce its effect on the overall performance of the designed structure.

Remark 1: The presence of the feedforward gain $L_{\omega}(\theta)$ does not add any complexity for deriving the controller design conditions in terms of LMIs since it would appear in a linear format in those mentioned control synthesis conditions [4].

By considering the Equations (4.5) and (4.7), the closed-loop system can be obtained as:

$$\Sigma_v(\theta): \begin{cases} \dot{x} = \hat{A}(\theta) x + \hat{B}_{\omega}(\theta) \omega \\ z = \hat{C}_z(\theta) x + \hat{D}_z(\theta) \omega' \end{cases} \tag{4.9}$$

with:

$$\hat{A}(\theta) = A(\theta) + B_u(\theta) K(\theta),$$
$$\hat{B}_{\omega}(\theta) = B_{\omega}(\theta) + B_u(\theta) L_{\omega}(\theta),$$
$$\hat{C}_z(\theta) = C_z(\theta) + D_z(\theta) K(\theta),$$
$$\hat{D}_z(\theta) = D_z(\theta) L_{\omega}(\theta),$$

where C_y is an identity matrix in the appropriate dimension.

Remark 2: An H_2 scheme will be utilized to design the control structure. According to [100], implementing an H_2 performance scheme for control synthesis requires the system matrix $\hat{D}_z(\theta)$ to be equal to zero. To achieve this, the steering torque, as the control input, is excluded from the performance output defined in Equations (2.15)-(2.17).

In the following, we develop the controller design conditions in terms of LMIs to have a state feedback controller in the form of Equation (4.8), stabilizing the polytopic LPV system (4.5) in an H_2 scheme framework where $\|\Sigma\|_2 < \gamma$, with γ as a positive scalar ($\gamma > 0$).

Definition 1 (H_2 nominal performance): The H_2 norm of an exponentially stable system $G:\begin{cases}\dot{x} = Ax + B\omega, \ \ x(0) = 0 \\ z = Cx\end{cases}$ is defined as follows [100]:

$$\|G\|_2^2 = \frac{1}{2\pi}\int_{-\infty}^{+\infty} Tr\{G(i\omega)^T G(i\omega)\}d\omega = \int_{-\infty}^{+\infty} Tr\big(g(t)^T g(t)\big)dt, \tag{4.10}$$

where $G(i\omega)$ is considered as the closed-loop transfer function from ω (here it is the disturbance signal) to z (here it is the output signal which regards the control system's performance), $g(t)$ is the convolution kernel of $G(i\omega)$, and $Tr(\cdot)$ denotes the trace of a matrix. The H_2 norm defined (4.10) is finite if the transfer function of the system G is strictly proper; that is, $G(\infty) = 0$. Therefore, the state-space representation of the system G must not contain the matrix D.

Definition 2 (Gramian) [98]**:** For the system $S:\begin{cases}\dot{x} = Ax + b\omega \\ Z = Cx + D\omega\end{cases}, x(0) = 0$, the controllability Gramian and the observability Gramian are defined as follows:

$$W_0 = \int_0^{\infty} e^{At}BB^T e^{A^T t}dt, \tag{4.11}$$

and

$$M_0 = \int_0^{\infty} e^{A^T t}C^T C e^{At}dt, \tag{4.12}$$

For the stable system S, i.e. A is Hurwitz, the controllability and observability Gramians satisfy, respectively:

$$AW_0 + W_0A^T + BB^T = 0, \tag{4.13}$$

and

$$A^T M_0 + M_0 A + C^T C = 0, \tag{4.14}$$

To verify Equations (4.13) from (4.11) consider that

$$\frac{d}{dt}\big(e^{At}BB^T e^{A^T t}\big) = Ae^{At}BB^T e^{A^T t} + e^{At}BB^T e^{A^T t}A^T, \tag{4.15}$$

Integrating (4.15) over the operation time gives

$$\int_0^{\infty} \frac{d}{dt}\left(e^{At}BB^Te^{A^Tt}\right)dt = A\int_0^{\infty} e^{At}BB^Te^{A^Tt}dt + \int_0^{\infty} e^{At}BB^Te^{A^Tt}A^Tdt. \tag{4.16}$$

Since for $t = \infty$, e^{At} converges zero (i.e. A is Hurwitz), (4.16) leads to

$$e^{At}BB^Te^{A^Tt}\Big|_{t=0}^{t=\infty} = A\int_0^{\infty} e^{At}BB^Te^{A^Tt}dt + \int_0^{\infty} e^{At}BB^Te^{A^Tt}A^Tdt \rightarrow \tag{4.17}$$
$$-BB^T = AW_0 + W_0B$$

The (4.17) equals (4.13). Considering the same procedure for (4.12) leads to (4.14).

Remark 3 [98]**:** For the stable system G, we have:

$$g(t) = \mathcal{L}^{-1}(G) = \begin{cases} Ce^{At}B, & t \geq 0 \\ 0 & t < 0 \end{cases}. \tag{4.18}$$

Therefore, the H_2 performance norm of the stable system G can be computed as

$$\begin{aligned} \|G\|_2^2 &= \int_{-\infty}^{+\infty} Tr\left(g(t)^Tg(t)\right)dt = \int_{-\infty}^{+\infty} Tr\left(B^Te^{A^Tt}C^TCe^{At}B\right)dt \\ &= \int_{-\infty}^{+\infty} Tr\left(Ce^{At}BB^Te^{A^Tt}C^T\right)dt \\ \|G\|_2^2 &= Trace(CW_0C^T) = Trace(B^TM_0B), \end{aligned} \tag{4.19}$$

where W_0 and M_0 are defined in Definition 2.

However, for the controller synthesis, the closed-loop system matrix is not available to analytically check the norm 2 performance by (4.13) and (4.14). The reason is that the closed-loop system matrix A is unknown due to the need for designing the stabilizing controller gain at the same time we handle its performance through the H_2 scheme. In other words, it is required that equalities (4.13) and (4.14) are solved to find the closed-loop system matrix and the Gramians together [100]. Therefore, the equalities (4.13) and (4.14) are transformed into inequalities that can be solved numerically since the analytical solution for the equalities cannot be addressed.

$$AW + WA^T + BB^T < 0, \tag{4.20}$$

and

$$A^T M + MA + C^T C < 0, \tag{4.21}$$

where $W_0 < W$ and $M_0 < M$. Consequently, an upper bound for the $\|G\|_2^2$ is achieved.

Definition 3 (Exponential stability): For the non-perturbed system S with $B_\omega = 0$ and a Lyapunov candidate $V(x)$, consider that the following inequality holds:

$$\dot{V}(x) + 2\alpha V(x) < 0, \tag{4.22}$$

where $\alpha \geq 0$ is the so-called decay rate. Then, the exponential stability is achieved and the Lyapunov function evolution is as follows:

$$V\big(x(t)\big) < -V\big((0)\big)e^{-2\alpha t}, \tag{4.23}$$

In the following, the controller design conditions are derived.

Theorem 4.3 [98]**:** Consider the polytopic LPV system $\Sigma_v(\theta)$ in (4.5), and a positive scalar $\alpha > 0$. Suppose there exists a symmetric positive definite $Q \in \mathbb{R}^{n_x} \times \mathbb{R}^{n_x}$, and a matrix $Z(\theta) \in \mathbb{R}^{n_\omega} \times \mathbb{R}^{n_\omega}$, and a positive scalar $\gamma > 0$, in the form of following constraints:

$$\begin{bmatrix} \hat{A}(\theta)Q + Q\hat{A}^T(\theta) + 2\alpha Q & \star \\ \hat{C}_z(\theta)Q & -I \end{bmatrix} < 0, \tag{4.24}$$

$$\begin{bmatrix} Z(\theta) & \star \\ \hat{B}_\omega(\theta) & Q \end{bmatrix} > 0, \tag{4.25}$$

$$Tarce\left(Z(\theta)\right) < \gamma^2, \tag{4.26}$$

then, the control law in (4.7) leads to the stable closed-loop system (4.9) with $\|\Sigma_v(\theta)\|_2^2 < \gamma^2$.

Proof [98]**:** Consider that (4.24) is feasible. Then, it follows that:

$$\begin{bmatrix} \hat{A}(\theta)Q + Q\hat{A}^T(\theta) & \star \\ \hat{C}_z(\theta)Q & -I \end{bmatrix} < -\begin{bmatrix} 2\alpha Q & * \\ 0 & 0 \end{bmatrix} \leq 0. \tag{4.27}$$

Therefore,

$$\begin{bmatrix} \hat{A}(\theta)Q + Q\hat{A}^T(\theta) & \star \\ \hat{C}_z(\theta)Q & -I \end{bmatrix} < 0. \tag{4.28}$$

Applying Schur complement on (4.28) results in that

$$\hat{A}(\theta)Q + Q\hat{A}^T(\theta) + Q\hat{C}_z^T(\theta)\hat{C}_z(\theta)Q < 0. \tag{4.29}$$

Pre and post-multiplying (4.29) to Q^{-1} and defining $M = Q^{-1}$ provides (4.21). Moreover, (4.25) guarantees that

$$\hat{B}_\omega^T(\theta)Q^{-1}\hat{B}_\omega(\theta) < Z(\theta), \tag{4.30}$$

Considering $M = Q^{-1}$, one has

$$\hat{B}_\omega^T(\theta)M\hat{B}_\omega(\theta) < Z(\theta). \tag{4.31}$$

Therefore,

$$Trace\left(\hat{B}_\omega^T(\theta)M\hat{B}_\omega(\theta)\right) < Trace\big(Z(\theta)\big), \tag{4.32}$$

Comparing (4.32) and (4.26), results in that

$$Trace\left(\hat{B}_\omega^T(\theta)M\hat{B}_\omega(\theta)\right) < \gamma^2. \tag{4.33}$$

Keeping (4.29) and (4.33) in mind, the H_2 performance is achieved. Moreover, since (4.24) is feasible, one has

$$\hat{A}(\theta)Q + Q\hat{A}^T(\theta) + 2\alpha Q < 0. \tag{4.34}$$

Pre- and post- multiplying (4.34) to $x^T Q^{-1}$ and $Q^{-1}x$, and defining $P = Q^{-1}$ provides:

$$x^T P\hat{A}(\theta)x + x^T\hat{A}^T(\theta)Px + 2\alpha x^T Px < 0. \tag{4.35}$$

Considering the candidate Lyapunov function of the form $V(x) = x^T Px$, for the non-perturbed LPV system, (4.34) equals:

$$\dot{V}(x) + 2\alpha V(x) < 0. \tag{4.36}$$

Therefore, the exponential stability with the decay rate α is assured. The proof is therefore complete. ■

Remark 4: The proof of Theorem 4.3 is decomposed into two parts. In the first part, it is shown that if the LMIs of Theorem 4.3 are feasible, then by defining the LMI variable $Q > 0$ as the observability Gramian, the H_2 performance is assured. In the second part, it is depicted that by

having a feasible solution for the LMIs and defining the LMI variable $Q > 0$ as the Lyapunov matrix, the exponential stability is guaranteed. In other words, the LMI constraints assure the exponential stability of the non-perturbed system and the H_2 performance simultaneously.

Remark 5: The constraints of Theorem 4.3 cannot be solved as LMIs, because i) they contain the time-varying parameters θ, and ii) the term $\hat{A}(\theta)Q$ contains the multiplication of the two unknown matrices. In the following, the constraints of Theorem 4.3 are derived in terms of LMIs.

Theorem 4.4 [4]**: C**onsider the polytopic LPV system $\Sigma_v(\theta)$ in (4.5), and a positive scalar $\alpha > 0$. Suppose there exists a symmetric positive definite $Q \in \mathbb{R}^{n_x} \times \mathbb{R}^{n_x}$, and matrices $Z_i \in \mathbb{R}^{n_\omega} \times \mathbb{R}^{n_\omega}$ for $i = 1,2$, and a positive scalar $\gamma > 0$, in the form of following LMIs:

$$\begin{gathered} T_{ii} < 0 \; for \; i = 1,2, \\ \frac{2}{L-1} T_{ii} + T_{ij} + T_{ji} < 0 \quad for \quad 1 \le i < j \le 2, \end{gathered} \tag{4.37}$$

$$\begin{bmatrix} Z_i & \star \\ \hat{B}_{\omega_i} & Q \end{bmatrix} > 0 \quad for \quad i = 1,2, \tag{4.38}$$

$$Tarce\,(Z_i) < \gamma^2 \quad for \quad i = 1,2, \tag{4.39}$$

where $L = 2$ and

$$T_{ij} = \begin{bmatrix} A_i Q + B_{u_i} K_j Q + Q A_i^T + Q K_j^T B_{u_i} + 2\alpha Q & \star \\ C_{z_i} Q + D_{z_i} K_j Q & -I \end{bmatrix}$$

then, the control law in (4.8) leads to the stable closed-loop system (4.9) with $\|\Sigma_v(\theta)\|_2^2 < \gamma^2$.

Proof [4] **and** [98]**:** Substituting the definition of the $\hat{A}(\theta)$ with convexity sum into (4.24) results in:

$$\begin{aligned} &\sum_{i=1}^{2}\sum_{j=1}^{2} \eta_i(\theta)\eta_j(\theta) \begin{bmatrix} A_i Q + B_{u_i} K_j Q + Q A_i^T + Q K_j^T B_{u_i} + 2\alpha Q & \star \\ C_{z_i} Q + D_{z_i} K_j Q & -I \end{bmatrix} \\ &= \sum_{i=1}^{2}\sum_{j=1}^{2} \eta_i(\theta)\eta_j(\theta) T_{ij} < 0, \end{aligned} \tag{4.40}$$

where

$$T_{ij} = \begin{bmatrix} A_i Q + B_{u_i} K_j Q + Q A_i^T + Q K_j^T B_{u_i} + 2\alpha Q & \star \\ C_{z_i} Q + D_{z_i} K_j Q & -I \end{bmatrix}$$

The left side of (4.60) is continued as follows:

$$\begin{aligned} &\sum_{i=1}^{2}\sum_{j=1}^{2} \eta_i(\theta)\eta_j(\theta) T_{ij} \\ &= \sum_{1\le i<j\le 2} \Big\{ \eta_i(\theta)^2 \frac{1}{L-1} T_{ii} + \eta_j^2(\theta) \frac{1}{L-1} T_{jj} + \frac{1}{2}\eta_i(\theta)\eta_j(\theta)\big(T_{ij} + T_{ji}\big) \\ &+ \frac{1}{2}\eta_j(\theta)\eta_i(\theta)\big(T_{ij} + T_{ji}\big) \Big\} \\ &= \sum_{1\le i<j\le 2} \left\{ [\eta_i(\theta) \quad \eta_j(\theta)] \begin{bmatrix} \frac{1}{L-1} T_{ii} & \frac{1}{2}\big(T_{ij} + T_{ji}\big) \\ \frac{1}{2}\big(T_{ij} + T_{ji}\big) & \frac{1}{L-1} T_{jj} \end{bmatrix} \begin{bmatrix} \eta_i(\theta) \\ \eta_j(\theta) \end{bmatrix}^T \right\} < 0, \end{aligned} \tag{4.41}$$

where $L = 2$. The time-varying parameters $\eta_i(\theta)$ and $\eta_j(\theta)$ in a polytopic LPV representation are non-negative. Therefore, by applying Tuan's relaxation lemma, given in Appendix 3, on (4.41), the LMIs (4.37) are achieved. The remaining LMIs in (4.38) and (4.39) can be obtained through the definition of the polytopic LPV representation of the system. Represented constraint in (4.25) results that:

$$\sum_{i=1}^{2} \eta_i(\theta) \begin{bmatrix} Z_i & \star \\ \hat{B}_{\omega_i} & Q \end{bmatrix} > 0, \tag{4.42}$$

Since $\eta_i(\theta) \ge 0$, (4.42) implies the LMI (4.38). In a similar way, the constraint (4.26) is re-written as follows:

$$Tarce\left(\sum_{i=1}^{2} \eta_i(\theta) Z_i\right) < \gamma^2, \tag{4.43}$$

Since $\eta_i(\theta) \le 1$, the constraint (4.43) holds if the LMIs (4.39) are satisfied. The proof is complete. ■

Theorem 4.5 [91]**:** Consider a scalar ϵ, and assuming initial condition of the system's state trajectories $x(0)$ is known. One can limit the amplitude bound of the controller's gain by adding the following constraints, which are in LMI form, to the control design conditions of theorem 4.4.

$$\begin{bmatrix} 1 & x(0)^T \\ x(0) & Q \end{bmatrix} \geq 0, \tag{4.44}$$

$$\begin{bmatrix} Q & M_j^T \\ M_j & \epsilon^2 I \end{bmatrix} \geq 0, j = 1,2, \tag{4.45}$$

where $I \in \mathbb{R}^{n_u}$, $Q = P^{-1}$, and M_j is defined as $K_j Q$. For the sake of brevity, readers may follow the information regarding Q and K_j in theorems 4.3 and/or 4.4.

Proof [91]**:** Consider that the Lyapunov function is as follows:

$$V\big(x(t)\big) = x^T(t)Px(t), \tag{4.46}$$

Also, consider that:

$$x^T(0)Px(0) \leq 1. \tag{4.47}$$

As a result,

$$1 - x^T(0)Q^{-1}x(0) \geq 0, \tag{4.48}$$

where $Q = P^{-1}$. By applying Schur complement on (4.48), the (4.44) is obtained.

By considering $\|u(t)\|_2 \leq \epsilon$, one has:

$$u^T(t)u(t) = \sum_{i=1}^{2}\sum_{j=1}^{2} \eta_i\eta_j x^T(t)K_i^T K_j x(t) \leq \epsilon^2, \tag{4.49}$$

Or through a mathematical simplification:

$$\frac{1}{\epsilon^2}\sum_{i=1}^{2}\sum_{j=1}^{2} \eta_i\eta_j x^T(t)K_i^T K_j x(t) \leq 1. \tag{4.50}$$

Knowing $x^T(t)X^{-1}x(t) < x^T(0)X^{-1}x(0) \leq 1, \forall t > 0$, (4.50) can be translated into:

$$u^T(t)u(t) = \sum_{i=1}^{2}\sum_{j=1}^{2} \eta_i\eta_j x^T(t)K_i^T K_j x(t) \leq x^T(t)X^{-1}x(t), \tag{4.51}$$

Taking the left side of (4.51) into consideration, the following can be deducted:

$$\begin{gathered} \frac{1}{2}\sum_{i=1}^{2}\sum_{j=1}^{2} \eta_i\eta_j x^T(t)\left(\frac{1}{\epsilon^2}K_i^T K_j + \frac{1}{\epsilon^2}K_j^T K_i - 2X^{-1}\right)x(t) = \\ \frac{1}{2}\sum_{i=1}^{2}\sum_{j=1}^{2} \eta_i\eta_j x^T(t) \times \left[\frac{1}{\epsilon^2}(K_i^T K_i + K_j^T K_j) - \frac{1}{\epsilon^2}(k_i^T - k_j^T)(k_i - k_j) - \right. \\ \left. 2X^{-1}\right]x(t) \leq \frac{1}{2}\sum_{i=1}^{2}\sum_{j=1}^{2} \eta_i\eta_j x^T(t) \times \left[\frac{1}{\epsilon^2}(K_i^T K_i + K_j^T K_j) - 2X^{-1}\right]x(t) = \end{gathered} \tag{4.52}$$

$$\sum_{i=1}^{2} \eta_i x^T(t) \left(\frac{1}{\epsilon^2} k_i^T k_i - X^{-1} \right) x(t).$$

As a result, (4.51) holds if the following is true:

$$\frac{1}{\epsilon^2} k_i^T k_i - X^{-1} \leq 0. \tag{4.53}$$

By pre and post-multiplying (4.53) by X, and defining $M_i = k_i X$, the following is derived:

$$\frac{1}{\epsilon^2} M_i^T M_i - X \leq 0. \tag{4.54}$$

Finally, by applying the Schur complement on (4.54), the matrix inequality (4.45) is obtained, completing the proof. ■

4.2.2. LPV Control Design with a Poly-Quadratic Lyapunov Function

In Subsection 4.2.1, the controller design is conducted by using the quadratic Lyapunov function. However, such consideration can increase the LMI conditions' conservativeness and degrade the closed-loop performance. In this subsection, the LPV controller is designed by using the poly-quadratic Lyapunov function.

Remark 6: To exploit the poly-quadratic Lyapunov function, it is required to investigate the H_2 norm (4.19) and observability Gramian inequality (4.21). Pre- and post- multiplying (4.21) into x^T and x, and defining the Lyapunov candidate as $V = x^T M x$ and its time-derivatives along with $\hat{B}_\omega(\theta) = 0$, one has

$$x^T(A^T M + MA + C^T C)x = \dot{V}(x) + z^T z < 0. \tag{4.55}$$

Moreover, by reminding exponential stability of Definition 3, i.e. (4.22), and merging it with (4.55) (see Remark 4 for more details), one gets:

$$\dot{V}(x) + 2\alpha V(x) + z^T z < 0. \tag{4.56}$$

In other words, the feasibility of (4.56) leads to the following results:

$$\dot{V}(x) + 2\alpha V(x) < -z^T z < 0 \rightarrow \dot{V}(x) + 2\alpha V(x) < 0: \quad \text{Exponential stability}$$
$$\dot{V}(x) + z^T z < -2\alpha V(x) < 0 \rightarrow \dot{V}(x) + z^T z < 0: \qquad H_2 \text{ control framework}$$

As is evident from Equation (4.56), by reversing the design procedure, one can replace the quadratic Lyapunov function, with a poly-quadratic one. Moreover, the H_2 norm (4.19) contains the Lyapunov matrix (the reader may see Equations (4.25),(4.30), and (4.31)).

The following theorem discusses sufficient constraints for the H_2 control framework with the poly-quadratic Lyapunov function and the controller of the form:

$$V = x^T Q^{-1}(\theta) x, \tag{4.57}$$

and

$$u = K(\theta) Q^{-1}(\theta) x, \tag{4.58}$$

where, same as (4.8), a feed-forward gain can be included in the represented control law in (4.58).

Theorem 4.6 [4]**:** Consider the polytopic LPV system $\Sigma_v(\theta)$ in (4.5), and a positive scalar $\alpha > 0$. Suppose there exists a symmetric positive definite $Q(\theta) \in \mathbb{R}^{n_x} \times \mathbb{R}^{n_x}$, and a matrix $Z(\theta) \in \mathbb{R}^{n_\omega} \times \mathbb{R}^{n_\omega}$, and a positive scalar $\gamma > 0$, in the form of following constraints:

$$\begin{bmatrix} \hat{A}(\theta)Q(\theta) + Q(\theta)\hat{A}^T(\theta) + 2\alpha Q(\theta) - \dot{Q}(\theta) & \star \\ \hat{C}_z(\theta)Q(\theta) & -I \end{bmatrix} < 0, \tag{4.59}$$

$$\begin{bmatrix} Z(\theta) & \star \\ \hat{B}_\omega(\theta) & Q(\theta) \end{bmatrix} > 0, \tag{4.60}$$

$$Trace\big(Z(\theta)\big) < \gamma^2, \tag{4.61}$$

then, the control law in (4.58) leads to the stable closed-loop system (4.9) with $\|\Sigma_v(\theta)\|_2^2 < \gamma^2$.

Proof [4] **and** [94]**:** Consider (4.56) and (4.57) along with the LPV system (4.9) with $\hat{B}_\omega(\theta) = 0$. Therefore,

$$\hat{A}(\theta)^T Q^{-1}(\theta) + Q^{-1}(\theta)\hat{A}(\theta) + 2\alpha Q^{-1}(\theta) + \frac{d}{dt}\big(Q^{-1}(\theta)\big) + C^T C < 0. \tag{4.62}$$

Pre- and post-multiplying Equation (4.62) into $Q(\theta)$ gives:

$$\begin{gathered} Q(\theta)\hat{A}(\theta)^T + \hat{A}(\theta)Q(\theta) + 2\alpha Q(\theta) + Q(\theta)\tfrac{d}{dt}\big(Q^{-1}(\theta)\big)Q(\theta) + \\ Q(\theta)C^T C Q(\theta) < 0. \end{gathered} \tag{4.63}$$

On the other hand, since $Q(\theta)Q^{-1}(\theta) = I$:

$$\dot{Q}(\theta)Q^{-1}(\theta) + Q(\theta)\frac{d}{dt}\left(Q^{-1}(\theta)\right) = 0$$
$$Q(\theta)\frac{d}{dt}\left(Q^{-1}(\theta)\right) = -\dot{Q}(\theta)Q^{-1}(\theta) \tag{4.64}$$
$$Q(\theta)\frac{d}{dt}\left(Q^{-1}(\theta)\right)Q(\theta) = -\dot{Q}(\theta).$$

Substituting Equation (4.64) into Equation (4.63) gives:

$$Q(\theta)\hat{A}(\theta)^T + \hat{A}(\theta)Q(\theta) + 2\alpha Q(\theta) - \dot{Q}(\theta) + Q(\theta)C^T CQ(\theta) < 0. \tag{4.65}$$

Applying Schur Complement on (4.65) results in the constraint (4.59). Substituting the Lyapunov matrix $Q^{-1}(\theta)$ into the (4.19) (See Remark 6) yields:

$$Trace\left(\hat{B}_\omega^T(\theta)Q^{-1}(\theta)\hat{B}_\omega(\theta)\right) < \gamma^2. \tag{4.66}$$

Defining the auxiliary polytopic matrix $Z(\theta)$, (4.66) is split into the following constraints:

$$\hat{B}_\omega^T(\theta)Q^{-1}(\theta)\hat{B}_\omega(\theta) < Z(\theta), \tag{4.67}$$

and

$$Trace(Z(\theta)) < \gamma^2. \tag{4.68}$$

Applying Schur Complement on (4.67) results in (4.60). Moreover (4.68) is equal to (4.61). The proof is complete. ■

Remark 7: The constraints of Theorem 4.6 cannot solved by LMIs, because i) they contain the time-varying parameters θ, ii) the term $\hat{A}(\theta)Q(\theta)$ contains the multiplication of the two unknown matrices, and iii) appearing $\dot{Q}(\theta)$. In the following, the constraints of Theorem 4.6 are derived in terms of LMIs.

Theorem 4.7 [4]**:** Consider the polytopic LPV system $\Sigma_v(\theta)$ in (4.5), and a positive scalar $\alpha > 0$. Suppose there exists a symmetric positive definite $Q_i \in \mathbb{R}^{n_x} \times \mathbb{R}^{n_x}$, and a matrix $Z_i \in \mathbb{R}^{n_\omega} \times \mathbb{R}^{n_\omega}$, and a positive scalar $\gamma > 0$, in the form of following constraints:

$$\frac{2}{L-1}S_{ii} + S_{ij} + S_{ji} < 0 \quad for \quad 1 \le i < j \le 2, \tag{4.69}$$

$$\begin{bmatrix} Z_i & \star \\ \hat{B}_{\omega_i} & Q_i \end{bmatrix} > 0 \quad for \quad i = 1,2, \tag{4.70}$$

$$Trace(Z_i) < \gamma^2 \quad for \quad i = 1,2, \tag{4.71}$$

where $L = 2$, and

$$S_{ij} = \begin{bmatrix} A_i Q_j + B_{u_i} K_j + Q_j A_i^T + K_j^T B_{u_i} + 2\alpha Q_j - \sum_{\substack{l=1 \\ l \neq k}}^{2} \sum_{m=1}^{2} w_{km}(\theta) \varphi_{km} (Q_k - Q_l) & \star \\ C_{z_i} Q_j + D_{z_i} K_j & -I \end{bmatrix}$$

then, the control law in (4.58) leads to the stable closed-loop system (4.9) with $\|\Sigma_v(\theta)\|_2^2 < \gamma^2$.

Proof [4] **and** [94]**:** Due to the appearance of the time-derivative term $\dot{Q}(\theta)$ in (4.59), some modifications are needed. it is known that:

$$Q(\theta) = \sum_{l=1}^{2} \eta_l(\theta) Q_l \rightarrow \dot{Q}(\theta) = \sum_{k=1}^{2} \dot{\eta}_k(\theta) Q_k. \tag{4.72}$$

On the other hand,

$$\sum_{k=1}^{2} \eta_k(\theta) = 1 \rightarrow \sum_{k=1}^{2} \dot{\eta}_k(\theta) = 0 \rightarrow \sum_{l=1}^{2} \dot{\eta}_l(\theta)(-Q_l) = 0, \tag{4.73}$$

Using (4.72) with the null term (4.73) provides:

$$\dot{Q}(\theta) = \sum_{k=1}^{2} \dot{\eta}_k(\theta)(Q_k - Q_l) = \sum_{\substack{l=1 \\ l \neq k}}^{2} \dot{\eta}_k(\theta)(Q_k - Q_l). \tag{4.74}$$

For any $\dot{\eta}_k(\theta)$ there exists lower and upper bounds φ_{k1} and φ_{k2} such that $\varphi_{k1} \leq \dot{\eta}_k(\theta) < \varphi_{k2}$. Therefore, by using the sector nonlinearity approach, one has

$$\dot{\eta}_k(\theta) = w_{k1}(\theta)\varphi_{k1} + w_{k2}(\theta)\varphi_{k2} = \sum_{m=1}^{2} w_{km}(\theta)\varphi_{km}, \tag{4.75}$$

where

$$w_{k1}(\theta) = \frac{\left(\varphi_{k2} - \dot{\eta}_k(\theta)\right)}{\varphi_{k2} - \varphi_{k1}}; w_{k2}(\theta) = 1 - w_{k1}(\theta). \tag{4.76}$$

Substituting (4.75) into (4.74) result that

$$\dot{Q}(\theta) = \sum_{k=1}^{2} \dot{\eta}_k(\theta)(Q_k - Q_l) = \sum_{\substack{l=1 \\ l \neq k}}^{2} \sum_{m=1}^{2} w_{km}(\theta)\varphi_{km}(Q_k - Q_l). \tag{4.77}$$

Keeping (4.77) in mind, (4.59) can be written as:

$$\begin{bmatrix} \hat{A}(\theta)Q(\theta) + Q(\theta)\hat{A}^T(\theta) + 2\alpha Q(\theta) - \dot{Q}(\theta) & \star \\ \hat{C}_z(\theta)Q(\theta) & -I \end{bmatrix} = \sum_{i=1}^{2} \sum_{j=1}^{2} \eta_i(\theta)\eta_j(\theta)S_{ij} \tag{4.78}$$

where $L = 2$ and

$$S_{ij} = \begin{bmatrix} A_i Q_j + B_{u_i} K_j + Q_j A_i^T + K_j^T B_{u_i} + 2\alpha Q_j - \sum_{\substack{l=1 \\ l \neq k}}^{2} \sum_{m=1}^{2} w_{km}(\theta)\varphi_{km}(Q_k - Q_l) & \star \\ C_{z_i} Q_j + D_{z_i} K_j & -I \end{bmatrix}$$

The time-varying parameters $\eta_i(\theta)$ and $\eta_j(\theta)$ in a polytopic LPV representation are non-negative. Therefore, by applying Tuan's relaxation lemma, given in Appendix 3, on (4.78), the LMIs (4.69) are achieved. Finally, by re-writing the polytopic representations in (4.60) and (4.61) and eliminating the $\eta_i(\theta)$, LMIs (4.70) and (4.71) are obtained. The proof is complete. ■

Theorem 4.8 [101]**:** Consider a scalar ϵ, and assuming the initial condition of the system's state trajectories $x(0)$ is known. One can limit the amplitude bound of the controller's gain by adding the following constraints, which are in the LMI form, to the control design conditions of theorem 4.7.

$$\begin{bmatrix} 1 & x(0)^T \\ x(0) & Q_j \end{bmatrix} \geq 0, j = 1,2, \tag{4.79}$$

$$\begin{bmatrix} Q_j & K_j^T \\ K_j & \epsilon^2 I \end{bmatrix} \geq 0, j = 1,2, \tag{4.80}$$

where $I \in \mathbb{R}^{n_u}$.

Proof: The theorem can be proved by following the provided proof procedure for theorem 4.5, alongside the definitions of the poly-quadratic Lyapunov function and the control law in (4.57) and (4.58) respectively.

4.3. Simulation Results and Comparisons

This section consists of the following subsections:

(i) An overview of the plots regarding the vehicle's global XY trajectory, the desired global XY trajectory, and the lateral position error.

(ii) The simulation results regarding the H_2 LPV state feedback controller with Quadratic Lyapunov Function (QLF), including tuning its decay rate (α parameter).

(iii) The simulation results regarding the H_2 LPV state feedback controller with Poly-Quadratic Lyapunov Function (PQLF), including tuning its decay rate.

(iv) A comparison between i) the H_2 LPV state feedback controller with QLF, ii) the H_2 LPV state feedback controller with PQLF, and iii) the tuned LQR for the road-vehicle model represented in Chapter 2.

(v) Considering practical aspects in the closed-loop road-vehicle model and implementing the final comparison between the H_2 LPV controller and the LQR one.

(vi) Simulation scenario iv with the lateral wind force (the gust wind), as the input disturbance.

- Subsection i:

Considering the following table, where ψ_{veh} is the yaw angle representing the orientation angle measured with respect to the global X axis.

Table 4.1 The useful parameters for simulation results

Parameter	Description
ψ_{des}	The desired yaw angle
X_{des}	The global position of the desired trajectory w.r.t. the X axis
Y_{des}	The global position of the desired trajectory w.r.t. the Y axis
ψ_{veh}	The vehicle's yaw angle
X_{veh}	The global position of the vehicle w.r.t. the X axis
Y_{veh}	The global position of the vehicle w.r.t. the Y axis
v_x	Vehicle longitudinal velocity
R	The constant radius of the test road
ρ_r	The road curvature
e_1 or y_{act}	Lateral position error
e_2 or ψ_L	Heading error
L_s	Look-ahead distance
y_l	Lateral deviation error at the look-ahead distance

From now on, the lateral position error is represented by e_1, and the heading error is represented by e_2 or ψ_L.

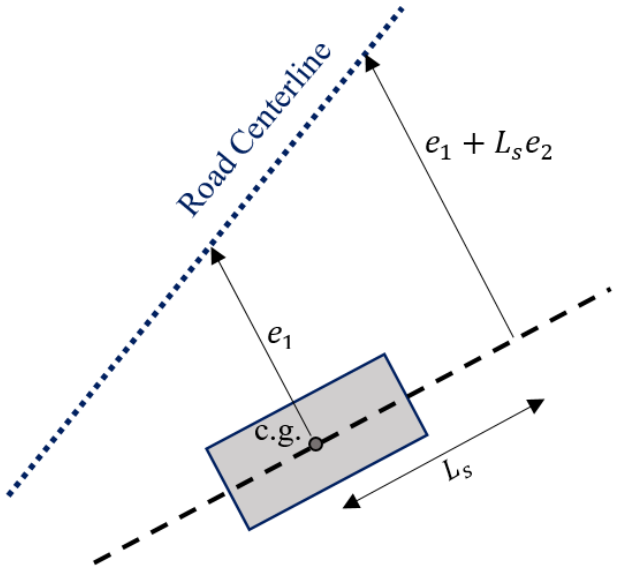

Fig. 4.1. Lateral deviation error measurement

Considering Fig. 4.1, as well as Fig. 2.1 in Chapter 2 and Table 4.1:

$$\rho_r = \frac{1}{R}$$

$$\dot{\psi}_{des} = \frac{V_x}{R} = V_x \rho_r$$

$$e_1 = y_L - d_s e_2$$

$$e_2 = \psi_{veh} - \psi_{des}$$

$$X_{veh} = X_{des} - e_1 \sin(\psi_{veh})$$

$$Y_{veh} = Y_{des} + e_1 \cos(\psi_{veh})$$

As a result, one has better insight into the produced results of this section. For the computational analysis, it is important to note that Matlab/Simulink R2022b [102] was used to generate the results, while the Yalmip toolbox [103] was employed to solve the convex optimization problems associated with the controller design conditions developed in Chapter 4.

As this thesis focuses on the path-following control of Autonomous Ground Vehicles (AGVs), two standard scenarios commonly used in autonomous vehicle control are employed to evaluate and verify the designed controllers: (i) the Single Lane Change (SLC) scenario and (ii) the Double Lane Change (DLC) scenario. These scenarios simulate real-world challenging conditions, allowing the controllers to demonstrate their effectiveness in path-following tasks. The road curvatures of these scenarios are depicted in Figs. 4.2 (a) and 4.2 (b) respectively.

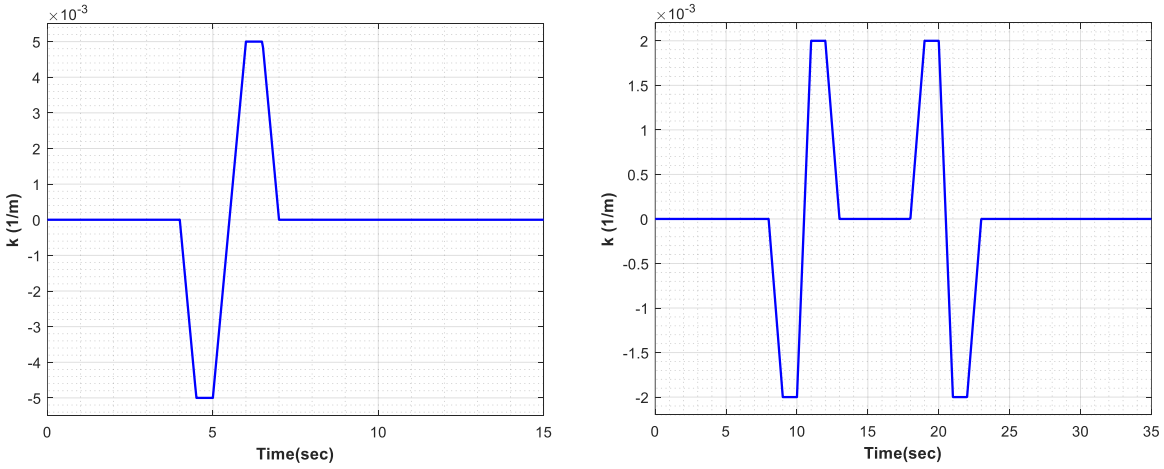

Fig. 4.2. Road curvature for **(a)** Single Lane Change (SLC) and **(b)** Double Lane Change (DLC) scenarios

Furthermore, as outlined in Chapter 1, this thesis incorporates the vehicle's longitudinal velocity as a varying parameter to develop control frameworks better suited to real-world conditions. Consequently, in the evaluation of the AGVs' performance, two distinct velocities are considered: (i) the nominal velocity used for designing the LQR controller, which serves as the benchmark in this dissertation (18 m/s), and (ii) a higher velocity (25 m/s) that deviates from the nominal value, subjecting the vehicle to more challenging test scenarios.

- Subsection ii:

In this subsection, the designed H_2 LPV state feedback controller, utilizing QLF in its design procedure, is employed to control the developed road-vehicle model inspected in equations (2.13)-(2.17) of Chapter 2. The resulting closed-loop road-vehicle system is investigated from both stability and performance points of view, where the states' trajectories and front and rear lateral forces are plotted in Fig. 4.6. Most importantly, the lateral position and heading errors are demonstrated in Fig. 4.3, and the control input (the generated steering torque) is depicted in Fig. 4.4. Finally, the global vehicle and desired XY trajectories are depicted in Fig. 4.5.

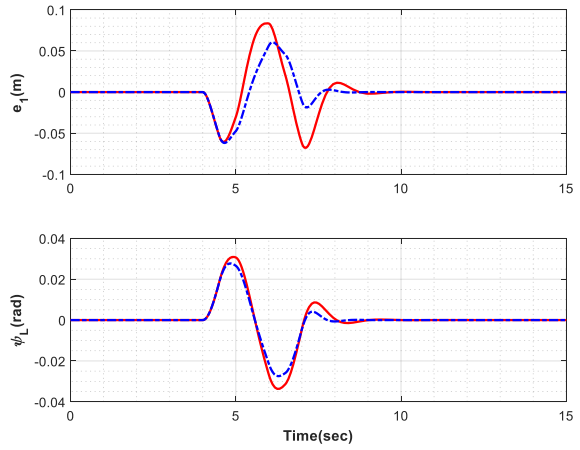

Fig. 4.3. **(Top)** Lateral position error, **(Bottom)** Heading error ($\alpha = 0$, $\alpha = 1.25$)

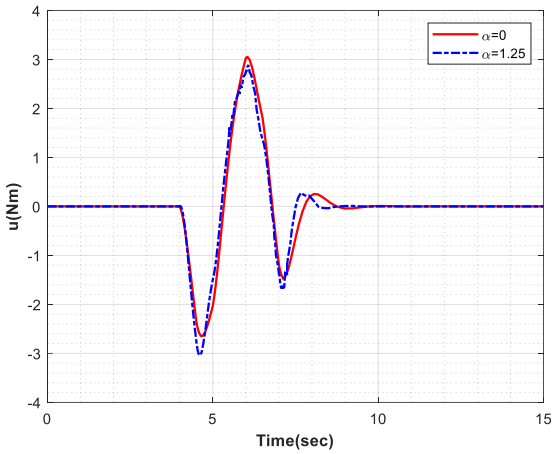

Fig. 4.4. Steering torque

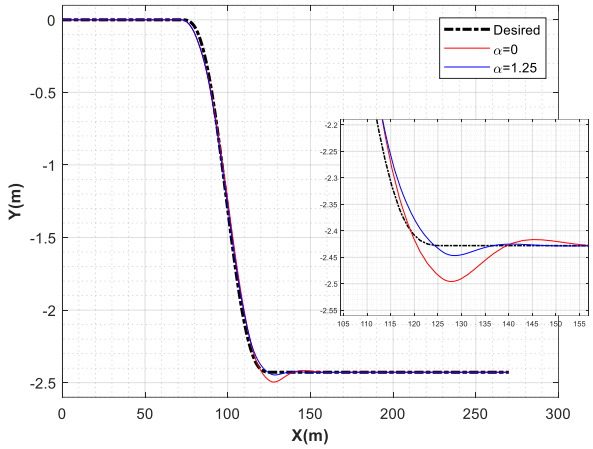

Fig. 4.5. Global vehicle XY trajectory

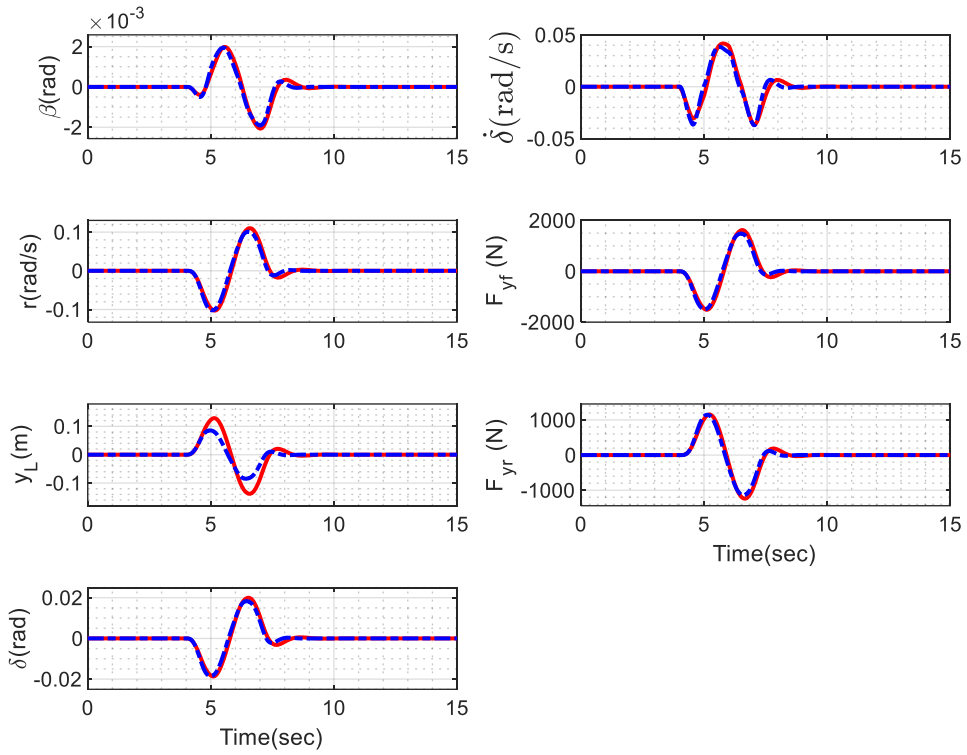

Fig. 4.6 From top to bottom: **(1)** Side-slip angle, **(2)** Yaw rate, **(3)** Lateral deviation error at the look-ahead distance, **(4)** Steering angle, **(5)** Steering rate, **(6)** Front lateral force, **(7)** Rear lateral force ($\alpha = 0$, $\alpha = 1.25$)

As shown in the plotted figures, the results are investigated for both having and not having the decay rate (α) in the structure of the developed controller. It is observed that having a decay rate in the design procedure not only increases the system's response rate but also reduces the lateral position error, as it leads to stricter upper and lower bounds on the stable exponential response (the reader may see Fig. 4.5).

- Subsection iii:

In this subsection, the H_2 LPV state feedback controller, utilizing PQLF in its design procedure, is hired to control the road-vehicle system represented in Chapter 2 to guarantee its stability and performance as two main agendas of a controlled system. This investigation includes the closed-loop states' trajectories along with the front and rear lateral forces (Fig. 4.10), the lateral position and heading errors (demonstrated in Fig. 4.7), the steering torque (Fig. 4.8), and the global vehicle XY trajectory versus the global desired XY trajectory (Fig. 4.9).

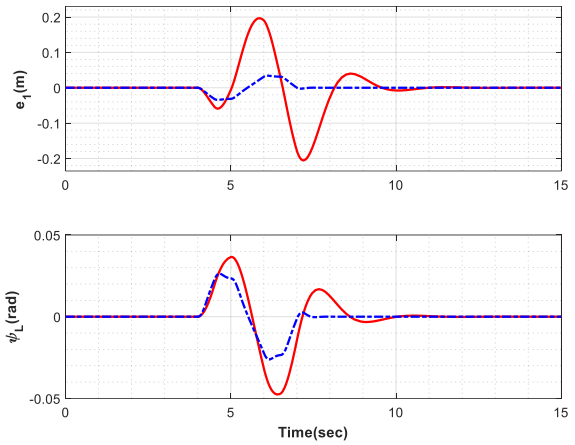

Fig. 4.7. **(Top)** Lateral position error, **(Bottom)** Heading error ($\alpha = 0$, $\alpha = 9.75$)

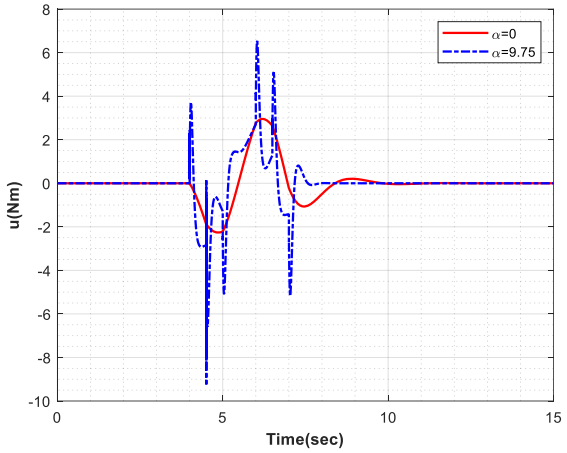

Fig. 4.8. Steering torque

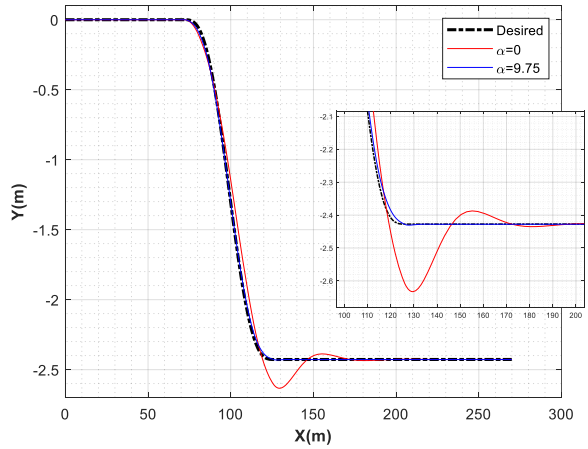

Fig. 4.9. Global vehicle XY trajectory

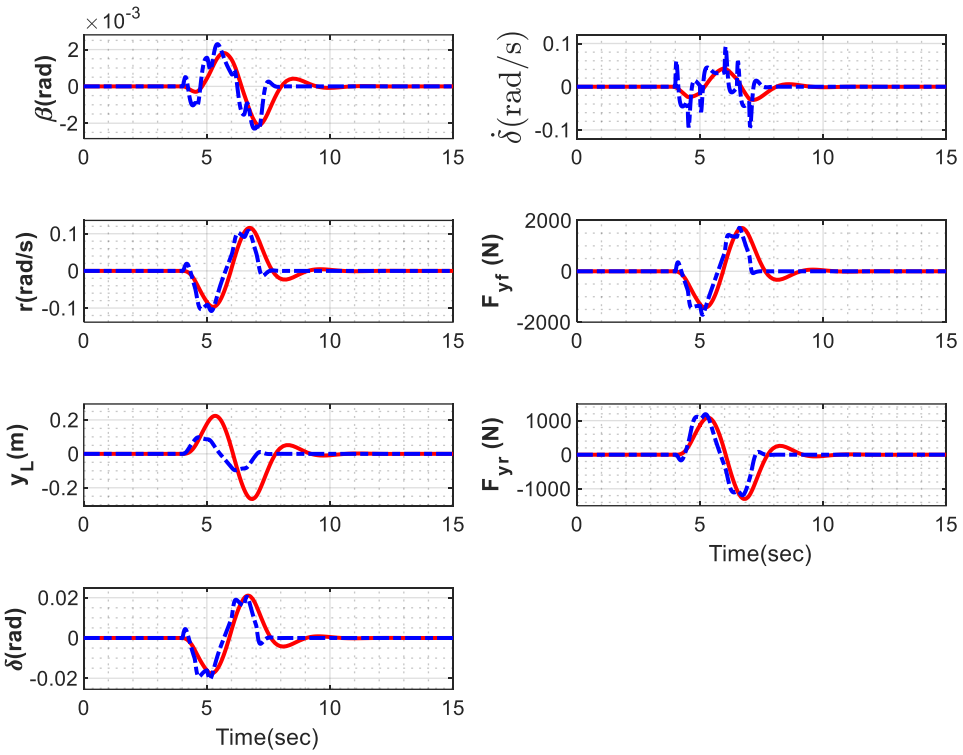

Fig. 4.10. From top to bottom: **(1)** Side-slip angle, **(2)** Yaw rate, **(3)** Lateral deviation error at the look-ahead distance, **(4)** Steering angle, **(5)** Steering rate, **(6)** Front lateral force, **(7)** Rear lateral force ($\alpha = 0$, $\alpha = 9.75$)

As in the previous subsection, the aforementioned results are analyzed for the control synthesis structure with and without including the α parameter as the decay rate. As expected, the same conclusion is drawn regarding the impact of incorporating a decay rate in the developed control framework. Consistent with the theoretical insights discussed in Chapter 4, the best achievable α is significantly improved when employing a Poly-Quadratic Lyapunov Function (PQLF) in the synthesis structure ($\alpha = 9.75$), compared to $\alpha = 1.25$ for the H_2 LPV controller with QLF. A higher α corresponds to improved system responses, which will be further examined in the following subsection.

- Subsection iv:

This subsection presents a general comparison between the LQR controller, designed in Chapter 3 as the benchmark, and the H_2 LPV state feedback controllers utilizing quadratic and poly-

quadratic Lyapunov functions. These H_2 controllers are tuned to their optimal performance by employing the best achievable decay rates, as detailed in their respective subsections. Comparisons are conducted for SLC standard test scenarios, where the nominal velocity ($v = 18\, m/s$) is considered as the vehicle longitudinal velocity. From here, the results are focused only on the lateral position and heading errors (Fig. 4.11), and the global vehicle and desired XY trajectories (Fig. 4.13). Additionally, to provide a comprehensive comparison between the optimal and robust approaches, the steering torques generated by each method, applied to their respective closed-loop systems as control inputs, are plotted in Fig. 4.12. Tables. 4.2 and 4.3 utilize the root mean square (RMS) and L_∞ norm of lateral position and heading errors of each strategy to better investigate their performance in the delegated path-following task.

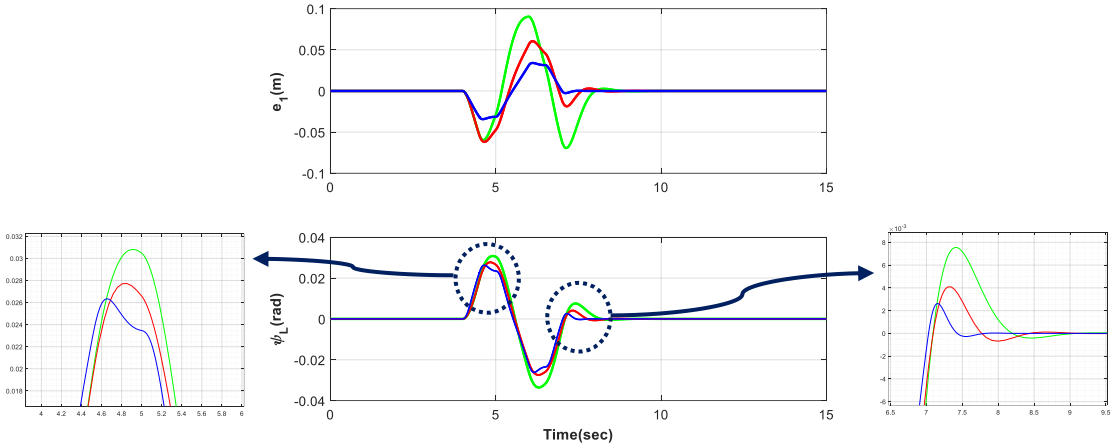

Fig. 4.11. **(Top)** Lateral position error, **(Bottom)** Heading error (LQR, H_2 *with QLF*, H_2 *with PQLF*)

Table 4.2. Comparison between LQR, H_2 with QLF, and H_2 with PQLF w.r.t. the lateral position error

	l_∞	rms
LQR	0.090333	0.030358
$H_2\ (QLF)$	0.061837	0.027662
$H_2\ (PQLF)$	0.03424	0.020781

Table 4.3. Comparison between LQR, H_2 with QLF, and H_2 with PQLF w.r.t. the heading error

	l_∞	rms
LQR	0.033571	0.011782
$H_2\ (QLF)$	0.027723	0.012949
$H_2\ (PQLF)$	0.026336	0.015312

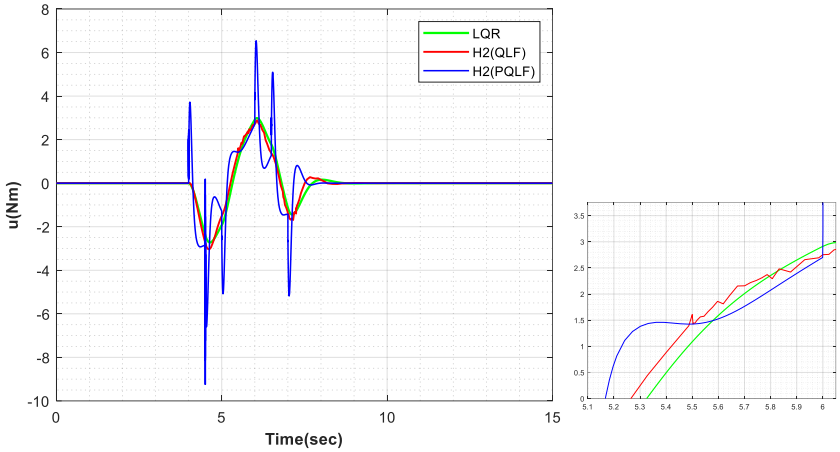

Fig. 4.12. Steering torque

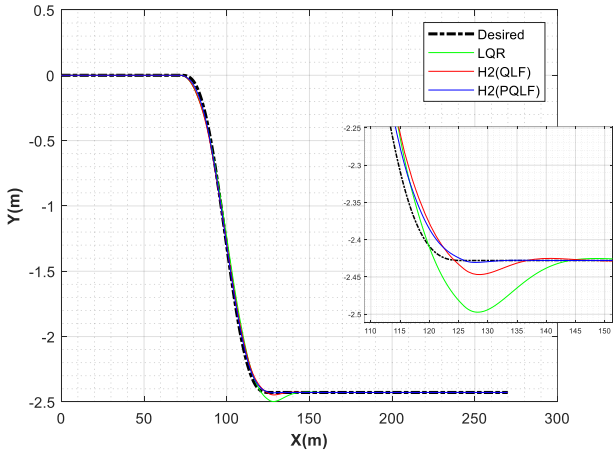

Fig. 4.13. Global vehicle XY trajectory

As it is observed, the performance of the closed-loop system is improved step by step by moving from the LQR controller to H_2 LPV controller with QLF, and from the latter to the H_2 LPV controller with PQLF. However, by observing the steering torque, one may conclude that although the mentioned enhancement is reached through the theoretical aspect, an AGV, in practice, encounters limitations in generating the steering torques that are commanded by the designed controllers. To tackle this issue, the H_2 LPV controller is tuned through its decay rate parameter to reach an acceptable performance in real-world applications, after which a fair and general comparison can be conducted between optimal and robust control methodologies.

- Subsection v:

Inspected simulation results in the previous subsections have a highlighted outcome, that is the H_2 LPV state feedback controller with PQLF has superiority in path-tracking mission in a controlled AGV. However, although the results are theoretically acceptable and confirm the developed strategies in this research, the practical applicability of the generated steering torques, as the control signals for use in a sample AGV must also be considered. Hence. The H_2 LPV state feedback controller is tuned with an acceptable decay rate parameter ($\alpha = 0.25$), and compared with the provided benchmark (the tuned LQR controller). The comparisons are conducted for both SLC and DLC standard test scenarios, where two longitudinal velocities are taken into consideration, the nominal velocity ($V = 18\ m/s$), and a high velocity deviated from the nominal one ($V = 25\ m/s$). The plots include generated steering torque, the lateral position error, the heading error, and the global vehicle and desired XY trajectories for each comparison case, where the represented tables give clearer investigation of the conducted comparison scenarios.

- **Single Lane Change (SLC) Scenario:**
- $\boldsymbol{V = 18\ m/s}$

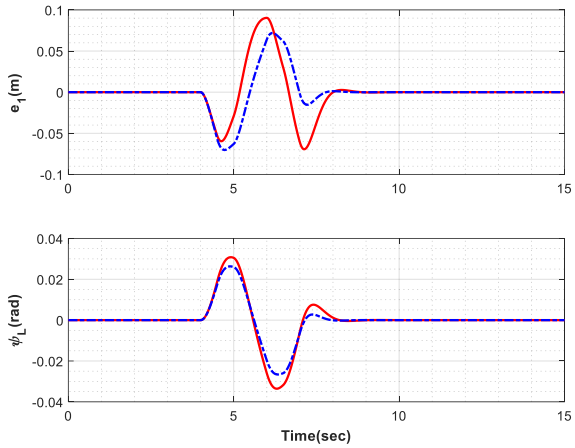

Fig. 4.14. **(Top)** Lateral position error, **(Bottom)** Heading error (LQR, H_2)

Table 4.4. Comparison between LQR, and H_2 w.r.t. the lateral position error

	$\boldsymbol{l_\infty}$	$\boldsymbol{rms}$
LQR	0.090333	0.030358
H_2	0.07192	0.037514

Table 4.5. Comparison between LQR, and H_2 w.r.t. the heading error

	$\boldsymbol{l_\infty}$	$\boldsymbol{rms}$
LQR	0.033571	0.011782
H_2	0.026625	0.013849

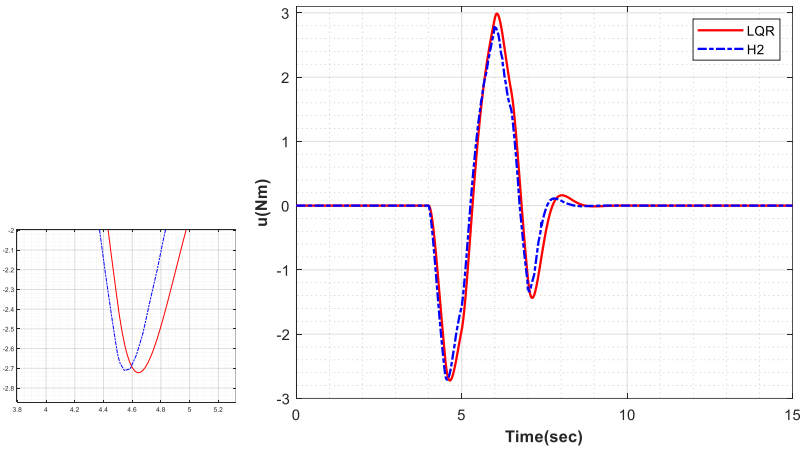

Fig. 4.15. Steering torque

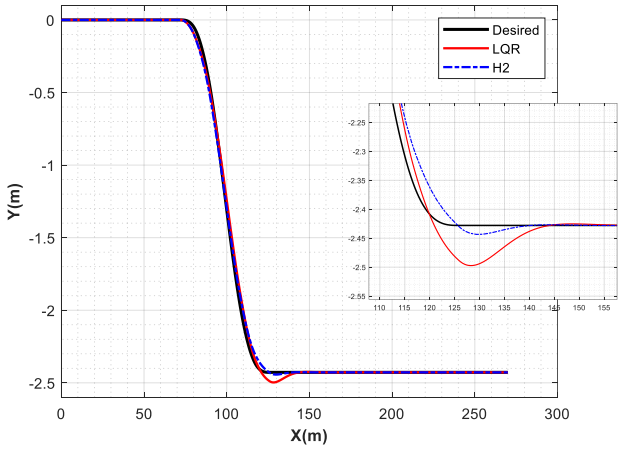

Fig. 4.16. Global vehicle XY trajectory

- $\boldsymbol{V = 25m/s}$

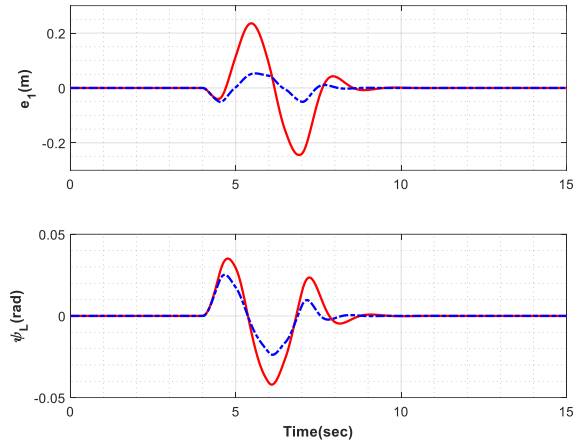

Fig. 4.17. **(Top)** Lateral position error, **(Bottom)** Heading error (LQR, H_2)

Table 4.6. Comparison between LQR, and H_2 w.r.t. the lateral position error

	$\boldsymbol{l_\infty}$	$\boldsymbol{rms}$
LQR	0.24433	0.085017
H_2	0.053232	0.027

Table 4.7. Comparison between LQR, and H_2 w.r.t. the heading error

	$\boldsymbol{l_\infty}$	$\boldsymbol{rms}$
LQR	0.042042	0.014075
H_2	0.025263	0.011188

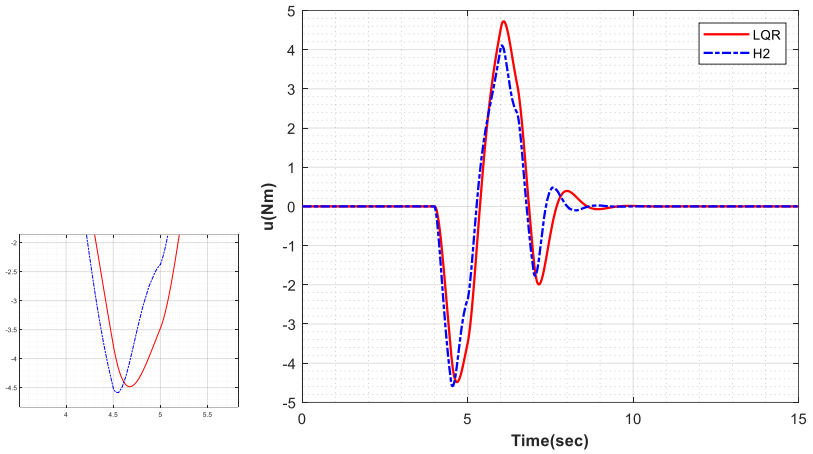

Fig. 4.18. Steering torque

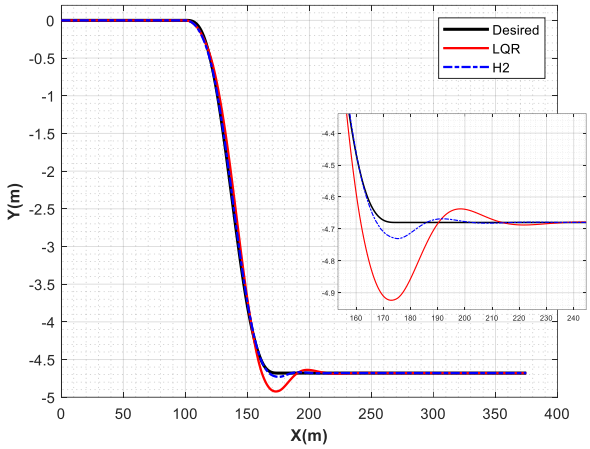

Fig. 4.19. Global vehicle XY trajectory

- **Double Lane Change (DLC) Scenario :**
- $\boldsymbol{V = 18\ m/s}$

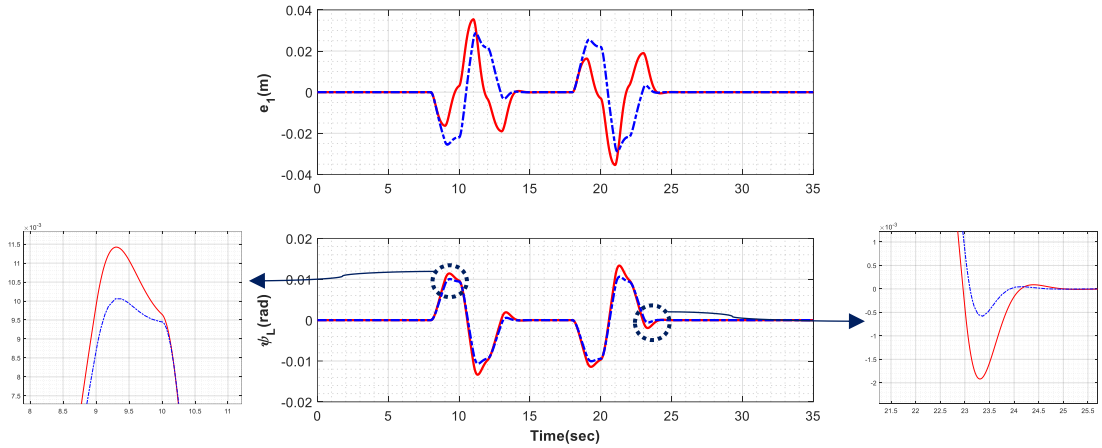

Fig. 4.20. **(Top)** Lateral position error, **(Bottom)** Heading error (LQR, H_2)

Table 4.8. Comparison between LQR, and H_2 w.r.t. the lateral position error

	$\boldsymbol{l_\infty}$	$\boldsymbol{rms}$
LQR	0.035427	0.010231
H_2	0.028798	0.01593

Table 4.9. Comparison between LQR, and H_2 w.r.t. the heading error

	$\boldsymbol{l_\infty}$	$\boldsymbol{rms}$
LQR	0.013352	0.0050909
H_2	0.010659	0.0058819

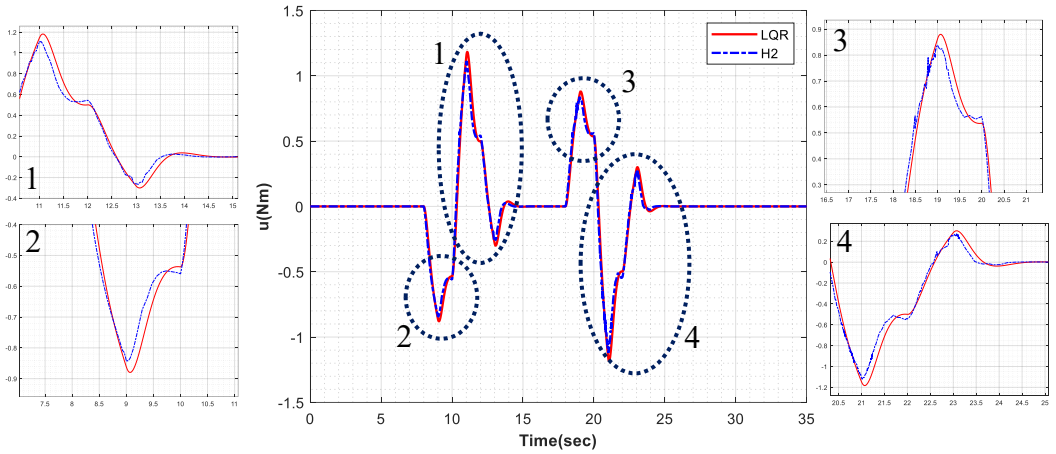

Fig. 4.21. Steering torque

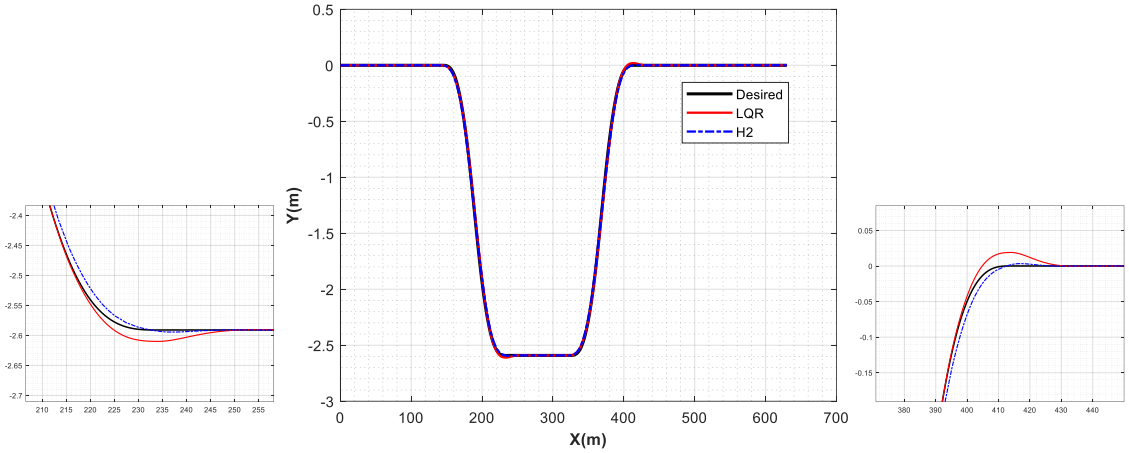

Fig. 4.22. Global vehicle XY trajectory

- $\boldsymbol{V = 25\ m/s}$
-

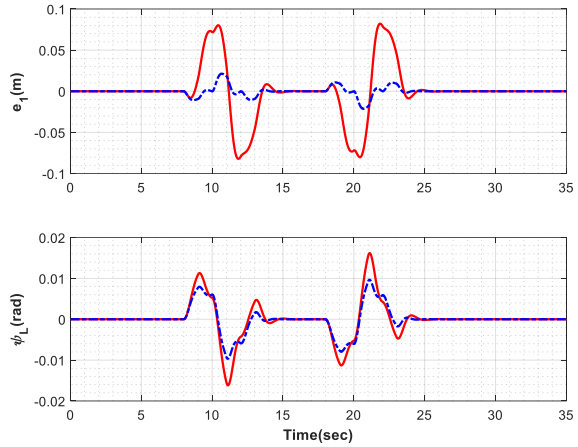

Fig. 4.23. **(Top)** Lateral position error, **(Bottom)** Heading error (LQR, H_2)

Table 4.10. Comparison between LQR, and H_2 w.r.t. the lateral position error

	$\boldsymbol{l_\infty}$	$\boldsymbol{rms}$
LQR	0.082094	0.034621
H_2	0.021436	0.0075031

Table 4.11. Comparison between LQR, and H_2 w.r.t. the heading error

	$\boldsymbol{l_\infty}$	$\boldsymbol{rms}$
LQR	0.016176	0.0048244
H_2	0.0096984	0.0043385

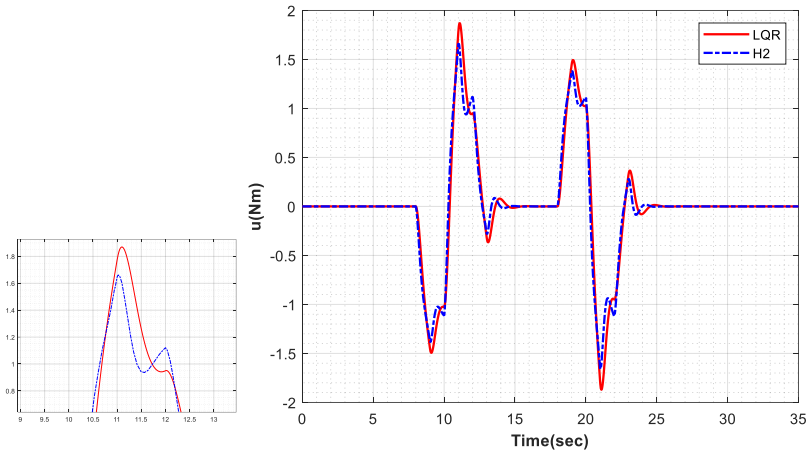

Fig. 4.24. Steering torque

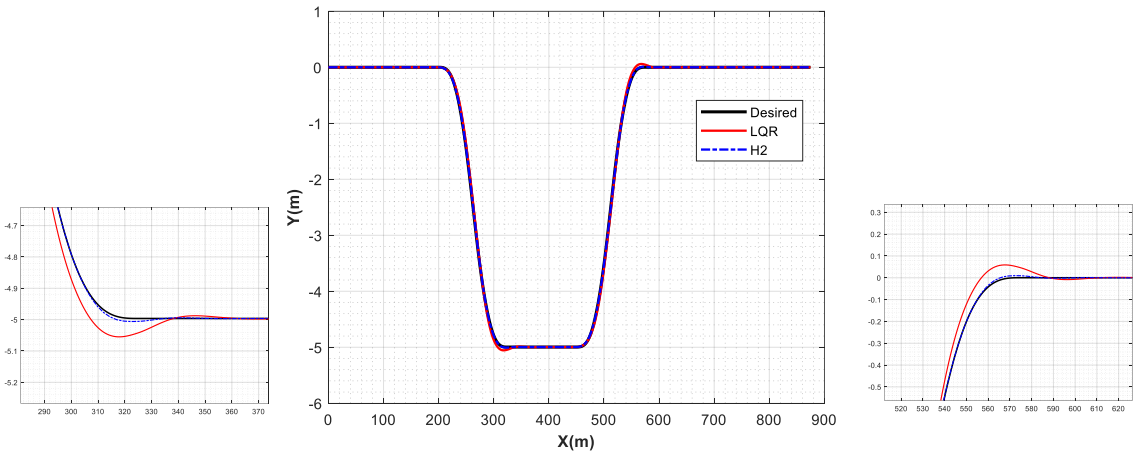

Fig. 4.25 Vehicle global XY trajectory

As anticipated, both optimal and robust controller shows almost the same performance at the nominal velocity ($V = 18\, m/s$) during the test scenarios. However, the developed H_2 LPV controller shows much better performance in the delegated path-following task when the road-vehicle system deviates from the nominal velocity since deviation from the nominal speed was considered in the design stages of the robust controller. In other words, in the H_2 LPV controller, the vehicle longitudinal velocity is considered as a varying parameter, whilst it is treated as a constant in the LQR synthesis.

One can better enhance the errors regarding the path-following task by having a feedforward gain, as another degree of freedom regarding the performance improvement, in the control law (one can refer to Chapter 2 or 4 for more information). However, since the diagrams related to the control structure with feedforward gain are very similar to those of the control structure without that gain, we have omitted the diagrams for the sake of brevity. The reason for this is that the magnitudes of road curvatures are small (see Fig. 4.2); and the effectiveness of this gain directly depends on the magnitudes of the considered road curvatures. Nevertheless, one can reduce the RMS value of the lateral position error, say for the last scenario, up to 4.10 %. In other words, the feedforward gain, in the last comparison scenario, decreases the RMS of lateral position error for the H_2 LPV controller from 0.0075301 to 0.0071955. Indeed, the greater the magnitude of the road curvature, the greater the effect of having a feedforward gain in the design structure of H_2 LPV controlling method.

- Subsection vi:

In this subsection, the performance of the LQR, and the tuned H_2 LPV state feedback controller are tested in the presence of a disturbance input. In more detail, the controlled AGV is assumed to be on the designated task of SLC scenario with the nominal velocity ($V = 18\ m/s$), when a lateral wind force is applied to the vehicle as the input disturbance, which is illustrated in Fig. 4.26. This choice, as a common natural phenomenon, is conventional in vehicle control applications. The reason behind the judicious choice of the time of applying the gust wind is that the reader can better observe and follow the performance of the mentioned optimal and robust controllers to face injected input disturbance. Unlike the previous subsection, the state trajectories, as well as the front and rear lateral forces, of the closed-loop systems are depicted in Fig. 4.30. This helps in understanding the effect of the gust wind on the side-slip angle, yaw rate, steering rate, etc., of the closed loop system. Moreover, the generated steering torques by these controllers are demonstrated in Fig. 4.28. One can observe the lateral position and heading errors in Fig. 4.27, and the vehicle global XY trajectory versus the desired path in Fig. 4.29. Tables. 4.12 and 4.13 conclude the robustness of each controller by investigating the RMS and L_∞ norm of both the lateral position and heading errors resulting from each method.

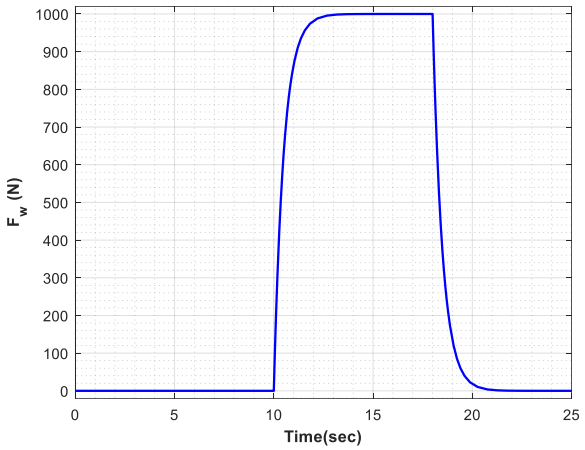

Fig. 4.26. Lateral wind force (injected disturbance)

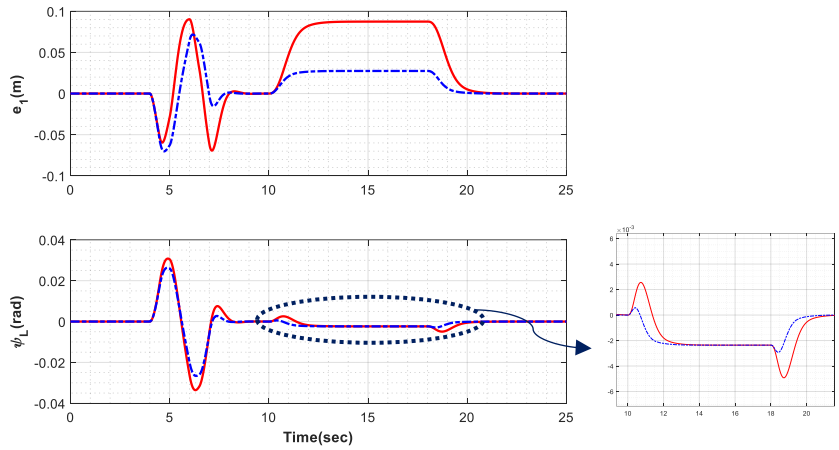

Fig. 4.27. Lateral position error

Table 4.12. Comparison between LQR, and H_2 w.r.t. the lateral position error

	l_∞	rms
LQR	0.090328	0.05599
H_2	0.071805	0.034765

Table 4.13. Comparison between LQR, and H_2 w.r.t. the heading error

	l_∞	rms
LQR	0.033573	0.0088795
H_2	0.026632	0.01232

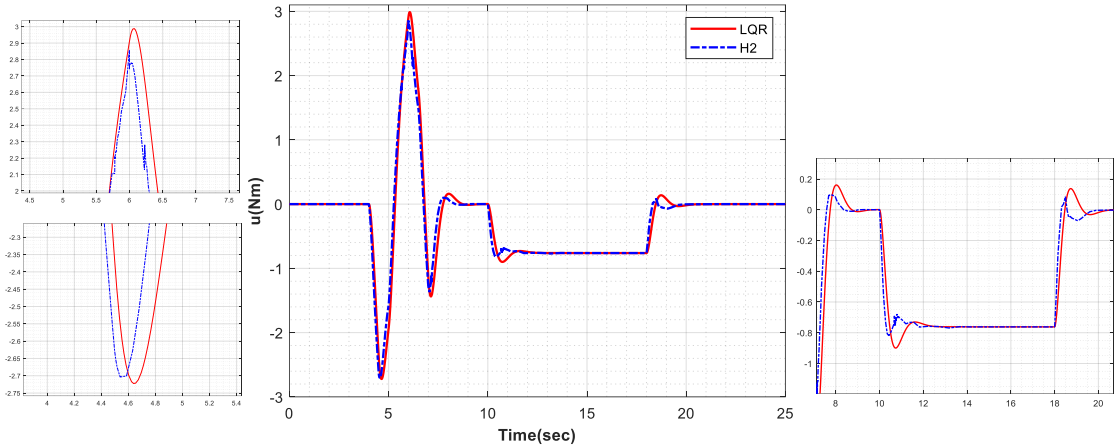

Fig. 4.28. Steering torque

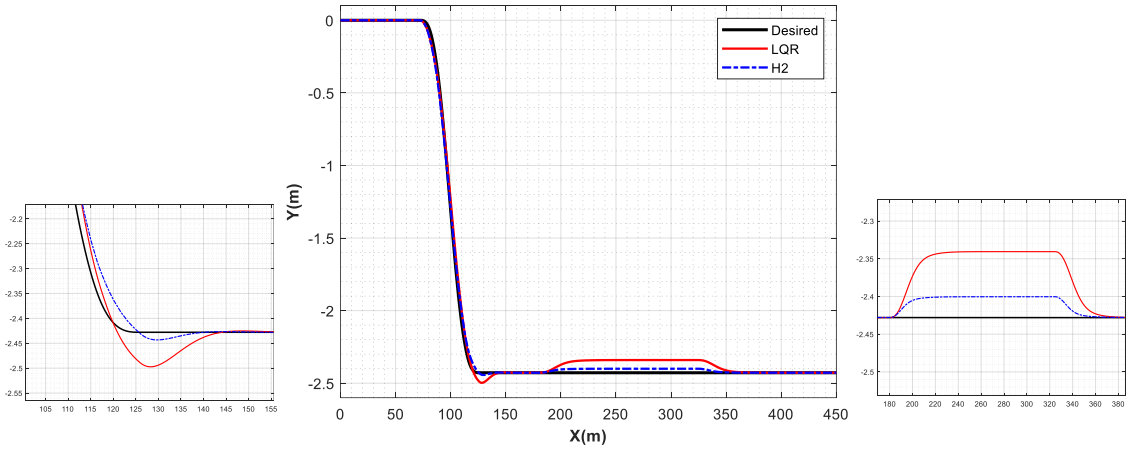

Fig. 4.29. Global vehicle XY trajectory

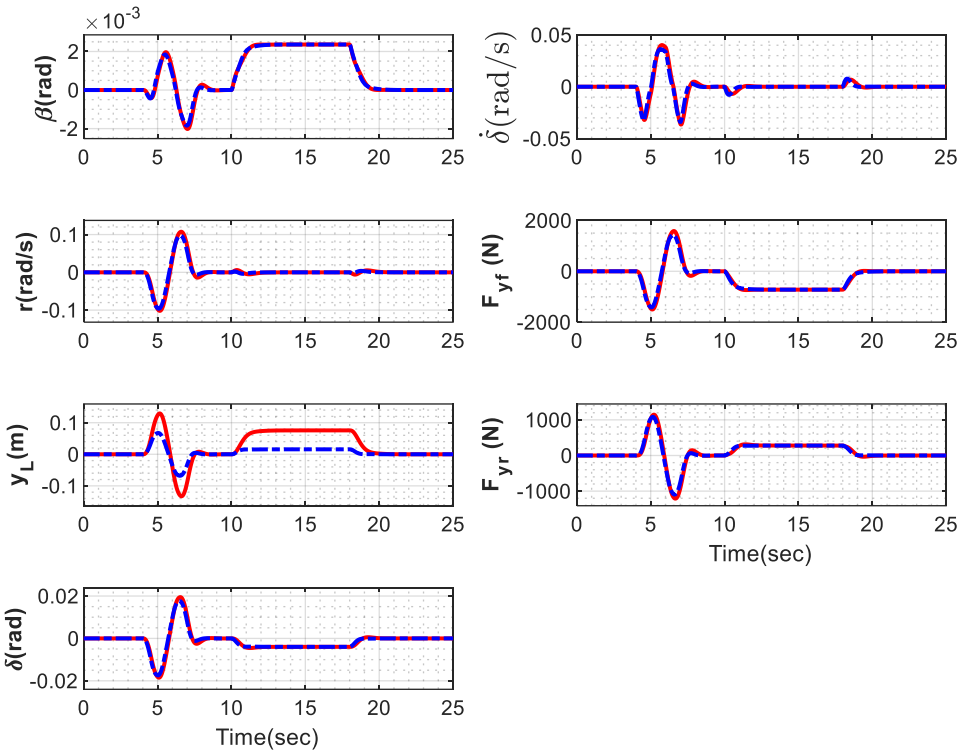

Fig. 4.30. From top to bottom: **(1)** Side-slip angle, **(2)** Yaw rate, **(3)** Lateral deviation error at the look-ahead distance, **(4)** Steering angle, **(5)** Steering rate, **(6)** Front lateral force, **(7)** Rear lateral force (LQR, H_2)

As intended, the H_2 LPV state feedback controller performs better in the disturbance attenuating task in comparison with the LQR controller even in the nominal velocity utilized for designing the LQR controller. The reason is that the H_2 scheme design minimizes the H_2 norm of the transfer function from the disturbance input ω to the performance output z, where the hired H_2 controller suppresses the impact of the disturbance by reducing the energy of the signal in the performance vector. On the other hand, the synthesize procedure of the LQR controller lacks considering the disturbance input, as well as performance output, including the weighted combinations of system states, outputs, and control inputs.

Chapter 5

Concluding Remarks and Future Work

5.1. Conclusion

In this thesis work, in the modeling phase, a general control-based road-vehicle system for AGVs was investigated. To obtain a more realistic model, the longitudinal velocity was considered as a varying parameter, forming a linear parameter varying (LPV) representation for the inspected road-vehicle system. It was shown that the represented LPV model mimics the nonlinear vehicle model behavior with fair precision. To support the control synthesis phase, a new scheduling variable was defined for the LPV model, and a polytopic LPV representation of the road-vehicle system was developed using first-order Taylor approximation. The accuracy of the polytopic LPV model was evaluated by comparing it with the nonlinear vehicle model, and the results demonstrated satisfactory alignment and reliability.

In the control design phase, a Linear Quadratic Regulator (LQR) controller was first designed for a linearized model of the nonlinear road-vehicle system. This approach was aimed to act as a benchmark for the developed controllers in this thesis study. To design this LQR controller, after defining a performance cost function and a state feedback control law, an optimization problem, in terms of Linear Matrix Inequalities (LMIs), was formulated to render the controller gain. The reason for such a design was rooted in integrating the control synthesis approaches between the benchmark and understudy control strategies in Chapter 4. It should be noted that the weighting parameters of the LQR controller, Q and R, were tuned to provide a context in which a fair and strict comparison could be conducted between all proposed controllers of this research study. In Chapter 4, an LPV controller was designed based on state feedback control law, where an H_2 scheme was considered in the design procedure to guarantee the performance of the controller in both reducing the lateral position and heading errors, whilst attenuating the effect of wind lateral forces as the disturbance input. These performance criteria lead to nothing but the passengers' comfort and safety. This thesis leveraged LMI techniques to form the controller design conditions as convex optimization problems. Such an approach resolves the serious problems existing regarding heuristic optimization approaches that suffer from computational costs and get trapped in local optima solutions. Moreover, a decay rate was introduced and tuned in the design procedure

ending in both fast tracking and less amount of errors (i.e. lateral position and heading errors) in the path-following task of autonomous vehicles. To ensure the stability of the controlled autonomous vehicle, the Lyapunov theory, and specifically, the Quadratic Lyapunov Function (QLF) and Poly-Quadratic Lyapunov Function (PQLF) were employed, leading to two different control approaches. The latter ensured deriving better decay rates, and less amount of errors for both lateral position and heading angle, by improving the upper bound of the H_2 norm in the H_2 scheme-based control methodology, which resulted in better performance of the closed-loop system. In addition, an extra condition was added to the developed optimization problem to limit the rendered controller's gain. This can be beneficial through practical aspects when it comes to the experimental implementation of the proposed controllers for AGVs. Furthermore, a feedforward gain was included in the defined control law to form a feedback-feedforward control structure. This framework takes advantage of the future information of the road geometry to enhance the path-following performance of the automated vehicle, and alleviate the lateral position and heading errors in comparison with the control structure which only benefits from the feedback loop.

The two designed controllers were tested in Single Lane Change (SLC) and Double Lane Change (DLC) situations, as the standard test scenarios in AGVs' applications, to verify the stability and effectiveness of the proposed controllers. Moreover, a comparison was conducted between the designed controllers and the LQR one, where designed controllers showed promising results in decreasing the targeted errors in the path-following operation. Moreover, the performance of the two designed controllers, as well as the LQR controller, were tested in a disturbance attenuation scenario with a significant wind gust as the injected disturbance. As shown, the designed controllers showed more favorable results in this aspect too. It should be noted that the represented control approaches of this thesis work show a decent performance in handling different longitudinal velocities rather than the nominal one, making them capable of handling varying longitudinal velocities, which is common in real-world applications.

All these outcomes illustrated the superiority of the synthesized controllers in i) well-established stability of the controlled autonomous vehicle, ii) passengers' comfort and safety, iii) disturbance attenuation, and (iv) applicability in real-world applications.

5.2. Future Work

Some future works that can be considered are as follows:

- To reduce reliance on costly vehicle sensors, the design procedures could be reformulated to implement an output feedback control law instead of a state feedback one. While this may result in slightly larger lateral position and heading errors during lane-keeping, it relies only on commonly available vehicle sensors, making it advantageous for both the commercialization of AGVs and real-time implementation.
- While the H_2 scheme was found more effective for minimizing the average errors over the entire trajectory rather than addressing specific overshoots, an H_∞ scheme could be adopted as an alternative design approach. This would allow the incorporation of the steering torque magnitude into the control performance specifications and enable the inclusion of a feedforward gain in the control law structure. The suitability of the H_∞ methodology lies in its lack of restrictions on the D matrix being zero in the state-space representation of the targeted systems.
- A switched-LPV control framework, which utilizes switched LPV models, can be developed to cover a wider range of variations in vehicle longitudinal velocity. In addition, since such a control structure utilizes multiple parameter-dependent Lyapunov functions, it can even more reduce the conservatism of the synthesis procedure. For this switched-LPV approach, a hysteresis switching law can be considered to guarantee a safe and smooth switching between the determined LPV subregions.
- Through an interpolation method, or more clearly, through the Youla-Koucera Parameterization-based interpolating controller, different controllers can be designed independently to serve different driving circumstances or objectives. Then, by conducting an interpolation between them, the desired performance in autonomous vehicles can be achieved in a safe, smooth, and blending fashion. This allows the control structure to have the required percentage of contribution from all designed controllers simultaneously, where a designed supervisory signal decides the aforementioned amount of contribution received from each controller.

Appendices

Appendix 1: Convex Optimization

The structure of a given optimization problem is as follows:

$$\min(f_x)$$
$$s.t.\ \ g_i(x) < 0,\ \ i = 1,2,\dots,m,\ \ x = (x_1,\dots,x_n). \tag{A.81}$$

An optimization problem can be divided into the three following main parts:

1) Objective function or optimization index
2) Constraints
3) Decision variables

The following are some standard definitions of convex optimization problems [104]:

- Convex set:

A set is convex if and only if for any two given points of that set in the linear vector space, the following relation holds true:

$$\{x_1, x_2\} \in S \Rightarrow \{x \coloneqq \alpha x_1 + (1-\alpha)x_2 \in S \ \ \forall \ \ \alpha \in (0,1)\}. \tag{A.82}$$

- Convex combinations:

Consider a subspace of a vector space S, then $x \coloneqq \Sigma_{i=1}^{n}\alpha_i x_i$ is a convex combination of $x_1, x_2, \dots, x_n$ such that $\Sigma_{i=1}^{n}\alpha_i = 1$, and $\alpha_i \geq 0$.

- Convex hull:

For any given set S, another set that results from all convex combinations of all members of S is called the convex hull of the set S and is denoted by $conv(S)$. The convex hull of a set is convex even if the set itself is not a convex set.

- Convex function:

A function $f: S \to R$ is convex if and only if i) its domain is convex, ii) for any given x_1 and x_2 that belong to the domain of that function, the following inequality is established:

$$f(\alpha x_1 + (1-\alpha)x_2) \leq \alpha f(x_1) + (1-\alpha)f(x_2). \tag{A.83}$$

- Affine function:

A function $f: S \to R$ is affine if and only if for any given x_1 and x_2 in the set S, and for any $\alpha \in \mathbb{R}$, the following is established:

$$f(\alpha x_1 + (1-\alpha)x_2) = \alpha f(x_1) + (1-\alpha) f(x_2). \quad \text{(A.84)}$$

An affine function is a convex function.

- Local and global minima:

The point $x_0 \in S$ is a minimum of function $f: S \to R$ if and only if $\epsilon > 0$ exists such that:

$$f(x_0) \leq f(x) \quad \forall \quad x \in S, \quad \|x - x_0\| < \varepsilon. \quad \text{(A.85)}$$

If:

$$f(x_0) \leq f(x) \quad \forall \quad x \in S, \quad \text{(A.86)}$$

Then x_0 is the global minimum.

Theorem A.1 [104]**:** If the function $f: S \to R$ is convex, then any local extremum of the function is its global extremum.

A common challenge in solving optimization problems is the risk of converging to a local extremum rather than the desired global extremum. This issue is eliminated in convex functions, as any local extremum of a convex function is also its global extremum. In other words, finding the global extremum of a convex function can be achieved by using standard optimization methods, such as the Newton-Raphson method, to identify its local extremum.

Theorem A.2 [104]**:** If the function $f: S \to R$ is a convex function, and if one has $S = conv(S_0)$, then:

$$f(x) < \gamma \quad \forall \quad x \in (S) \Leftrightarrow f(x) < \gamma \quad \forall \quad x \in S_0. \quad \text{(A.87)}$$

In other words, if the condition $f(x) < \gamma$ is valid for all the corner points (S_0), the mentioned relation, $f(x) < \gamma$, holds true for any points in the convex hull resulting from those corner points.

Based on the abovementioned definitions, one has the following definition for the convex optimization:

- Convex optimization:

If the domain of the answer is convex, in addition to the convexity of its objective function, the optimization problem is a convex programming problem. It should be pointed out that two numerical tools, i) the Interior Point method and ii) the Ellipsoidal method, can be employed to solve such optimization problems.

Appendix 2: Introduction to Linear Matrix Inequalities

The structure of Linear Matrix Inequalities (LMIs) is defined as follows [94]:

$$F(x) = F_0 + x_1F_1 + \cdots + x_nF_n < 0, \tag{A.88}$$

where $x = [x_1, \dots, x_n]$ are matrix variables recognized as decision variables. In addition, $F_0, \dots, F_n$ are real symmetric matrices. As a result, $F(x)$ is an affine function of decision variables. Since $F(x)$ is a convex function, the set of decision variables in $F(x) < 0$ constitute a convex function. Therefore, the Interior Point method and the Ellipsoidal method can be used to solve LMIs [104] and [94]. In the following, different LMI problems will be investigated [94].

- Feasibility problem:

Consider the following general form:

$$F(x) < 0. \tag{A.89}$$

The goal of this kind of LMI problem is to find decision variables that satisfy (A.89). In other words, only the existence of the answer is concerned, and no optimization is performed.

- Linear Objective Minimization problem:

Consider the following expression:

$$\begin{aligned} &minimize \quad \alpha(x_1, \dots, x_n) \\ &s.t. \quad F(x_1, \dots, x_n) < 0. \end{aligned} \tag{A.90}$$

In these problems, the target is to optimize the scalar function $\alpha(.)$ with decision variables of (A.90) acting as constraints for the given optimization problem.

- Generalized Eigenvalue problem:

The general form of a Generalized Eigenvalue problem is given as follows:

$$\begin{aligned} &minimize \quad \lambda \\ &s.t. \quad F_1(x_1, \dots, x_n) + \lambda F_2(x_1, \dots, x_n) < 0, \end{aligned} \tag{A.91}$$

$$F_2(x_1, \dots, x_n) < 0,$$
$$F_3(x_1, \dots, x_n) < 0.$$

In some control design procedures, the problems are in a Nonlinear Matrix Inequalities form. In other words, the in-hand problem is in the form of a nonlinear function of decision variables. In such problems, one can try to transform the problem into an LMI and solve that optimization problem via convex LMI solvers. In this context, some lemmas are provided and widely used for transforming a Nonlinear Matrix Inequality to an LMI [94].

- Lemma 1: Congruence Transformation

If $Q \in \mathbb{R}^{n\times n}$ is positive (negative) definite, another real matrix $W \in \mathbb{R}^{n\times n}$ with the rank n can be considered such that:

$$W^T Q W > 0 \quad or \quad W^T Q W < 0. \tag{A.92}$$

In other words, the definiteness of a matrix is not changed if it is pre and post-multiplied by a real full-rank matrix.

- Lemma 2: Schur Complement

Schur complement expresses that the three following expressions are equal:

$$\begin{aligned} &1)\ F = \begin{bmatrix} A & B \\ B^T & C \end{bmatrix} < 0 \\ &2)\ \mathrm{A} < 0\ \&\ \mathrm{C} - \mathrm{B}^{\mathrm{T}} A^{-1} B < 0 \\ &3)\ C < 0\ \&\ A - BC^{-1}B^T < 0 \end{aligned} \tag{A.93}$$

Appendix 3: Tuan's Relaxation Lemma [105] and [4]

Given the symmetric matrices of appropriate dimensions ($\mathrm{T}_{ij}, i, j \in \Omega_N$), and a family of functions ($\{\eta_i\}, i \in \Omega_N$) with the following characteristics:

$$\eta_i \geq 0, \sum_{i=1}^{N} \eta_i = 1, \sum_{i=1}^{N} \dot{\eta}_i = 0\,, \tag{A.14}$$

The inequality

$$\sum_{i=1}^{N}\sum_{j=1}^{N} \eta_i \eta_j \mathrm{T}_{ij} < 0\,, \tag{A.15}$$

is satisfied if

$$\begin{cases} \mathrm{T}_{ii} < 0, & i \in \Omega_N \\ \dfrac{2}{N-1}\mathrm{T}_{ii} + \mathrm{T}_{ij} + \mathrm{T}_{ji} < 0, & i, j \in \Omega_N, \text{and } i < j \end{cases} \tag{A.16}$$

References:

[1] B. Paden, M. Cap, S. Z. Yong, D. Yershov, and E. Frazzoli, "A Survey of Motion Planning and Control Techniques for Self-Driving Urban Vehicles," *IEEE Trans. Intell. Veh.*, vol. 1, no. 1, pp. 33–55, Mar. 2016, doi: 10.1109/TIV.2016.2578706.

[2] A.-T. Nguyen, C. Sentouh, H. Zhang, and J.-C. Popieul, "Fuzzy Static Output Feedback Control for Path Following of Autonomous Vehicles With Transient Performance Improvements," *IEEE Trans. Intell. Transp. Syst.*, vol. 21, no. 7, pp. 3069–3079, Jul. 2020, doi: 10.1109/TITS.2019.2924705.

[3] S. El Hamdani and N. Benamar, "Autonomous Traffic Management: Open Issues and New Directions," in *2018 International Conference on Selected Topics in Mobile and Wireless Networking (MoWNeT)*, Tangier: IEEE, Jun. 2018, pp. 1–5. doi: 10.1109/MoWNet.2018.8428937.

[4] A.-T. Nguyen, P. Chevrel, and F. Claveau, "On the Effective Use of Vehicle Sensors for Automatic Lane Keeping via LPV Static Output Feedback Control," *IFAC-Pap.*, vol. 50, no. 1, pp. 13808–13815, Jul. 2017, doi: 10.1016/j.ifacol.2017.08.2072.

[5] C. Hu, H. Jing, R. Wang, F. Yan, and M. Chadli, "Robust H ∞ output-feedback control for path following of autonomous ground vehicles," *Mech. Syst. Signal Process.*, vol. 70–71, pp. 414–427, Mar. 2016, doi: 10.1016/j.ymssp.2015.09.017.

[6] J.-M. Park, D.-W. Kim, Y.-S. Yoon, H. J. Kim, and K.-S. Yi, "Obstacle avoidance of autonomous vehicles based on model predictive control," *Proc. Inst. Mech. Eng. Part J. Automob. Eng.*, vol. 223, no. 12, pp. 1499–1516, Dec. 2009, doi: 10.1243/09544070JAUTO1149.

[7] P. Talwar, "Autonomous Vehicle Safety Overview," *Int. Res. J. Mod. Eng. Technol. Sci.*, vol. 03, no. 05, May 2021.

[8] A. Broggi, P. Medici, P. Zani, A. Coati, and M. Panciroli, "Autonomous vehicles control in the VisLab Intercontinental Autonomous Challenge," *Annu. Rev. Control*, vol. 36, no. 1, pp. 161–171, Apr. 2012, doi: 10.1016/j.arcontrol.2012.03.012.

[9] L. Li, D. Wen, N.-N. Zheng, and L.-C. Shen, "Cognitive Cars: A New Frontier for ADAS Research," *IEEE Trans. Intell. Transp. Syst.*, vol. 13, no. 1, pp. 395–407, Mar. 2012, doi: 10.1109/TITS.2011.2159493.

[10] C. Sentouh, A.-T. Nguyen, M. A. Benloucif, and J.-C. Popieul, "Driver-Automation Cooperation Oriented Approach for Shared Control of Lane Keeping Assist Systems," *IEEE Trans. Control Syst. Technol.*, vol. 27, no. 5, pp. 1962–1978, Sep. 2019, doi: 10.1109/TCST.2018.2842211.

[11] Wenda Xu, Junqing Wei, J. M. Dolan, Huijing Zhao, and Hongbin Zha, "A real-time motion planner with trajectory optimization for autonomous vehicles," in *2012 IEEE International Conference on Robotics and Automation*, St Paul, MN, USA: IEEE, May 2012, pp. 2061–2067. doi: 10.1109/ICRA.2012.6225063.

[12] S. Zhu and B. Aksun-Guvenc, "Trajectory Planning of Autonomous Vehicles Based on Parameterized Control Optimization in Dynamic on-Road Environments," *J. Intell. Robot. Syst.*, vol. 100, no. 3–4, pp. 1055–1067, Dec. 2020, doi: 10.1007/s10846-020-01215-y.

[13] W. Lim, S. Lee, M. Sunwoo, and K. Jo, "Hierarchical Trajectory Planning of an Autonomous Car Based on the Integration of a Sampling and an Optimization Method," *IEEE Trans. Intell. Transp. Syst.*, vol. 19, no. 2, pp. 613–626, Feb. 2018, doi: 10.1109/TITS.2017.2756099.

[14] C. Liu, S. Lee, S. Varnhagen, and H. E. Tseng, “Path planning for autonomous vehicles using model predictive control,” in *2017 IEEE Intelligent Vehicles Symposium (IV)*, Los Angeles, CA, USA: IEEE, Jun. 2017, pp. 174–179. doi: 10.1109/IVS.2017.7995716.
[15] S. Magdici and M. Althoff, “Adaptive Cruise Control with Safety Guarantees for Autonomous Vehicles,” *IFAC-Pap.*, vol. 50, no. 1, pp. 5774–5781, Jul. 2017, doi: 10.1016/j.ifacol.2017.08.418.
[16] C. Wang, S. Gong, A. Zhou, T. Li, and S. Peeta, “Cooperative adaptive cruise control for connected autonomous vehicles by factoring communication-related constraints,” *Transp. Res. Part C Emerg. Technol.*, vol. 113, pp. 124–145, Apr. 2020, doi: 10.1016/j.trc.2019.04.010.
[17] R. Rajamani and C. Zhu, “Semi-autonomous adaptive cruise control systems,” *IEEE Trans. Veh. Technol.*, vol. 51, no. 5, pp. 1186–1192, Sep. 2002, doi: 10.1109/TVT.2002.800617.
[18] C. Desjardins and B. Chaib-draa, “Cooperative Adaptive Cruise Control: A Reinforcement Learning Approach,” *IEEE Trans. Intell. Transp. Syst.*, vol. 12, no. 4, pp. 1248–1260, Dec. 2011, doi: 10.1109/TITS.2011.2157145.
[19] Z. Gacovski and S. Deskovski, “Different Control Algorithms for a Platoon of Autonomous Vehicles,” *IAES Int. J. Robot. Autom. IJRA*, vol. 3, no. 3, Sep. 2014, doi: 10.11591/ijra.v3i3.5591.
[20] B. Peng, D. Yu, H. Zhou, X. Xiao, and Y. Fang, “A Platoon Control Strategy for Autonomous Vehicles Based on Sliding-Mode Control Theory,” *IEEE Access*, vol. 8, pp. 81776–81788, 2020, doi: 10.1109/ACCESS.2020.2990644.
[21] K. Li, J. Wang, and Y. Zheng, “Cooperative Formation of Autonomous Vehicles in Mixed Traffic Flow: Beyond Platooning,” *IEEE Trans. Intell. Transp. Syst.*, vol. 23, no. 9, pp. 15951–15966, Sep. 2022, doi: 10.1109/TITS.2022.3146612.
[22] J. Wang, S. Gong, S. Peeta, and L. Lu, “A real-time deployable model predictive control-based cooperative platooning approach for connected and autonomous vehicles,” *Transp. Res. Part B Methodol.*, vol. 128, pp. 271–301, Oct. 2019, doi: 10.1016/j.trb.2019.08.002.
[23] K. Min and J. Choi, “A control system for autonomous vehicle valet parking,” in *2013 13th International Conference on Control, Automation and Systems (ICCAS 2013)*, Gwangju, Korea (South): IEEE, Oct. 2013, pp. 1714–1717. doi: 10.1109/ICCAS.2013.6704211.
[24] K.-W. Min and J.-D. Choi, “Design and implementation of autonomous vehicle valet parking system,” in *16th International IEEE Conference on Intelligent Transportation Systems (ITSC 2013)*, The Hague, Netherlands: IEEE, Oct. 2013, pp. 2082–2087. doi: 10.1109/ITSC.2013.6728536.
[25] M. R. Heinen, F. S. Osorio, F. J. Heinen, and C. Kelber, “SEVA3D: Using Arti cial Neural Networks to Autonomous Vehicle Parking Control,” in *The 2006 IEEE International Joint Conference on Neural Network Proceedings*, Vancouver, BC, Canada: IEEE, 2006, pp. 4704–4711. doi: 10.1109/IJCNN.2006.247124.
[26] P. Cheedalla and M. Karanam, “Parallel Parking and Parking Assist System for Autonomous and Semi-Autonomous Vehicles,” in *2022 10th International Conference on Reliability, Infocom Technologies and Optimization (Trends and Future Directions) (ICRITO)*, Noida, India: IEEE, Oct. 2022, pp. 1–6. doi: 10.1109/ICRITO56286.2022.9964917.
[27] X. Meng, H. Wang, and B. Liu, “A Robust Vehicle Localization Approach Based on GNSS/IMU/DMI/LiDAR Sensor Fusion for Autonomous Vehicles,” *Sensors*, vol. 17, no. 9, p. 2140, Sep. 2017, doi: 10.3390/s17092140.

[28] G. Wan *et al.*, “Robust and Precise Vehicle Localization Based on Multi-Sensor Fusion in Diverse City Scenes,” in *2018 IEEE International Conference on Robotics and Automation (ICRA)*, Brisbane, QLD: IEEE, May 2018, pp. 4670–4677. doi: 10.1109/ICRA.2018.8461224.
[29] W. Farag, “Kalman-filter-based sensor fusion applied to road-objects detection and tracking for autonomous vehicles,” *Proc. Inst. Mech. Eng. Part J. Syst. Control Eng.*, vol. 235, no. 7, pp. 1125–1138, Aug. 2021, doi: 10.1177/0959651820975523.
[30] F. A. Butt, J. N. Chattha, J. Ahmad, M. U. Zia, M. Rizwan, and I. H. Naqvi, “On the Integration of Enabling Wireless Technologies and Sensor Fusion for Next-Generation Connected and Autonomous Vehicles,” *IEEE Access*, vol. 10, pp. 14643–14668, 2022, doi: 10.1109/ACCESS.2022.3145972.
[31] J. Wu, J. Zhang, Y. Tian, and L. Li, “A Novel Adaptive Steering Torque Control Approach for Human–Machine Cooperation Autonomous Vehicles,” *IEEE Trans. Transp. Electrification*, vol. 7, no. 4, pp. 2516–2529, Dec. 2021, doi: 10.1109/TTE.2021.3083679.
[32] A.-T. Nguyen, J. J. Rath, C. Lv, T.-M. Guerra, and J. Lauber, “Human-Machine Shared Driving Control for Semi-Autonomous Vehicles Using Level of Cooperativeness,” *Sensors*, vol. 21, no. 14, p. 4647, Jul. 2021, doi: 10.3390/s21144647.
[33] U. E. Manawadu, M. Kamezaki, M. Ishikawa, T. Kawano, and S. Sugano, “A multimodal human-machine interface enabling situation-adaptive control inputs for highly automated vehicles,” in *2017 IEEE Intelligent Vehicles Symposium (IV)*, Los Angeles, CA, USA: IEEE, Jun. 2017, pp. 1195–1200. doi: 10.1109/IVS.2017.7995875.
[34] C. Huang, C. Lv, F. Naghdy, and H. Du, “Reference-free approach for mitigating human–machine conflicts in shared control of automated vehicles,” *IET Control Theory Appl.*, vol. 14, no. 18, pp. 2752–2763, Dec. 2020, doi: 10.1049/iet-cta.2020.0289.
[35] Y. S. Son, W. Kim, S.-H. Lee, and C. C. Chung, “Robust Multirate Control Scheme With Predictive Virtual Lanes for Lane-Keeping System of Autonomous Highway Driving,” *IEEE Trans. Veh. Technol.*, vol. 64, no. 8, pp. 3378–3391, Aug. 2015, doi: 10.1109/TVT.2014.2356204.
[36] X. Li, Z. Sun, D. Cao, D. Liu, and H. He, “Development of a new integrated local trajectory planning and tracking control framework for autonomous ground vehicles,” *Mech. Syst. Signal Process.*, vol. 87, pp. 118–137, Mar. 2017, doi: 10.1016/j.ymssp.2015.10.021.
[37] M. Brown, J. Funke, S. Erlien, and J. C. Gerdes, “Safe driving envelopes for path tracking in autonomous vehicles,” *Control Eng. Pract.*, vol. 61, pp. 307–316, Apr. 2017, doi: 10.1016/j.conengprac.2016.04.013.
[38] L. Menhour, B. d’Andrea-Novel, M. Fliess, D. Gruyer, and H. Mounier, “An Efficient Model-Free Setting for Longitudinal and Lateral Vehicle Control: Validation Through the Interconnected Pro-SiVIC/RTMaps Prototyping Platform,” *IEEE Trans. Intell. Transp. Syst.*, vol. 19, no. 2, pp. 461–475, Feb. 2018, doi: 10.1109/TITS.2017.2699283.
[39] R. Marino, S. Scalzi, and M. Netto, “Nested PID steering control for lane keeping in autonomous vehicles,” *Control Eng. Pract.*, vol. 19, no. 12, pp. 1459–1467, Dec. 2011, doi: 10.1016/j.conengprac.2011.08.005.
[40] G. Tagne, R. Talj, and A. Charara, “Design and Comparison of Robust Nonlinear Controllers for the Lateral Dynamics of Intelligent Vehicles,” *IEEE Trans. Intell. Transp. Syst.*, vol. 17, no. 3, pp. 796–809, Mar. 2016, doi: 10.1109/TITS.2015.2486815.

[41] K. Lee, S. E. Li, and D. Kum, “Synthesis of Robust Lane Keeping Systems: Impact of Controller and Design Parameters on System Performance,” *IEEE Trans. Intell. Transp. Syst.*, vol. 20, no. 8, pp. 3129–3141, Aug. 2019, doi: 10.1109/TITS.2018.2873101.
[42] U. Rosolia, S. De Bruyne, and A. G. Alleyne, “Autonomous Vehicle Control: A Nonconvex Approach for Obstacle Avoidance,” *IEEE Trans. Control Syst. Technol.*, vol. 25, no. 2, pp. 469–484, Mar. 2017, doi: 10.1109/TCST.2016.2569468.
[43] R. Attia, R. Orjuela, and M. Basset, “Combined longitudinal and lateral control for automated vehicle guidance,” *Veh. Syst. Dyn.*, vol. 52, no. 2, pp. 261–279, Feb. 2014, doi: 10.1080/00423114.2013.874563.
[44] P. Falcone, F. Borrelli, J. Asgari, H. E. Tseng, and D. Hrovat, “Predictive Active Steering Control for Autonomous Vehicle Systems,” *IEEE Trans. Control Syst. Technol.*, vol. 15, no. 3, pp. 566–580, May 2007, doi: 10.1109/TCST.2007.894653.
[45] E. Kayacan, H. Ramon, and W. Saeys, “Robust Trajectory Tracking Error Model-Based Predictive Control for Unmanned Ground Vehicles,” *IEEEASME Trans. Mechatron.*, vol. 21, no. 2, pp. 806–814, Apr. 2016, doi: 10.1109/TMECH.2015.2492984.
[46] J. Funke, M. Brown, S. M. Erlien, and J. C. Gerdes, “Collision Avoidance and Stabilization for Autonomous Vehicles in Emergency Scenarios,” *IEEE Trans. Control Syst. Technol.*, vol. 25, no. 4, pp. 1204–1216, Jul. 2017, doi: 10.1109/TCST.2016.2599783.
[47] J. Suh, H. Chae, and K. Yi, “Stochastic Model-Predictive Control for Lane Change Decision of Automated Driving Vehicles,” *IEEE Trans. Veh. Technol.*, vol. 67, no. 6, pp. 4771–4782, Jun. 2018, doi: 10.1109/TVT.2018.2804891.
[48] J. Wang, G. Zhang, R. Wang, S. C. Schnelle, and J. Wang, “A Gain-Scheduling Driver Assistance Trajectory-Following Algorithm Considering Different Driver Steering Characteristics,” *IEEE Trans. Intell. Transp. Syst.*, vol. 18, no. 5, pp. 1097–1108, May 2017, doi: 10.1109/TITS.2016.2598792.
[49] M. Chilali and P. Gahinet, “H/sub ∞/ design with pole placement constraints: an LMI approach,” *IEEE Trans. Autom. Control*, vol. 41, no. 3, pp. 358–367, Mar. 1996, doi: 10.1109/9.486637.
[50] J. Wang, M. Dai, G. Yin, and N. Chen, “Output-feedback robust control for vehicle path tracking considering different human drivers’ characteristics,” *Mechatronics*, vol. 50, pp. 402–412, Apr. 2018, doi: 10.1016/j.mechatronics.2017.05.001.
[51] A.-T. Nguyen, C. Sentouh, and J.-C. Popieul, “Sensor Reduction for Driver-Automation Shared Steering Control via an Adaptive Authority Allocation Strategy,” *IEEEASME Trans. Mechatron.*, vol. 23, no. 1, pp. 5–16, Feb. 2018, doi: 10.1109/TMECH.2017.2698216.
[52] M. Shimakage, “Design of lane-keeping control with steering torque input,” *JSAE Rev.*, vol. 23, no. 3, pp. 317–323, Jul. 2002, doi: 10.1016/S0389-4304(02)00194-7.
[53] A.-T. Nguyen, C. Sentouh, and J.-C. Popieul, “Fuzzy steering control for autonomous vehicles under actuator saturation: Design and experiments,” *J. Frankl. Inst.*, vol. 355, no. 18, pp. 9374–9395, Dec. 2018, doi: 10.1016/j.jfranklin.2017.11.027.
[54] V. Cerone, M. Milanese, and D. Regruto, “Combined Automatic Lane-Keeping and Driver’s Steering Through a 2-DOF Control Strategy,” *IEEE Trans. Control Syst. Technol.*, vol. 17, no. 1, pp. 135–142, Jan. 2009, doi: 10.1109/TCST.2008.924558.
[55] V. Cerone and D. Regruto, “Vehicle lateral controller design exploiting properties of SITO systems,” in *Proceedings of the 2003 American Control Conference, 2003.*, Denver, CO, USA: IEEE, 2003, pp. 4365–4370. doi: 10.1109/ACC.2003.1240525.

[56] N. Minoiu Enache, M. Netto, S. Mammar, and B. Lusetti, “Driver steering assistance for lane departure avoidance,” *Control Eng. Pract.*, vol. 17, no. 6, pp. 642–651, Jun. 2009, doi: 10.1016/j.conengprac.2008.10.012.
[57] S. M. Erlien, S. Fujita, and J. C. Gerdes, “Shared Steering Control Using Safe Envelopes for Obstacle Avoidance and Vehicle Stability,” *IEEE Trans. Intell. Transp. Syst.*, vol. 17, no. 2, pp. 441–451, Feb. 2016, doi: 10.1109/tits.2015.2453404.
[58] A.-T. Nguyen, C. Sentouh, and J.-C. Popieul, “Driver-Automation Cooperative Approach for Shared Steering Control Under Multiple System Constraints: Design and Experiments,” *IEEE Trans. Ind. Electron.*, vol. 64, no. 5, pp. 3819–3830, May 2017, doi: 10.1109/tie.2016.2645146.
[59] A.-T. Nguyen, C. Sentouh, J.-C. Popieul, and B. Soualmi, “Shared lateral control with on-line adaptation of the automation degree for driver steering assist system: A weighting design approach,” in *2015 54th IEEE Conference on Decision and Control (CDC)*, Osaka: IEEE, Dec. 2015. doi: 10.1109/cdc.2015.7402336.
[60] A. Nguyen, C. Sentouh, and J.-C. Popieul, “Online adaptation of the authority level for shared lateral control of driver steering assist system using dynamic output feedback controller,” in *IECON 2015 - 41st Annual Conference of the IEEE Industrial Electronics Society*, Yokohama: IEEE, Nov. 2015. doi: 10.1109/iecon.2015.7392688.
[61] T. Raharijaona, P. Chevrel, and G. Duc, “Reduced order gain scheduled h-infinity control design for lateral driving assistance,” in *Proceedings of 2005 IEEE Conference on Control Applications, 2005. CCA 2005.*, Toronto, Canada: IEEE, pp. 233–238. doi: 10.1109/cca.2005.1507130.
[62] L. Saleh, P. Chevrel, F. Claveau, J.-F. Lafay, and F. Mars, “Shared Steering Control Between a Driver and an Automation: Stability in the Presence of Driver Behavior Uncertainty,” *IEEE Trans. Intell. Transp. Syst.*, vol. 14, no. 2, pp. 974–983, Jun. 2013, doi: 10.1109/TITS.2013.2248363.
[63] N. M. Enache, S. Mammar, M. Netto, and B. Lusetti, “Driver Steering Assistance for Lane-Departure Avoidance Based on Hybrid Automata and Composite Lyapunov Function,” *IEEE Trans. Intell. Transp. Syst.*, vol. 11, no. 1, pp. 28–39, Mar. 2010, doi: 10.1109/TITS.2009.2026451.
[64] A.-T. Nguyen, P. Chevrel, and F. Claveau, “LPV Static Output Feedback for Constrained Direct Tilt Control of Narrow Tilting Vehicles,” *IEEE Trans. Control Syst. Technol.*, vol. 28, no. 2, pp. 661–670, Mar. 2020, doi: 10.1109/TCST.2018.2882345.
[65] C. Hu *et al.*, “MME-EKF-Based Path-Tracking Control of Autonomous Vehicles Considering Input Saturation,” *IEEE Trans. Veh. Technol.*, vol. 68, no. 6, pp. 5246–5259, Jun. 2019, doi: 10.1109/TVT.2019.2907696.
[66] V. Turri, A. Carvalho, H. E. Tseng, K. H. Johansson, and F. Borrelli, “Linear model predictive control for lane keeping and obstacle avoidance on low curvature roads,” in *16th International IEEE Conference on Intelligent Transportation Systems (ITSC 2013)*, The Hague, Netherlands: IEEE, Oct. 2013, pp. 378–383. doi: 10.1109/ITSC.2013.6728261.
[67] J. E. Naranjo, C. Gonzalez, R. Garcia, T. dePedro, and R. E. Haber, “Power-Steering Control Architecture for Automatic Driving,” *IEEE Trans. Intell. Transp. Syst.*, vol. 6, no. 4, pp. 406–415, Dec. 2005, doi: 10.1109/TITS.2005.858622.
[68] X. Huang, H. Zhang, G. Zhang, and J. Wang, “Robust Weighted Gain-Scheduling $H_{\infty }$ Vehicle Lateral Motion Control With Considerations of Steering System Backlash-Type

Hysteresis," *IEEE Trans. Control Syst. Technol.*, vol. 22, no. 5, pp. 1740–1753, Sep. 2014, doi: 10.1109/tcst.2014.2317772.
[69] Y. Liang, Y. Li, Y. Yu, Z. Zhang, L. Zheng, and Y. Ren, "Path-Following Control of Autonomous Vehicles Considering Coupling Effects and Multi-source System Uncertainties," *Automot. Innov.*, vol. 4, no. 3, pp. 284–300, Aug. 2021, doi: 10.1007/s42154-021-00155-z.
[70] A. Mohammadzadeh and H. Taghavifar, "A robust fuzzy control approach for path-following control of autonomous vehicles," *Soft Comput.*, vol. 24, no. 5, pp. 3223–3235, Mar. 2020, doi: 10.1007/s00500-019-04082-4.
[71] Y. Zhang, W. Wang, W. Wang, C. Yang, and Y. Zhang, "An Adaptive Constrained Path Following Control Scheme for Autonomous Electric Vehicles," *IEEE Trans. Veh. Technol.*, vol. 71, no. 4, pp. 3569–3578, Apr. 2022, doi: 10.1109/TVT.2022.3146134.
[72] N. Tork, A. Amirkhani, and S. B. Shokouhi, "An adaptive modified neural lateral-longitudinal control system for path following of autonomous vehicles," *Eng. Sci. Technol. Int. J.*, vol. 24, no. 1, pp. 126–137, Feb. 2021, doi: 10.1016/j.jestch.2020.12.004.
[73] H. Wang, T. Zhang, W. Quan, and Q. Li, "Observer-based path following control for autonomous vehicles with localization errors and tire slip effects," *Asian J. Control*, vol. 25, no. 2, pp. 1526–1541, Mar. 2023, doi: 10.1002/asjc.2948.
[74] Z. Liang, Y. Chen, and J. Zhao, "Real-time Parameter Updating and Path-following Control for Autonomous Vehicles on Slope Roads," *Int. J. Control Autom. Syst.*, vol. 20, no. 7, pp. 2178–2190, Jul. 2022, doi: 10.1007/s12555-021-0269-8.
[75] Q. Liu, S. Song, H. Hu, T. Huang, C. Li, and Q. Zhu, "Extended model predictive control scheme for smooth path following of autonomous vehicles," *Front. Mech. Eng.*, vol. 17, no. 1, p. 4, Mar. 2022, doi: 10.1007/s11465-021-0660-4.
[76] P. Li, J. Lam, and R. Lu, "Robust Switched Velocity-Dependent Path-Following Control for Autonomous Ground Vehicles," *IEEE Trans. Intell. Transp. Syst.*, vol. 24, no. 5, pp. 4815–4826, May 2023, doi: 10.1109/TITS.2023.3236113.
[77] Z. Xue, S. Cheng, L. Li, and Z. Zhong, "Nonlinear H∞ path following control for autonomous ground vehicles via neural network and policy iteration algorithm," *Proc. Inst. Mech. Eng. Part J. Automob. Eng.*, vol. 238, no. 6, pp. 1670–1683, May 2024, doi: 10.1177/09544070221145468.
[78] H. Zhang, R. Wang, and J. Wang, "Robust $$\mathcal {H}_\infty $$ Path Following Control for Autonomous Ground Vehicles with Delay and Data Dropout," in *Robust Gain-Scheduled Estimation and Control of Electrified Vehicles via LPV Technique*, in Key Technologies on New Energy Vehicles. , Singapore: Springer Nature Singapore, 2023, pp. 153–171. doi: 10.1007/978-981-19-8509-6_6.
[79] X. Jin, Q. Wang, Z. Yan, H. Yang, and G. Yin, "Integrated robust control of path following and lateral stability for autonomous in-wheel-motor-driven electric vehicles," *Proc. Inst. Mech. Eng. Part J. Automob. Eng.*, p. 09544070241227266, Jan. 2024, doi: 10.1177/09544070241227266.
[80] H. B. Pacejka, *Tire and Vehicle Dynamics*, Third. Elsevier, Butterworth-Heinemann, 2012. doi: 10.1016/C2010-0-68548-8.
[81] R. Rajamani, *Vehicle Dynamics and Control*. in Mechanical Engineering Series. Boston, MA: Springer US, 2012. doi: 10.1007/978-1-4614-1433-9.
[82] S. Sastry, *Nonlinear Systems*, vol. 10. in Interdisciplinary Applied Mathematics, vol. 10. New York, NY: Springer New York, 1999. doi: 10.1007/978-1-4757-3108-8.

[83] W. J. Rugh and J. S. Shamma, “Research on gain scheduling,” *Automatica*, vol. 36, no. 10, pp. 1401–1425, Oct. 2000, doi: 10.1016/S0005-1098(00)00058-3.
[84] S. M. Shahruz and S. Behtash, “Gain scheduling: potential hazards and possible remedies,” *J. Math. Anal. Appl.*, vol. 168, no. 1, pp. 195–217, Jul. 1992, doi: 10.1016/0022-247X(92)90199-N.
[85] C. Briat, *Linear Parameter-Varying and Time-Delay Systems: Analysis, Observation, Filtering & Control*, vol. 3. in Advances in Delays and Dynamics, vol. 3. Berlin, Heidelberg: Springer Berlin Heidelberg, 2015. doi: 10.1007/978-3-662-44050-6.
[86] R. Tóth, *Modeling and Identification of Linear Parameter-Varying Systems*, vol. 403. in Lecture Notes in Control and Information Sciences, vol. 403. Berlin, Heidelberg: Springer Berlin Heidelberg, 2010. doi: 10.1007/978-3-642-13812-6.
[87] O. Sename, P. Gaspar, and J. Bokor, Eds., *Robust Control and Linear Parameter Varying Approaches: Application to Vehicle Dynamics*, vol. 437. in Lecture Notes in Control and Information Sciences, vol. 437. Berlin, Heidelberg: Springer Berlin Heidelberg, 2013. doi: 10.1007/978-3-642-36110-4.
[88] J. Mohammadpour and C. W. Scherer, Eds., *Control of Linear Parameter Varying Systems with Applications*. Boston, MA: Springer US, 2012. doi: 10.1007/978-1-4614-1833-7.
[89] H. Atoui, “Switching/interpolating lpv control based on youla-kucera parameterization: Application to autonomous vehicles,” Doctoral dissertation, Université Grenoble Alpes [2020-....], 2022.
[90] J. P. Switkes, E. J. Rossetter, I. A. Coe, and J. C. Gerdes, “Handwheel Force Feedback for Lanekeeping Assistance: Combined Dynamics and Stability,” *J. Dyn. Syst. Meas. Control*, vol. 128, no. 3, pp. 532–542, Sep. 2006, doi: 10.1115/1.2229256.
[91] K. Tanaka and H. O. Wang, *Fuzzy Control Systems Design and Analysis: A Linear Matrix Inequality Approach*, 1st ed. Wiley, 2001. doi: 10.1002/0471224596.
[92] Kirk, D. E., *Optimal control theory: an introduction*. Courier Corporation, 2004.
[93] B. Li, S. Wen, Z. Yan, G. Wen, and T. Huang, “A Survey on the Control Lyapunov Function and Control Barrier Function for Nonlinear-Affine Control Systems,” *IEEECAA J. Autom. Sin.*, vol. 10, no. 3, pp. 584–602, Mar. 2023, doi: 10.1109/JAS.2023.123075.
[94] S. Boyd, L. El Ghaoui, E. Feron, and V. Balakrishnan, *Linear Matrix Inequalities in System and Control Theory*. Society for Industrial and Applied Mathematics, 1994. doi: 10.1137/1.9781611970777.
[95] J. Daafouz and J. Bernussou, “Parameter dependent Lyapunov functions for discrete time systems with time varying parametric uncertainties,” *Syst. Control Lett.*, vol. 43, no. 5, pp. 355–359, Aug. 2001, doi: 10.1016/S0167-6911(01)00118-9.
[96] H. K. Lam, “Stability analysis of T–S fuzzy control systems using parameter-dependent Lyapunov function,” *IET Control Theory Appl.*, vol. 3, no. 6, pp. 750–762, Jun. 2009, doi: 10.1049/iet-cta.2008.0196.
[97] N. Vafamand, “Global non-quadratic Lyapunov-based stabilization of T–S fuzzy systems: A descriptor approach,” *J. Vib. Control*, vol. 26, no. 19–20, pp. 1765–1778, Oct. 2020, doi: 10.1177/1077546320904817.
[98] C. Scherer and S. Weiland, *Linear matrix inequalities in control*, Lecture Notes., vol. 3(2). Dutch Institute for Systems and Control, Delft, The Netherlands, 2000.
[99] Daizhan Cheng, Lei Guo, and Jie Huang, “On quadratic lyapunov functions,” *IEEE Trans. Autom. Control*, vol. 48, no. 5, pp. 885–890, May 2003, doi: 10.1109/TAC.2003.811274.

[100] C. Scherer, P. Gahinet, and M. Chilali, “Multiobjective output-feedback control via LMI optimization,” *IEEE Trans. Autom. Control*, vol. 42, no. 7, pp. 896–911, Jul. 1997, doi: 10.1109/9.599969.
[101] M. Bernal, P. Hušek, and V. Kučera, “Nonquadratic stabilization of continuous-time systems in the Takagi-Sugeno form,” *Kybernetika*, vol. 42, no. 6, pp. 665–672, 2006.
[102] *MATLAB version: 9.13.0 (R2022b)*. The Mathworks INc., Natick, Massachusetts, United States. [Online]. Available: https://www.mathworks.com
[103] J. Lofberg, “YALMIP : a toolbox for modeling and optimization in MATLAB,” in *2004 IEEE International Conference on Robotics and Automation (IEEE Cat. No.04CH37508)*, Taipei, Taiwan: IEEE, 2004, pp. 284–289. doi: 10.1109/CACSD.2004.1393890.
[104] S. Boyd and L. Vandenberghe, *Convex Optimization*, 1st ed. Cambridge University Press, 2004. doi: 10.1017/CBO9780511804441.
[105] H. D. Tuan, P. Apkarian, T. Narikiyo, and Y. Yamamoto, “Parameterized linear matrix inequality techniques in fuzzy control system design,” *IEEE Trans. Fuzzy Syst.*, vol. 9, no. 2, pp. 324–332, Apr. 2001, doi: 10.1109/91.919253.